

FreedomCAR & Fuel Partnership



U.S. DEPARTMENT OF
ENERGY

USCAR
UNITED STATES COUNCIL FOR AUTOMOTIVE RESEARCH LLC



ConocoPhillips

ExxonMobil



SOUTHERN CALIFORNIA
EDISON
An EDISON INTERNATIONAL® Company

FreedomCAR and Fuel Partnership

2010

Highlights of Technical Accomplishments

Table of Contents

<i>Item</i>	<i>Page</i>
Preface	v
<u>Vehicle Technologies</u>	
Advanced Combustion & Emissions Control	
• <i>Dual-Fuel (Gasoline+Diesel) RCCI Offers High Efficiency and Low Emissions in Engines</i>	1
• <i>Turbocharger Technology to Deliver Better Performance and Reduced Fuel Consumption</i>	2
• <i>Late Intake Valve Closing Improves Tradeoff Between Diesel-Engine Smoke and NO_x Emissions</i>	3
• <i>Modeling of Lean NO_x Trap Chemistry</i>	4
• <i>Neutron Radiography Non-Destructive Image of EGR Cooler and DPF Build-ups</i>	5
• <i>Accurate Detailed Chemical Kinetic Surrogate Model for Gasoline</i>	6
• <i>Sources of Inefficiency Identified in Light-Duty, Low-Temperature Diesel Combustion</i>	7
• <i>2010 FreedomCAR Engine Milestone for 45% Brake Thermal Efficiency Met</i>	8
Electrical & Electronics	
• <i>Novel Power Semiconductor Packaging Reduces Die Area, Volume, Weight and Cost</i>	9
• <i>Direct Water-Cooled Power Electronics Packaging Concept Reduces Size and Weight</i>	10
• <i>Segmented Drive Inverter Topology Enables Smaller and Lower Cost DC Bus Capacitor</i>	11
• <i>Effect of Enhanced Surfaces on Single and Two-Phase Heat Transfer is Quantified</i>	12
• <i>Reduced Cost Permanent Magnets for High-Speed Interior Permanent Magnet Motors</i>	13
• <i>Compact Bi-Directional Charger for Plug-in Vehicles</i>	14

Table of Contents (continued)

Item	Page
Electrochemical Energy Storage	
• <i>Novel Battery Thermal Management System Developed</i>	15
• <i>Nanophosphate Battery Technology for HEVs</i>	16
• <i>Advanced PHEV Cathode Material Developed</i>	17
• <i>Design, Build and Testing of NMC-Prismatic Format Cell and System</i>	18
• <i>High Temperature Melt Integrity Separator and Test Suite Developed</i>	19
• <i>19 Amp-Hour Prismatic Cell Delivered</i>	20
• <i>Advanced Separators for HEV/PHEVs</i>	21
• <i>Surface-Coated, High-Energy Battery Cathode Demonstrates Improved Cycling and Capacity</i>	22
• <i>Pre-Lithiating Graphite, Silicon, and Tin Anodes Reduces First Cycle Irreversible-Capacity-Loss</i>	23
• <i>Synthesis of a High-Voltage Cathode Material with Improved Stability</i>	24
• <i>Improved Performance of High-Energy Battery Anodes</i>	25
• <i>New Electrolyte Additive for Lithium-Ion and Lithium-Air Batteries</i>	26
• <i>Improved Thermal Performance Using a Coated Cathode Material</i>	27
• <i>In Situ NMR Observation of the Formation of Metallic Lithium Microstructures</i>	28
• <i>Development of High Rate Anode Using Graphene Building Blocks</i>	29
Fuel Cells	
• <i>Automotive Fuel Cell System Cost Modeling Shows Progress Toward Cost Targets</i>	30
• <i>New Ultra-Low Platinum Loading Fuel Cell Catalyst has 7X Improved Activity and High Stability</i>	31
• <i>Systems Analysis Shows Significant Cost Savings Possible by Easing Peak-Power Efficiency Target</i>	32
• <i>New Composite Membranes show Improved Durability without Compromising Performance</i>	33
• <i>Improved Resolution for Imaging Water in Operating Fuel Cells Aids Developers</i>	34
• <i>Improved Performance and Stability of Non-Precious Metal Cathode Catalysts</i>	35
• <i>Hollow Platinum Nanoparticles Developed for Stable, High-Activity Fuel Cell Catalysts</i>	36
• <i>Fuel Cells Can Recover from Ammonia Contamination in Both Fuel and Air Streams</i>	37
• <i>Better Water Management Improves Transient Performance of Low Platinum-Loading Catalysts</i>	38
• <i>Fuel Cell Membranes Show Promise to Meet High Temperature Operation Targets</i>	31
• <i>Simultaneous Water Visualization and Resistance Measurements Can Be Used to Develop Fuel Cell Shut-Down Strategy</i>	39
• <i>New Fuel Cell Membranes Show Promise to Meet High-Temperature Operation Targets</i>	40

Table of Contents (continued)

Item	Page
Materials	
• <i>Advanced High-Strength Steel Matches Aluminum Performance and Light Weight with Reduced Cost</i>	41
• <i>Minimum Weight SMC Assemblies Free from Bond-Line Read-Through</i>	42
• <i>Reliability Tools for Resonance Inspection</i>	43
• <i>Development of High-Volume Warm Forming of Low-Cost Magnesium Sheet</i>	44
• <i>Friction Stir and Ultrasonic Solid State Welding Enable Joining of Magnesium to Steel</i>	45
• <i>Friction Stir Spot Welding of Advanced High Strength Steel</i>	46
• <i>Stabilization Time of Lignin Precursor Fiber Reduced from Days to Minutes</i>	47
Vehicle Systems Analysis	
• <i>Accelerating Advanced Technology Introduction through Plug-and-Play Architecture Modeling</i>	48
• <i>Accelerating Control Development Using Hardware in a Virtual System Environment</i>	49
• <i>Grid-Connected Electric Drive Vehicle and Charging Studies Demonstrate Petroleum Reductions</i>	50
• <i>A Standard Practice for Testing PHEVs Developed and Balloted</i>	51
• <i>European Hybrid Vehicle Benchmarked for Fuel Consumption Benefits and Emissions Trade-Offs</i>	52
• <i>PHEV Bus Reduces Fuel Consumption Up to 50%</i>	53
• <i>Thermal Preconditioning Restores Range Up to 19%</i>	54
<u>Fuel Infrastructure Technologies</u>	
Fuel Pathway Integration	
• <i>Hydrogen Threshold Cost Updated</i>	55
• <i>Hydrogen Costs from Fuel Cell Combined Heat and Power</i>	56
• <i>Infrastructure Costs for Coal-Based Hydrogen Production</i>	57
Hydrogen Delivery	
• <i>Development of a Centrifugal Hydrogen Pipeline Gas Compressor</i>	58
Hydrogen Production	
• <i>Hydrogen Selective Membranes as Reactors/Separators for Distributed Hydrogen Production</i>	59
• <i>New Benchmark Efficiency for Photoelectrochemical Water-Splitting Devices</i>	60

Table of Contents (continued)

<i>Item</i>	<i>Page</i>
<u>Crosscutting Technologies</u>	
Codes & Standards	
• <i>SAE J2579 TIR and GTR Coordination</i>	61
• <i>SAE J2601 Hydrogen Fueling Protocol</i>	62
Onboard Hydrogen Storage	
• <i>Cryo-Compressed Tank Exceed 2015 Weight and Volume Targets</i>	63
• <i>12 Weight Percent Hydrogen Reversibility Demonstrated for Magnesium Borohydride</i>	64
• <i>“Optimized” Sorbents Designed and Synthesized for Hydrogen Storage</i>	65
• <i>New Class of Lightweight Metal Hydrides Show Promise for Hydrogen Storage</i>	66
• <i>New Techniques for Safe Hydride Containment</i>	67
• <i>Performance and Cost Analyses Accelerate Development of Hydrogen Storage Technologies</i>	68
Grid Interaction	
• <i>Universal Vehicle Energy-Use Communications Technology Developed</i>	69
• <i>Compact Low-Cost Revenue-Grade Sub-Meter Demonstrated</i>	70

Preface

This report summarizes key technical accomplishments achieved in support of the FreedomCAR and Fuel Partnership in 2010.

The FreedomCAR and Fuel Partnership is a voluntary government-industry partnership focused on advanced automotive and related infrastructure technology research and development (R&D). Specifically, the partnership is a forum for pre-competitive technical information exchange among experts who interact as equal partners to discuss R&D needs, develop goals and technology roadmaps and evaluate R&D progress.

Partners are the United States Department of Energy (DOE); the United States Council for Automotive Research LLC (USCAR), a consortium composed of Chrysler Group LLC, Ford Motor Company and General Motors Company; five energy companies, (BP America, Chevron Corporation, ConocoPhillips, ExxonMobil Corporation and Shell Oil Products US); and two electric utilities, DTE Energy and Southern California Edison.

By providing a framework for frequent and regular interaction among technical experts in a common area of expertise, the partnership –

- Accelerates technical progress; peers in the technical community discuss pre-competitive, technology-specific R&D needs and challenges, identify possible solutions and evaluate progress toward jointly-developed technical goals.
- Helps to avoid duplication of efforts and ensure that publicly-funded research delivers high-value results and overcomes high-risk barriers to technology commercialization.

The partnership selected technical highlights from many hundreds of DOE-funded projects in 2010. Each one-page highlight represents what DOE and the automotive, energy and utility industry partners collectively consider to be significant progress in the development of advanced automotive and infrastructure technologies. The report is organized by technical area, with highlights that fall into three groups:

Vehicles

- Advanced Combustion & Emissions Control
- Electrical and Electronics
- Electrochemical Energy Storage
- Fuel Cells
- Materials
- Vehicle Systems Analysis

Fuels

- Fuel Pathway Integration
- Hydrogen Delivery
- Hydrogen Production

Crosscutting

- Codes and Standards
- Onboard Hydrogen Storage
- Grid Interaction

Prior year accomplishments reports are available on the FreedomCAR and Fuel Partnership page on the USCAR website at www.uscar.org and the DOE website at www.vehicles.energy.gov/about/partnerships/freedomcar/index.html.

Through cooperation and partnership among industry and government, advanced automotive technology research continues to make tremendous progress. Advanced technologies are beginning to enter the market in increasing numbers, and technologies that were only concepts less than a decade ago are now approaching initial commercial readiness. These advancements are the result of partners working together to achieve a common goal. With continued progress resulting from the joint efforts of government, industry and academic experts, the FreedomCAR and Fuel Partnership is helping to increase the competitiveness of American industry, safeguard American R&D and manufacturing jobs and secure U.S. leadership in the development of advanced automotive technologies to enable a clean and sustainable transportation energy future.

Note: Common abbreviations used through this report

ANL – Argonne National Laboratory
BNL – Brookhaven National Laboratory
EPA – Environmental Protection Agency
EDV – Electric Drive Vehicle
EUCAR – European Council for Automotive R&D
EV – Electric Vehicle
EVSE – Electric Vehicle Supply Equipment
DOE – Department of Energy
FCV – Fuel Cell Electric Vehicle
HEV – Hybrid Electric Vehicle
INL – Idaho National Laboratory
LANL – Los Alamos National Laboratory
NIST – National Institute of Standards and Technology
NREL – National Renewable Energy Laboratory
ORNL – Oak Ridge National Laboratory
PHEV – Plug-In Hybrid Electric Vehicle
PNNL – Pacific Northwest National Laboratory
SNL – Sandia National Laboratories
SRNL – Savannah River National Laboratory
USABC – United States Advanced Battery Consortium
USAMP – United States Automotive Materials Partnership

2010 FreedomCAR and Fuel Partnership Highlight

Dual-Fuel (Gasoline+Diesel) RCCI Offers High Efficiency and Low Emissions in Engines

University of Wisconsin-Madison

Recent experiments conducted on a heavy-duty diesel research engine at the University of Wisconsin-Madison have demonstrated that dual-fuel operation can offer high-efficiency with low engine-out emissions. In this study, single cylinder engine experiments were used to further investigate the dual-fuel Reactivity Controlled Compression Ignition (RCCI) concept in both light-duty (LD) and heavy-duty (HD) engines, and comparisons were made between the two engine classes. The RCCI concept uses in-cylinder blending of two fuels with different auto-ignition characteristics to achieve controlled high efficiency clean combustion. The study uses gasoline port injection in combination with optimized in-cylinder multiple diesel injections.

It was found that with only small changes in the injection parameters, the excellent combustion characteristics of the HD engine could be reproduced in the LD engine. Comparisons of the emissions and performance showed that both engines can simultaneously meet NO_x and soot emissions targets without the need for after-treatment (i.e., achieve NO_x below 0.2 g/kW-hr and soot below 0.03 g/kW-hr in-cylinder). HC and CO emissions were higher than conventional diesel operation; however the exhaust temperatures appear to be sufficient for reduction using a standard oxidation catalyst and do not pose a challenge. Furthermore, it was found that stratification in fuel reactivity can be used to maintain acceptable pressure rise rates, such that knocking combustion is avoided.

The peak gross indicated efficiencies of the light- and heavy-duty engines were 50 and 57 percent, respectively. Note that the HD engine is inherently more efficient than the LD engine due to the smaller surface area-to-volume ratio. The efficiency of the LD RCCI engine was compared to LD conventional diesel and LD low temperature combustion (LTC) diesel operation. This comparison showed that LD RCCI has the potential to achieve a 10 to 20 percent improvement in indicated efficiency. Recent advances have also demonstrated satisfactory RCCI operation at loads below 6 bar IMEP, including idle.

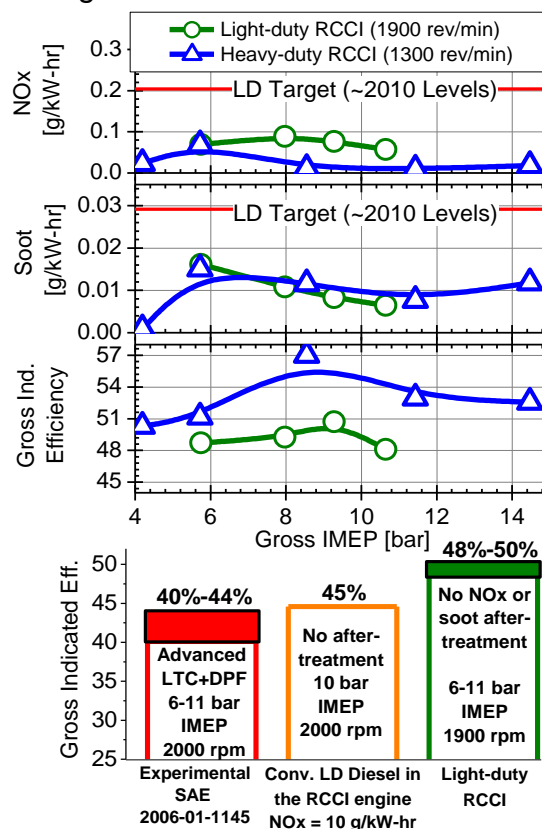


Figure 1: Comparison of LD and HD engine experimental results over load range (top). Comparison of RCCI with conventional (high NO_x) diesel and advanced after-treatment-equipped diesel that meets Tier 2 Bin 5 emissions targets (bottom).

2010 FreedomCAR and Fuel Partnership Highlight

Turbocharger Technology to Deliver Better Performance and Reduced Fuel Consumption

Ford Motor Company, Wayne State University and Concepts NREC

The turbocharger is one of the most important components enabling engine downsizing for better fuel economy. Typically the turbocharger is sized large enough to enable high engine horsepower yet small enough to have a prompt transient response for drivability. High efficiency on customer drive cycles is also important for improving fuel economy.

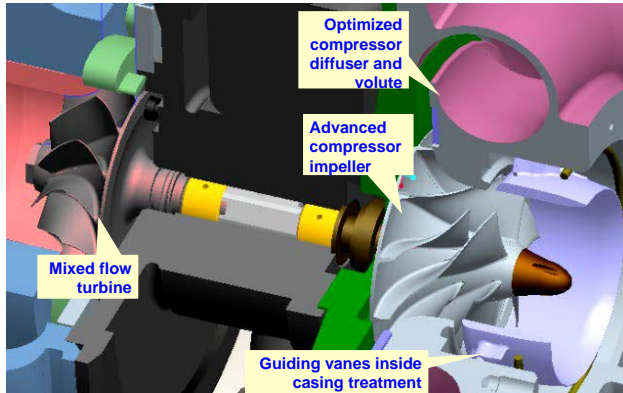


Figure 1. CAD rendering showing areas of focus.

The primary focus of this research is to extend the turbocharger operation range and maintain or improve engine efficiency on regular customer driving cycles. This is accomplished through a variety of new concepts which improve gas flows through the turbine and compressor. Various advanced numerical simulation tools have been applied to guide the optimization of existing turbocharger technologies as well as the assessment of new technologies such as: mixed flow turbine, advanced compressor impeller with compressor variable inlet guiding vane and advanced casing treatment, optimized compressor variable diffuser and dual sequential compressor volute as shown in Figure 1.

vane and advanced casing treatment, optimized compressor variable diffuser and dual sequential compressor volute as shown in Figure 1.

Based on numerical analyses, the most promising technologies were fabricated and are being tested. The preliminary bench test flow data has validated the computer prediction of the extension of compressor flow capacity in the near choking condition. (The performance near the surge condition is not yet tested due to hardware constraints). Figure 2, a combination of analytical and test data, shows the optimal design of compressor blades coupled with advanced casing treatment can extend compressor operation range up to 25 percent and improve efficiency up to 10 percent on regular customer driving cycles. This will lead to engine efficiency improvements of approximately 3 percent on city driving cycles.

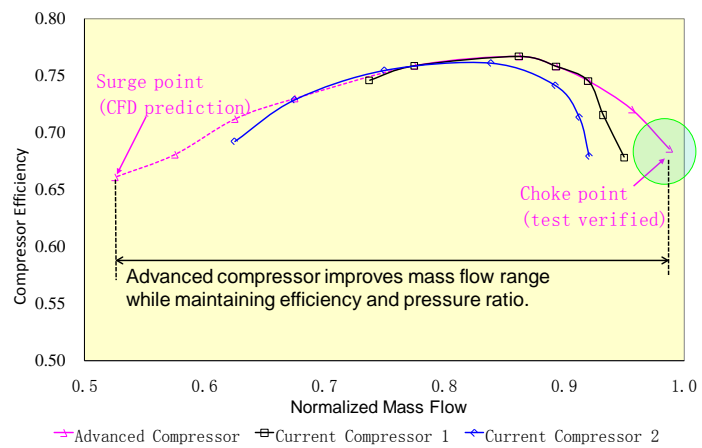


Figure 2. Advanced compressor technology improves efficiency and operation range.

extend compressor operation range up to 25 percent and improve efficiency up to 10 percent on regular customer driving cycles. This will lead to engine efficiency improvements of approximately 3 percent on city driving cycles.

2010 FreedomCAR and Fuel Partnership Highlight

Late Intake Valve Closing Improves Tradeoff Between Diesel-Engine Smoke and NO_x Emissions

General Motors

In diesel combustion, a reduction in smoke usually leads to an increase in NO_x. Late Intake Valve Closing (LIVC) has the potential to improve this emission tradeoff. LIVC was studied in an experimental, 8-cylinder, 4-valve per cylinder, diesel engine with cooled external exhaust gas recirculation (EGR). The engine was operated at steady conditions at several Federal Test Procedure (FTP) key points with load ranging from 2- to 7-bar brake mean effective pressure (BMEP). The operating conditions were selected to reach Tier 2 Bin5 NO_x emission levels with an aftertreatment system. During the tests, the valve event of one intake valve was delayed relative to the other intake valve that operated at normal timing. The combination of both valves created an effective intake valve event where the intake valve was open during the early part of the compression stroke and intake valve closing was later than normal timing as shown in Figure 1.

At the key points and when NO_x emissions equaled the baseline engine, the LIVC strategy improved smoke and fuel consumption due to improved in-cylinder fuel-air mixing by control of swirl and increased ignition delay by reduction of effective compression ratio and lower compression pressure and temperature. These changes increased hydrocarbons and CO. On the FTP schedule, the impact estimated by weighting results from all the key points, was 0.5 percent improvement in fuel consumption, 25 percent lower particulates, and 17 percent higher hydrocarbons as shown in Figure 2. With LIVC, the engine volumetric efficiency is reduced. An improved turbocharger system may be needed to compensate for this change and match the baseline air flow and air-fuel ratios.

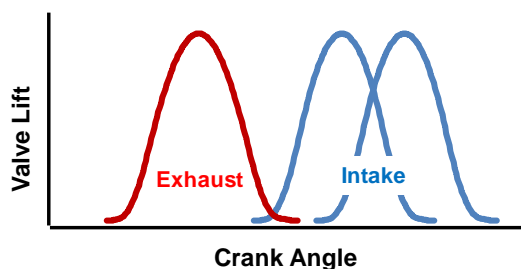


Figure 1. LIVC Valve Lift profiles.

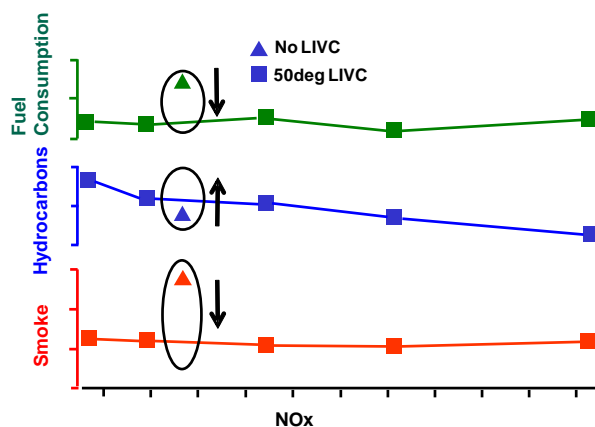


Figure 2. Fuel consumption, hydrocarbon, and smoke as a function of NO_x at 1200r/min, 3.9-bar BMEP for base and LIVC with 50° shift. NO_x changed by varying EGR from 30% to 42%.

2010 FreedomCAR and Fuel Partnership Highlight

Modeling of Lean NO_x Trap Chemistry

Oak Ridge National Laboratory, Sandia National Laboratories

Lean NO_x Traps (LNTs) represent one technology for meeting stringent new standards for emission of NO_x from lean-burn engines. Oak Ridge and Sandia National Laboratories are developing models that accurately describe the chemistry in LNTs. The goal is to be able to predict both the NO_x conversion efficiency and the distribution of products throughout the vehicle lifetime. This long term view is critical, since sulfur in the fuel can have a cumulative effect on the chemistry, and exposure of the catalysts to high temperatures during operation can eventually affect the reactivity. Understanding the chemistry and how it changes over the life of a vehicle allows optimization of controls for maximum fuel economy with a minimum of pollutants.

The laboratories have pursued two complementary routes to account for the complex behavior in LNTs. First, a set of single-step chemical reactions was assembled that describe the functionality of LNTs at a fundamental level. The rates of those reactions were then determined by matching reactor simulations to the results of an extensive set of experiments. To account for fuel-borne sulfur that accumulates in the LNT during use, a supplementary mechanism was also developed to account for sulfur poisoning of the catalyst and its subsequent desulfation. Figure 1 shows results for the outlet NO_x concentration during a normal cycle (60 second lean for NO_x storage, 5 second rich for NO_x release) for three different levels of sulfation. The model reproduces the experimental observation that low sulfation levels can be tolerated, while higher levels cause a disproportionate increase in NO_x emissions.

A global approach to modeling was also implemented which accounts for the basic steps that occur in an LNT, including by-product formation (Figure 2). This ability to track by-products is critical, as it has been demonstrated that ammonia (NH₃) can form in LNTs. Minimizing the emission of NH₃ is often a goal, but NH₃ can also be a useful by-product when employed in an LNT+SCR (Selective Catalytic Reduction) NO_x control strategy. The ability to simulate all facets of the chemistry should facilitate the optimal use of LNTs, and in the longer term, the development of improved and less-expensive catalysts.

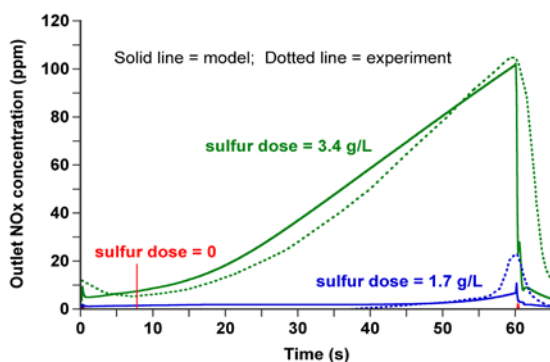


Figure 1. Fundamental model reproduces effect of sulfur on NO_x trapping efficiency.

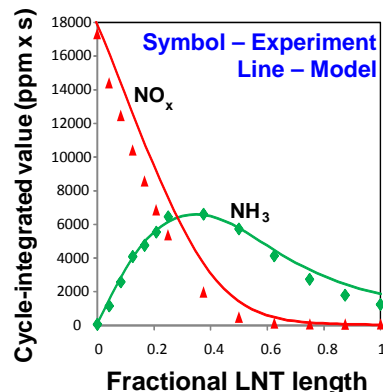


Figure 2. Global model predicts NH₃ formation inside LNT catalyst. Data averaged over entire lean+rich cycle.

2010 FreedomCAR and Fuel Partnership Highlight

Neutron Radiography Non-Destructive Image of EGR Cooler and DPF Build-ups

Oak Ridge National Laboratory

Oak Ridge National Laboratory (ORNL) developed a technique for imaging emissions control devices using neutron radiography. This non-destructive technique utilizes the neutron capabilities uniquely available at ORNL's High Flux Isotope Reactor (HFIR) and Spallation Neutron Source (SNS) and allows the imaging of a range of processes. This imaging is possible because neutrons can penetrate certain materials, e.g. metals and ceramics, while being absorbed by other materials such as hydrocarbons and water. Thus, detailed analysis of undisturbed layers inside emissions control devices can be observed without cutting open the device. The improved understanding will aid design and control of these complex systems and help to ensure that they are operating at peak efficiency. Efforts to date have aimed at developing the technique for 3-D tomography, improving image resolution and establishing limitations with respect to material contrasts, i.e. what can be seen and to what level can it be quantified. Initial focus has been on investigating fouling in exhaust gas recirculation (EGR) coolers and soot/ash deposition inside of diesel particulate filters (DPFs).

EGR coolers are employed to control the temperature of recirculated exhaust, but build-up of soot and hydrocarbons on the walls reduces cooling efficiency. As shown in Figure 1, neutron tomography enables imaging within the cooler and thus can help identify operating conditions that exacerbate fouling. DPFs are another key component of the emissions control system for modern diesel engines. Their main purpose is to trap the carbonaceous soot in exhaust. They are then periodically regenerated through high temperature oxidation. There remain significant questions about the basic behavior of the DPFs, specifically on the location of the soot and the effectiveness of the regeneration techniques being employed. Figure 2 illustrates a clean DPF and one that has been filled with soot. The bright rounded squares in the bottom image are the inlet side of the DPF. Applying this approach systematically will help explain where particulate is deposited and where it is removed during partial regeneration, which in turn will help minimize overheating, control the oxidation and minimize the associated fuel consumption penalty in DPFs.

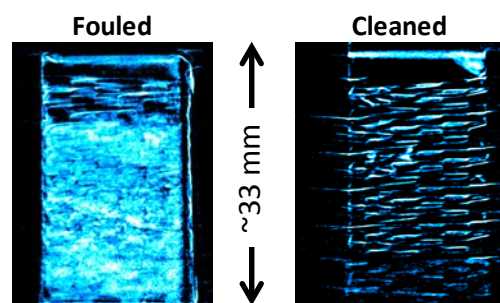


Figure 1. Neutrons enable non-destructive imaging of EGR cooler fouling. White areas indicate soot and hydrocarbons.

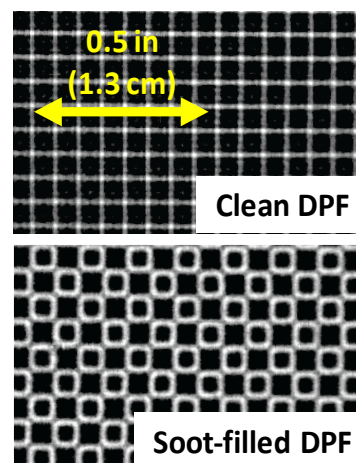


Figure 2. Soot deposits within DPF imaged using neutron tomography.

2010 FreedomCAR and Fuel Partnership Highlight

Accurate Detailed Chemical Kinetic Surrogate Model for Gasoline

Lawrence Livermore National Laboratory

Real fuel kinetics are needed in computational fluid dynamics models for engines to enable their use in developing more efficient engine designs with low emissions and in predicting the effect of fuel properties on engine performance. Gasoline and diesel fuels typically contain hundreds to thousands of constituents which can be grouped into chemical classes including n-alkanes, iso-alkanes, alkenes, cycloalkenes and aromatics. The use of real fuel kinetics has been inhibited by lack of kinetic models that cover the major chemical classes. Chemical kinetic models need to be developed for components to represent each chemical class so they can then be merged together to make fuel “surrogate models” to accurately represent real fuels.

Major improvements have been made to chemical kinetic models for gasoline. Kinetic component models have been developed to represent all the chemical classes of n-alkanes, iso-alkanes, cycloalkanes, alkenes, aromatics and ethanol in gasoline. These models include low temperature chemistry that is important for simulating low temperature combustion strategies such as Homogeneous Charge Compression Ignition (HCCI). The component models have also been merged together to form a complete fuel surrogate model for gasoline. Consequently, the fuel chemistry of gasoline can now be accurately represented, and for example, gasoline HCCI combustion can now be successfully simulated. Model predictions have been compared with recent gasoline HCCI experiments from Sandia National Laboratories. The operating parameters for the simulated engine cycle have been varied to obtain optimal combustion phasing with boosted pressures as done in the experiments, covering a wide range of conditions. The model correctly reproduced both qualitatively and quantitatively the measured engine data, as shown in Figure 1, where the measured and calculated bottom dead center temperatures required for optimal phasing are shown over a range of intake pressures for HCCI combustion of gasoline.

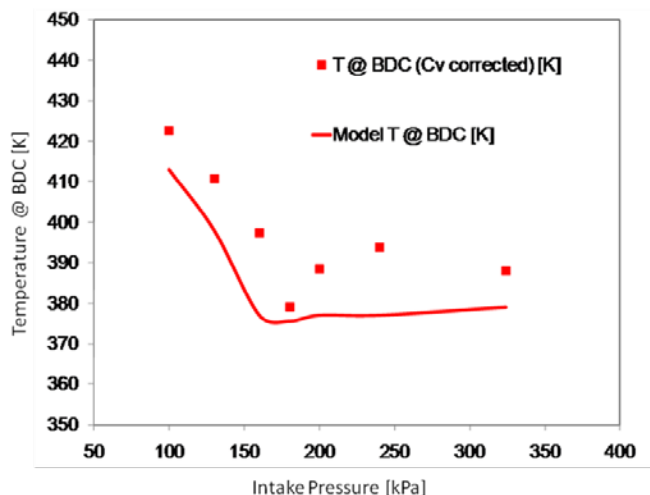


Figure 1. Gasoline surrogate accurately reproduces bottom-dead center (BDC) temperature required to achieve measured HCCI combustion timing over a range of intake pressures for 87 octane gasoline.

2010 FreedomCAR and Fuel Partnership Highlight

Sources of Inefficiency Identified in Light-Duty, Low-Temperature Diesel Combustion

Sandia National Laboratories, University of Wisconsin

Low-temperature diesel combustion strategies offer promise for the in-cylinder control of NO_x and soot emissions, but can suffer from a loss in combustion efficiency that results in increased emissions of unburned hydrocarbons (UHC) and carbon monoxide (CO). Identifying the in-cylinder sources of these emissions, and developing a predictive modeling and simulation capability are keys to the future development of clean and efficient advanced diesel engines.

Researchers at Sandia National Laboratories have developed unique capabilities to image the spatial distributions of UHC and CO in the cylinder of an operating diesel engine. Coupled with conventional emissions analysis, and additional measurements and simulations performed by collaborators at the University of Wisconsin, a comprehensive picture of the in-cylinder sources of these emissions has emerged.

The middle image in Figure 1 shows that at moderately light load (3 bar IMEP), UHC arises mainly from injector fuel dribble (~15%), crevices and fuel films (~20%), and overly lean bulk gas mixture (~60%) found largely in the squish volume but also found in the center of the cylinder near the injector. Likewise, the CO (top image) is dominated by an overly lean mixture which is especially concentrated within the squish volume.

Comparison of the measurements to the results of computer simulations, shown in the bottom image of Figure 1, reveals that in-cylinder UHC distributions are poorly predicted. The simulations predict that UHC is dominated by a rich plume of mixture leaving the bowl. Simulated CO distributions (not shown) are similar. Although this plume is occasionally observed experimentally, it contributes only ~5 percent to the engine-out UHC emissions. Identification of this discrepancy has led to a 50 percent improvement in the prediction of engine-out UHC. Further improvement of the prediction of mixing processes within the bowl is still required and is the focus of ongoing work.

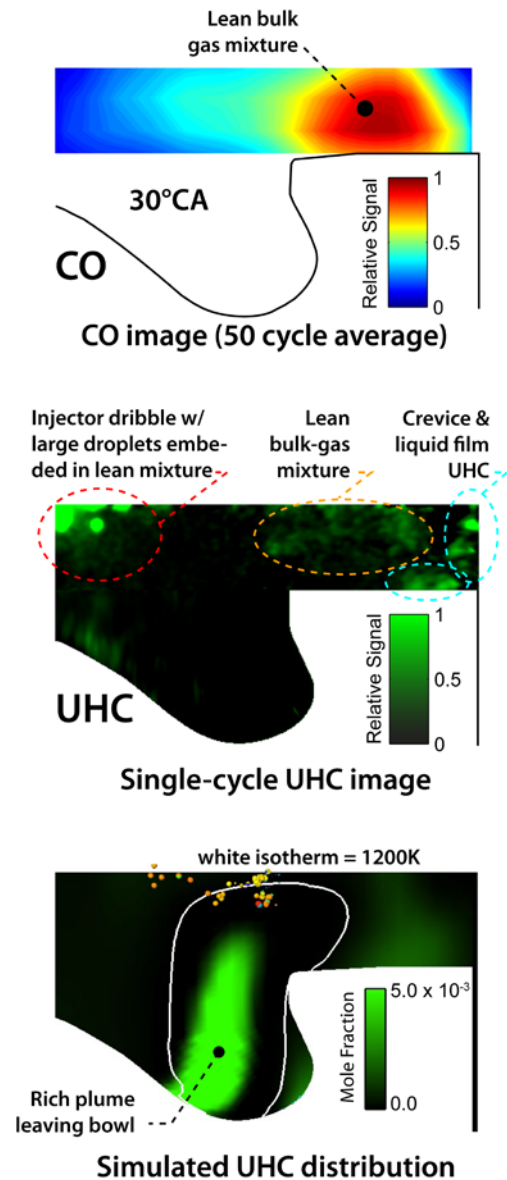


Figure 1. Measured UHC distributions contrasted with current, state-of-the-art computer simulations. 3 bar load and 1500 rpm.

2010 FreedomCAR and Fuel Partnership Highlight

2010 FreedomCAR Engine Milestone for 45% Brake Thermal Efficiency Met

Oak Ridge National Laboratory

A 15 percent improvement in peak brake thermal efficiency (39 percent to 45 percent BTE), was demonstrated on a light-duty diesel engine through improvements in engine technology, operational parameters, lubrication and the recovery of thermal exhaust energy which is normally discarded to the environment. This achievement of 45 percent BTE is the final milestone in the path to demonstrating the 2010 DOE FreedomCAR and Fuel Partnership efficiency objective.

Experiments were conducted on a General Motors 1.9-L diesel engine to evaluate technologies required to achieve this efficiency milestone as shown in Figure 1. The critical technology used was an organic rankine cycle (ORC) to convert heat from the exhaust gases into electrical power that could be used to drive vehicle loads or to drive a hybrid system. A heat exchanger (boiler) on the exhaust system is used to heat the ORC working fluid (refrigerant R245fa) to a superheated vapor which is then expanded through a turbine to generate electrical power. The vapor exiting the turbine is then cooled to a liquid in a condenser and pumped back to the boiler. The ORC generated 3.9 kW of net electrical power. Combined with the 66 kW of power generated by the engine (at an efficiency of 42.5 percent), the combined output yields an overall system BTE of 45 percent.

A detailed model was also developed for the ORC and integrated with an engine model to evaluate the potential of the thermal energy recovery system under road-load conditions as well as across a light-duty drive cycle. The model, using more efficient heat exchangers than those used in the experiments, predicts a potential gain of 2 percent in BTE for an optimized ORC system at 1500 rpm, 2 bar BMEP (brake mean effective pressure) and a potential gain of 3 percent (vs. 2.5 percent in the experiment) at 2250 rpm, 18 bar BMEP. These points were chosen to represent a typical operating point for urban driving and the most efficient operating point for the engine. Ongoing modeling will explore on-board energy recovery and details of integrating the ORC into a vehicle.

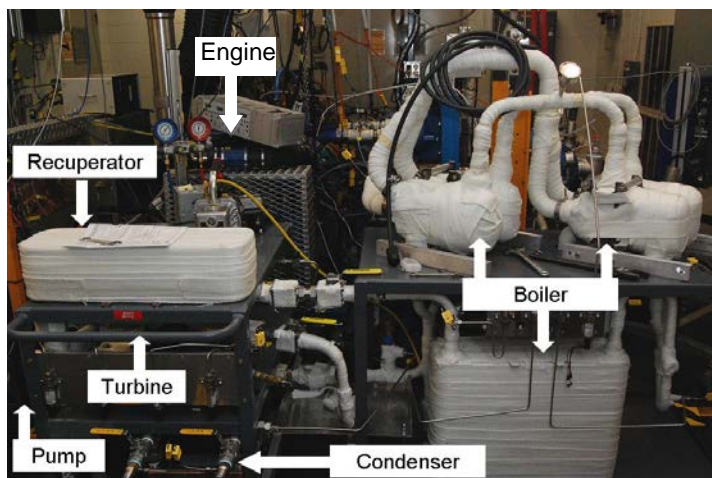


Figure 1. Test cell installation of the ORC system used to achieve the milestone of 45 percent combined BTE.

2010 FreedomCAR and Fuel Partnership Highlight

Novel Power Semiconductor Packaging Reduces Die Area, Volume, Weight and Cost

Delphi Automotive

As governments enact stricter regulations for fuel economy and emissions, vehicle manufacturers are seeking economical and reliable ways to comply. To satisfy projected regulations, automakers around the globe are implementing strategies to increase penetration of electrified powertrains across their fleets. Currently, mass market adoption of hybrid and full electric vehicles is hindered by the cost of electrified powertrain systems. To increase acceptance of these vehicles, the cost of electrification must be reduced. One way to help is with an affordable traction inverter. Delphi has developed a high-power traction inverter using innovative power semiconductor packaging technology to reduce the cost, size and weight of the inverter while increasing overall reliability. The unique power semiconductor package includes an insulated gate bipolar transistor (IGBT) and a diode in an electrically isolated package that is thermally conductive on both sides (Figure 1.)



Figure 1. Delphi's Power Semiconductor Packaging.

The innovative package enables higher current and power density that, when coupled with double-side cooling, reduces cost by requiring less power semiconductor area. Reducing power semiconductor area also reduces inverter volume and weight by making compact inverter building blocks possible (Figure 2). The innovative power device package is capable of withstanding the rigorous demands of the automotive environment and forms the basis for a portfolio of low-cost, high-reliability inverters that will be produced within Delphi's existing engineering and manufacturing processes.



Figure 2. Delphi's Power Semiconductor Package Incorporated into Assembly.

	Leading Module Die Area (mm ²)	Leading Module $\Theta_{J-Coolant}$ °C/W	Delphi Double Sided Cooled Die Area (mm ²)	Delphi Double Sided Cooled $\Theta_{J-Coolant}$ °C/W
IGBT	198 (99X2)	0.46	144	0.15
Diode	110 (55X2)	1.06	72	0.21

Figure 3. Delphi's double-side cooling reduces required silicon die area (and potentially cost, weight and size) by at least 30 percent.

Delphi has worked with several semiconductor companies to identify and incorporate world-class advanced silicon device technology in its innovative package. This newly developed package offers the flexibility to utilize world-class silicon or wide

bandgap devices to help reduce system losses and increase efficiencies (Figure 3). The design also builds in the flexibility for vehicle manufacturers to scale the semiconductor technology and size based on the application and drive profile.

2010 FreedomCAR and Fuel Partnership Highlight

Direct Water-Cooled Power Electronics Packaging Concept Reduces Size and Weight

Oak Ridge National Laboratory, National Renewable Energy Laboratory

Successful use of high-temperature coolants for power electronics requires innovative packaging to meet FreedomCAR and Fuel partnership volume and weight targets. The Direct Water-Cooled Power Electronics Substrate Packaging concept promises to reduce inverter size and weight by eliminating the traditional base plate and heat sink while operating with a high temperature coolant. The ORNL package, shown in Figure 1, is projected to achieve a weight reduction of approximately 17% as compared to the approach used on the Toyota Camry and a power density of 14.1kW/kg.

Flowing coolant directly through the ceramic substrate delivers cooling more efficiently to the semiconductor dies. Experimental results using module prototypes show that a 175°C rated silicon insulated gate bipolar transistor can operate reliably using 105°C Water-Ethylene Glycol (WEG) coolant. This concept enables use of existing silicon devices rather than more costly silicon carbide devices, eliminating the base plate, thermal interface material and cooling plate, as well as integrating the power electronics cooling loop with the engine coolant.

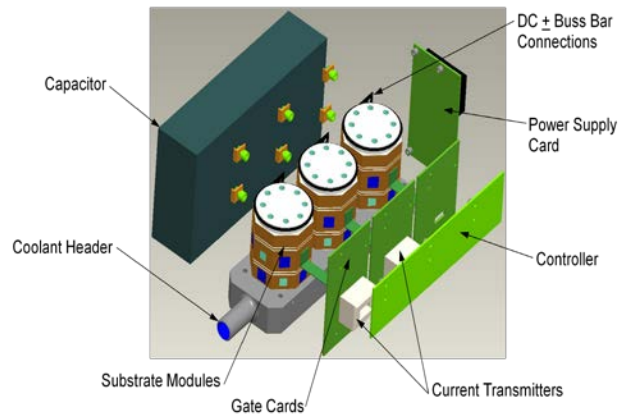
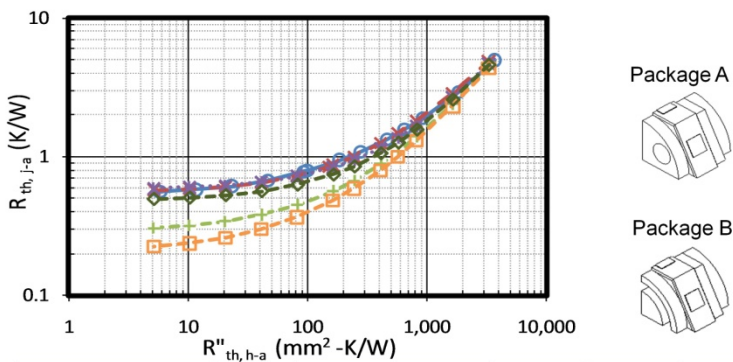


Figure 1. ORNL Direct Water-Cooled Power Electronics Substrate Inverter Package.



Package	A	B1	B2	B3	B4	B5
Legend						
Metallization	Cu	Cu	Cu	Cu	Cu	Cu
Ceramic Insulator	Al ₂ O ₃	AlN	AlN			
TIM R'' _{th} [mm ² -K/W]	NA	NA	2.5	66.7	2.5	66.7
Heat Sink	Al ₂ O ₃	Al ₂ O ₃	Al	Al	Al	Al

Figure 2. NREL thermal systems analysis results.

The project also demonstrated collaboration of the ORNL inverter activity and the NREL thermal control work. The NREL thermal simulation results matched those performed at ORNL within 4%. Using its thermal system analysis tool NREL determined that the ORNL design made maximum use of the thermal aspects of the design concept (see Figure 2).

2010 FreedomCAR and Fuel Partnership Highlight

Segmented Drive Inverter Topology Enables Smaller and Lower Cost DC Bus Capacitor

Oak Ridge National Laboratory

The DC bus capacitor is an essential component for maintaining a stable DC bus voltage for the traction drive system in HEVs, PHEVs and EVs. It must absorb large ripple currents and suppress voltage transients, which occur on the DC bus at every instant of inverter switching and are detrimental to the battery life and reliability of the semiconductor switches in the inverter. The large ripple currents generated in a typical 55 kW HEV inverter necessitate the use of bulky and costly DC bus capacitors of about 1000 μ F, contributing to 15~20 percent of inverter cost and 25~30 percent volume. It would be beneficial in achieving the FreedomCAR and Fuel Partnership targets to minimize this bulky component by significantly reducing the ripple current.

ORNL has developed a segmented drive system that does not add additional power components but can significantly reduce the ripple current and thus the requirement on the bus capacitors through reconfiguring the inverter switches and motor connections in a way that allows the use of simple interleaved switching and optimized PWM schemes. ORNL has devised an optimal pulse width modulation (PWM) control scheme, designed, built and successfully tested a 55 kW prototype (Figure 1). Test results (Figure 2) indicate that compared to the standard inverter, the ripple currents can be reduced with the segmented inverter by 55~75 percent depending on the operating points and the DC bus capacitor volume can be decreased 60 percent.

Performance improvements with the technology applied to the Toyota Camry inverter are estimated as follows: (a) 39 percent increase in specific power, (b) 36 percent increase in power density, and (c) 11 percent decrease in cost. Table 1 lists the performance metrics as well as the DOE inverter targets with those exceeded by the segmented inverter highlighted.

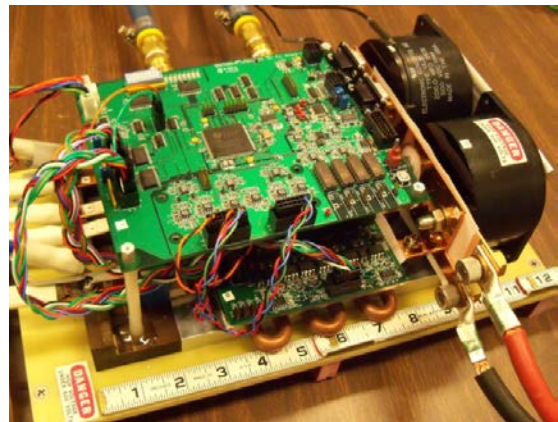


Figure 1. ORNL Segmented Drive Inverter.

		Metrics		
		kW/kg	kW/L	\$/kW
Segmented Inverter		12.9	15.9	11.6
DOE targets	2015	12	12	5
	2020	14.1	13.4	3.3

Table 1. Estimated Performance Metrics.

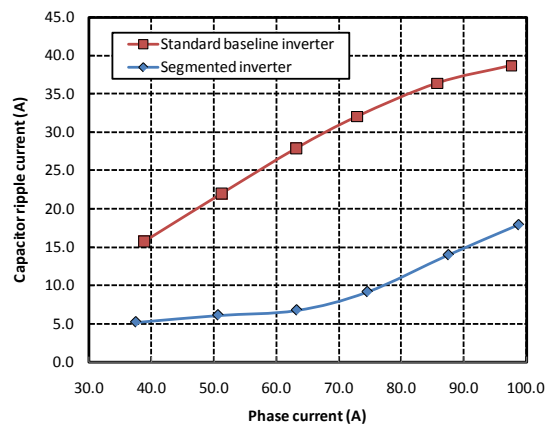


Figure 2. Test Results.

2010 FreedomCAR and Fuel Partnership Highlight

Effect of Enhanced Surfaces on Single and Two-Phase Heat Transfer is Quantified

National Renewable Energy Laboratory, 3M, Wolverine Tube, Inc.

Inverters are key power electronic devices used in hybrid electric vehicles (HEVs) and electric vehicles (EVs) to convert battery power into a form usable for electric drive motors. Aggressive thermal management is essential in increasing power density and specific power of these electronic devices to levels necessary to meet program targets and goals.

In collaboration with 3M and Wolverine Tube, Inc., NREL has demonstrated significantly increased heat transfer rates for single-phase and two-phase flows using surface enhancements. Using HFE-7100 as the coolant, up to a 100% enhancement in heat transfer coefficients (Figure 1a) was demonstrated for submerged single-phase jets impinging on the Wolverine MicroCool™ enhanced surface, and up to a 500% enhancement (Figure 1b) in pool boiling heat transfer coefficients was demonstrated for the 3M microporous coating compared to a plain surface. These results have significant implications for reducing overall thermal resistance of power electronics packages. Figure 1c shows the junction-to-ambient resistance as a function of fluid heat transfer coefficient for the heat transfer technologies investigated.

Immersion boiling implemented in conjunction with enhanced surfaces can decrease the total thermal resistance (junction-to-liquid) of an automotive power module by over 50% compared to a traditional single-phase water-ethylene glycol (WEG) cooling system. This decrease in thermal resistance may have a major impact on program targets of cost, weight, volume and efficiency. It was estimated that the improved thermal performance can decrease insulated gate bipolar transistor die count or area by half, with potential IGBT die cost savings exceeding 50%. Similar savings were found in the 2007 ORNL floating loop inverter project. Additionally, this passive two-phase cooling scheme would eliminate the dedicated power electronics cooling loop which would also provide significant savings in weight, volume and cost, along with permitting increased efficiency through the elimination of parasitic pump losses.

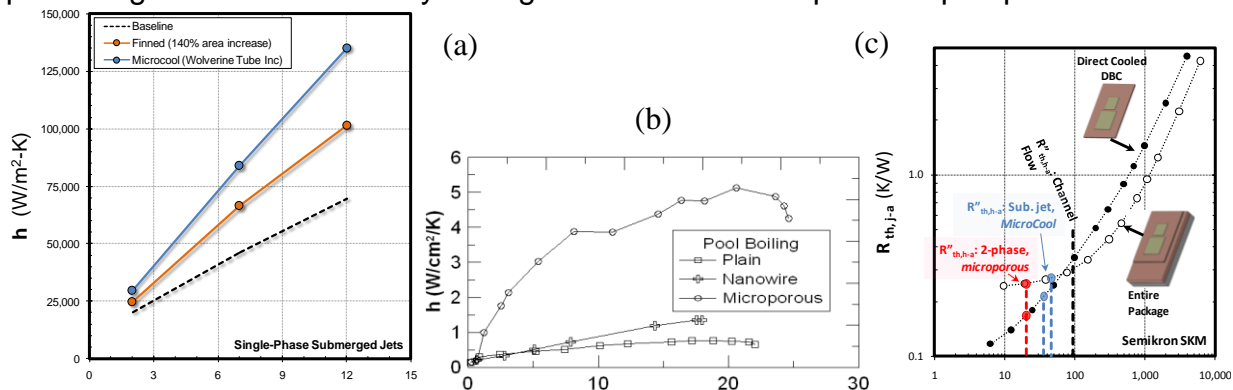


Figure 1: (a) Heat transfer performance of different enhancements as a function of jet velocities in a submerged configuration; (b) Heat transfer coefficient as a function of heat flux in pool boiling; (c) Impact of aggressive cooling technologies on package junction-to-ambient thermal resistance.

2010 FreedomCAR and Fuel Partnership Highlight

Reduced Cost Permanent Magnets for High-Speed Interior Permanent Magnet Motors

GE Global Research

GE Global Research has developed a scalable, high performance interior permanent motor (IPM) solution utilizing novel designs and materials. In particular, high electrical resistivity, high energy-product permanent magnet materials are required to minimize eddy current losses while achieving high power density, which enables smaller motor designs. To meet this need, multiphase composite permanent magnets have been developed that display an effective resistivity 3X that of sintered neodymium iron boron (NdFeB), as shown in Figure 1. The reduction in power loss is achieved by the presence of an insulating phase in the composite impeding the flow of eddy currents in the magnet structure. The insulating phase is introduced into the composite structure during sintering of the NdFeB permanent magnet. This process enables a manufacturing cost reduction of at least 10% relative to externally segmented permanent magnets (as shown in Figure 2) while maintaining an energy product (BH_{MAX}) effectively the same as externally segmented magnets.

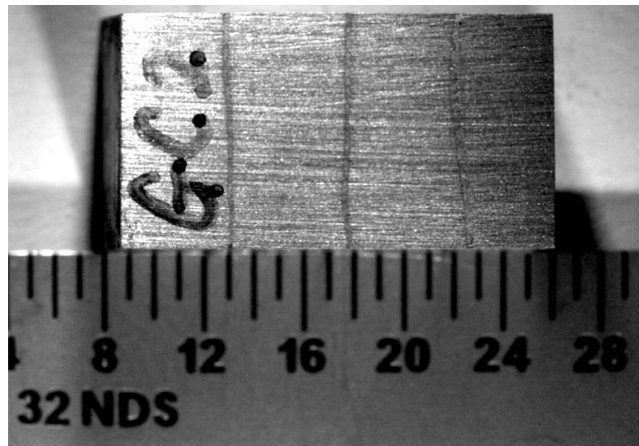


Figure 1. Multiphase internally segmented NdFeB magnet with effective resistivity 3X that of conventional NdFeB sintered magnet.

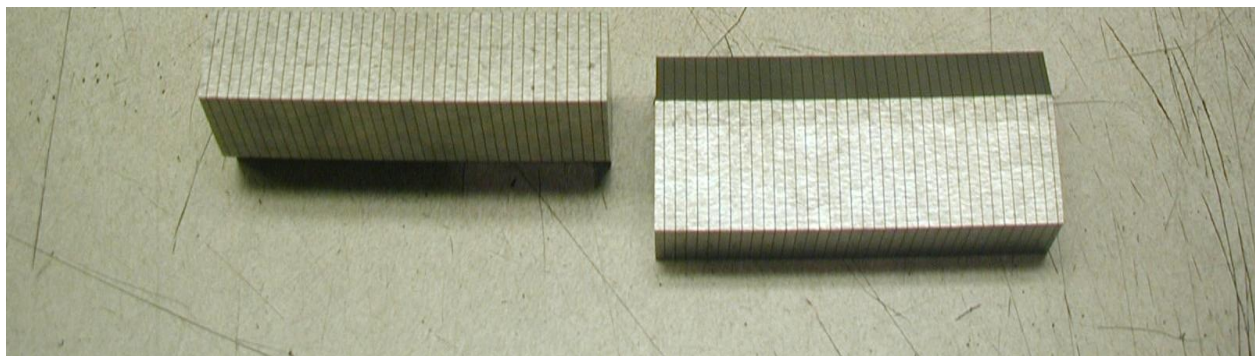


Figure 2. Externally segmented magnets currently used in high-speed motors. Internal segmentation by the GE design will reduce manufacturing cost by at least 10%.

2010 FreedomCAR and Fuel Partnership

Compact Bi-Directional Charger for Plug-in Vehicles

General Motors

Range Extended Electric Vehicles (REEVs) and Battery Electric Vehicles (BEVs) provide transportation and societal benefits, but additional consumer benefits can be created. The ability to provide true sinusoidal 120Vac/220Vac electric power from the vehicle battery system would enable the consumer to run any household tools or appliances. Additionally in the future, with the same power electronics, services may be provided to the electric grid to help enable a smart grid. These additional benefits will be considerations in the purchase of an EREV or BEV.

The current industry approach is to process energy from grid to the vehicle Electrical Storage System (ESS) using the charging system based on a two power converter design, namely: a Front End Boost Converter which provides Power Factor Correction (PFC), low Total Harmonic Distortion (THD) and high voltage bus, usually 400VDC; and an Isolation Buck Converter which provides galvanic isolation between the grid/ESS and regulates charging voltage and current. This approach provides two stages that can be optimized individually but typically are less efficient, not cost effective and limited to unidirectional power flow (no vehicle-to-grid function).

General Motors has developed a Bi-Directional Matrix Converter (BMC) for an on-board charger for a plug-in vehicle, shown in Figure 1, which provides two modes of operation. First mode is the charging mode, in which the BMC processes energy from the grid to charge the vehicle electrical storage system. The second mode is electrical power take off. In this mode the BMC processes energy from the ESS to provide AC output power for consumer usages, e.g. home appliances, construction tools, emergency power, etc. Also the converter could be configured to supply energy from vehicle ESS to the grid and be integrated in a smart grid. It is a building block in smart grid/green energy applications.

The BMC charger is a single stage 3.3 kW bidirectional isolated unity PFC matrix converter architecture that can be scaled up to a 10kW system. This innovative design provides additional functionality and improved power density and lower cost compared to today's on-board chargers. To further develop the functionality, General Motors is collaborating with Electric Power Research Institute (EPRI) for the research and development of vehicle-to-grid and helping to enable the smart grid.

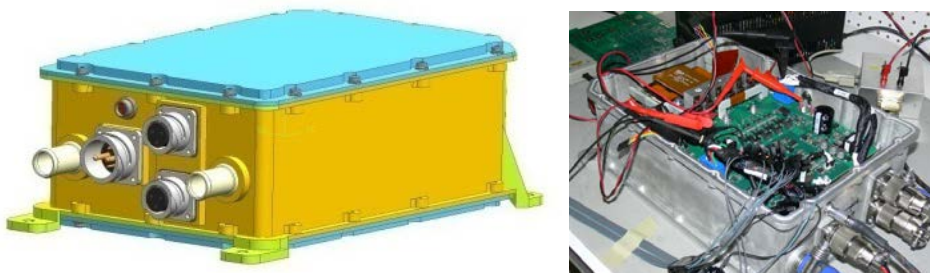


Figure 1. BMC Charger for Plug-in Vehicles.

2010 FreedomCAR and Fuel Partnership Highlight

Novel Battery Thermal Management System Developed

CPI/LG Chem, United States Advanced Battery Consortium

Management of battery temperature is critical to electrified vehicle performance and battery life. CPI/LG Chem and the U.S. Advanced Battery Consortium (USABC) developed a unique thermal management system, which was included as a key element of battery pack system deliverables to USABC. Figure 1 below illustrates the pack system in its as-delivered-to-USABC state.

This advanced thermal management system incorporates a pack-internal refrigerant loop, which is used to cool the air within the battery pack, while that same defined pack-internal air volume is slowly circulated around the cells. The large temperature gradient between the air and the cells facilitates efficient heat transfer without the need for high velocity air circulation.

Vehicle usage situations where high environmental heat loads are present and conditioned cabin air is not readily available were addressed with this design approach. Further, the need for complex coolant manifolds within the pack as well as the need for coolant maintenance and periodic filling operations is also mitigated.

Over the course of this program a number of deliverables were provided to USABC as noted in Figure 2 below, ranging from cell-level deliverables in the earlier portion of the program to the full pack systems provided near the end of the program, which concluded in 2010.



Figure 1. Developed CPI/LG Chem PHEV Lithium-ion battery pack system as delivered to USABC.

	<i>Month 9 (Sep, 08)</i>	<i>Month 22 (October, 09)</i>	<i>Month 27 (March, '10)</i>
INL	20 Cells	40 Cells	3 Packs
SNL	12 Cells (Safety tests)	16 Cells	3 packs (+ 8 modules)
NREL	4 Cells (Thermal)	3 Cells (Thermal)	One of SNL packs makes a detour to NREL prior to SNL tests

Figure 2. Program deliverables leading from early cell samples through 2010 pack system samples.

2010 FreedomCAR and Fuel Partnership Highlight

Nanophosphate Battery Technology for HEVs

A123 Systems, United States Advanced Battery Consortium

A cylindrical cell (32113 format) which meets U.S. Advanced Battery Consortium (USABC) FreedomCAR and Fuel Partnership targets for power, energy and cycle life has been developed by A123 Systems and USABC. Efforts in this HEV program included optimization of materials and design to reduce the Battery Scaling Factor (BSF) and, consequently reduce system cost.

Development of this cell has progressed through several generations during the three years of this program and has concluded with a 22 percent increase in capacity and a 67 percent reduction in BSF. The Gen 1 cylindrical cell has completed the 25 Wh cycle life test through 360k cycles, and projections indicate that >450k cycles will be achieved prior to 20 percent capacity fade. The Gen 2 cells have completed over 280k cycles, and the cycle life projection indicates that the FreedomCAR target can be met at 300k cycles, prior to 20 percent capacity fade. Available energy is well above target, at 300k cycles for Gen 1, and 260k cycles for Gen 2.

Standard USABC abuse test protocols were completed for Gen 1 and Gen 2 32113 cells, and resulted in acceptable European Council for Automotive R&D (EUCAR) ratings of 4 or less. Gen 2 cells were tested and resulted in better EUCAR ratings of 3 or lower.

This HEV development program formally ended in 2010, and remaining activities are focused on modification of an electrochemical thermal model to provide insight into optimal current collector and tab dimensions and locations for future product improvements.



Figure 1. A123 10-cell Module Design.

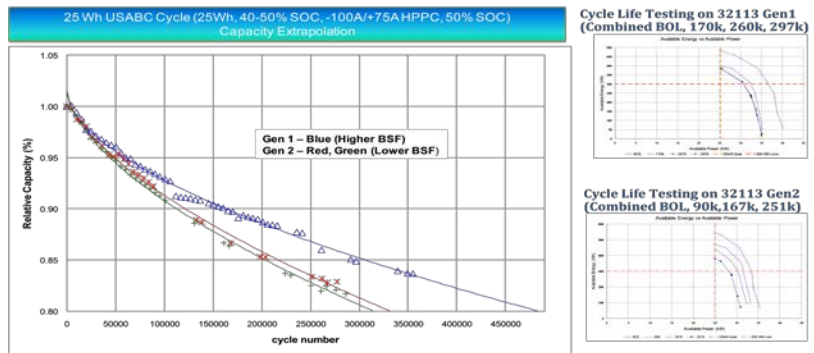


Figure 2. 25 Wh cycle life results for A123 System 32113 HEV cell demonstrates capability to meet 300K target.

2010 FreedomCAR and Fuel Partnership Highlight

Advanced PHEV Cathode Material Developed

3M, United States Advanced Battery Consortium

An advanced cathode material made from $\text{Li}[\text{Ni}_x\text{Mn}_y\text{Co}_{1-x-y}]\text{O}_2$ with $x \neq 1/3$ (advanced Nickel Manganese Cobalt or NMC) has been developed by 3M and USABC that provides 5~10 percent higher capacity (mAh/g) and ~15 percent lower raw material cost compared to the baseline NMC $x=y=1/3$ for PHEV applications, while maintaining comparable or higher thermal stability and cycle life performance

The raw materials costs associated with a kilogram of various cathode active materials based on high volume metals costs from 2009 are shown below in Figure 1. The baseline NMC has become a popular material in both electronics and larger format applications like automotive batteries because of its beneficial abuse tolerance and energy density as

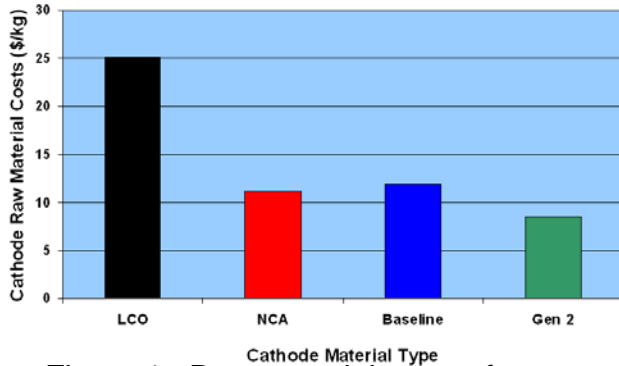


Figure 1. Raw materials costs for cathode materials based on 2009 high volume metals costs

compared to LCO (Lithium Cobalt Oxide) and NCA (Nickel Cobalt Aluminum). The Gen 2 material is intended to reduce cost per kWh while maintaining or improving upon all of the benefits associated with the baseline NMC material. This was accomplished by a reduction in raw materials costs per kg and an increase in Ah capacity per kg.

Figure 2 below depicts specific capacity in mAh/g vs. specific current in C-rate, with data collected at both 30°C and -30°C. The graphs show that the rate capability of both materials are similar but the Gen 2 material

offers increased capacity as compared to the baseline material, which further increases the advantage of the Gen 2 material in terms of decreased \$/kWh.

Figure 3 shows that both cells containing NMC, either baseline or Gen 2, performed almost identically in terms of hot block and thermal ramp abuse response, indicating that the Gen 2 material can offer similar abuse tolerance with decreased cost per kWh.

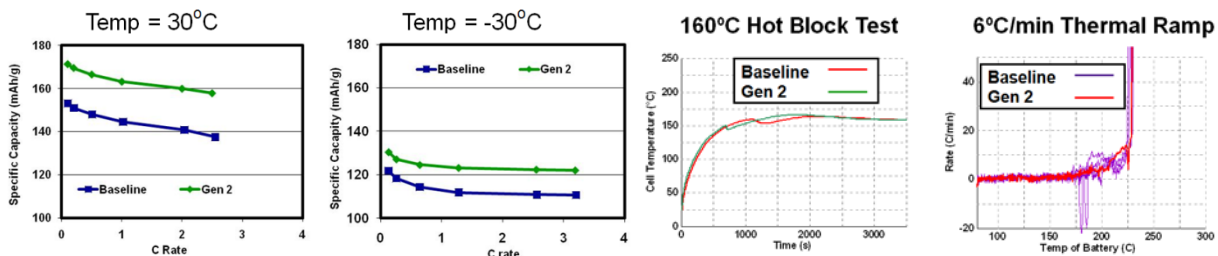


Figure 2. Specific capacity vs. specific current (as C-rate) for the Gen 2 material vs. the baseline material for both 30°C and -30°C.

Figure 3. Results of the Hot Block and Thermal Ramp tests comparing abuse response of cells using baseline and Gen 2 materials.

2010 FreedomCAR and Fuel Partnership Highlight

Design, Build and Testing of NMC-Prismatic Format Cell and System

Johnson Controls - SAFT, United States Advanced Battery Consortium

A central goal of this program was to deliver battery systems/designs that combined Saft cell technology with JCI automotive system expertise to meet USABC goals of life, cost and high energy density.

In the second quarter of 2009, a radical program scope-change was implemented, motivated by the need to implement a step-change in energy density improvement. The redefined program moved from Saft-developed NCA (Nickel Cobalt Aluminum)-graphite cylindrical cells to new JCS-designed NMC (Nickel Manganese Cobalt)-graphite rigid prismatic cells. This required fundamental development on all technical fronts: electrochemistry, cell mechanical design and system design and initial cell hardware builds to support early baseline performance characterization.

Mechanical design, chemistry optimization and in-house build capability were the focus of 2010. Two Proof-of-Concept builds had previously been executed in collaboration with JCS's Saft partner in Cockeysville, MD. Since then, the Milwaukee Technical Center has aggressively developed equipment and skill-base resources to execute full in-house builds of prismatic cells, associated modules and systems. The latter two are new JCS designs, developed within this USABC program.

These builds, executed entirely in Milwaukee, demonstrate JCS's new prismatic technology manufacturing capability. The 2010 A1-build included hundreds of prismatic cells used for baseline deliverables, characterization, life testing, and module

and system builds for internal evaluation and design verification as shown in Figure 1. Builds included wound and stacked electrodes for direct comparison of the two formats. Cylindrical and prismatic cells using identical NMC electrodes were also fabricated, enabling a unique, valuable comparison of the decoupled impact of form factor on degradation rate.

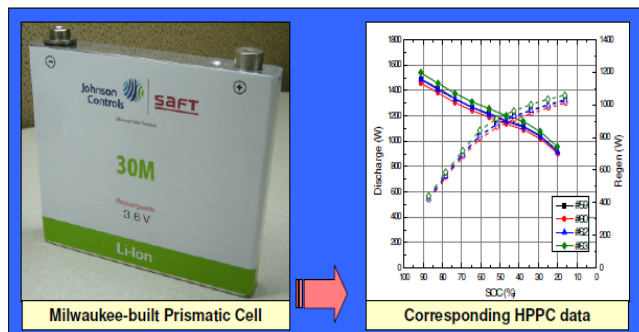


Figure 1.

The promised system-level energy density improvement will be achieved. The final pre-scope-change gap analysis for the 10-mi AER system predicted an end-of-program volume of 84 L. The current end-of-program projection for the production-intent prismatic system with twice the range (20-mi AER) is 65 L. Preliminary abuse tests of prismatic cells have also yielded promising results, showing tangible improvement over phase I counterparts. This demonstrated rapid engineering response in pursuit of what will be a fundamentally new and compelling product for the automotive sector. JCS plans to commercialize the technology developed within this program in 2013.

2010 FreedomCAR and Fuel Partnership Highlight

High Temperature Melt Integrity Separator and Test Suite Developed

Celgard LLC, United States Advanced Battery Consortium

One of the two major tasks identified in the creation of a High Temperature Melt Integrity (HTMI) separator was the need for a standard methodology to rapidly screen materials for their potential HTMI behavior without building a complete battery. This tactic allows for the quick production of prospective materials on a small scale. Then, with little extra time, the samples can be validated against these standard tests outside of the battery system.

Celgard determined that there are three tests which simulate conditions within a hot battery that can focus efforts on important thermal failure modes: hot tip, hot electrical resistance and thermomechanical analysis, as shown in Figure 1, left. With support from USABC, Celgard was able to successfully develop and test a HTMI lithium-ion battery separator (Figure 1, right) that can maintain structural integrity at temperatures where typical shutdown mechanisms can fail.

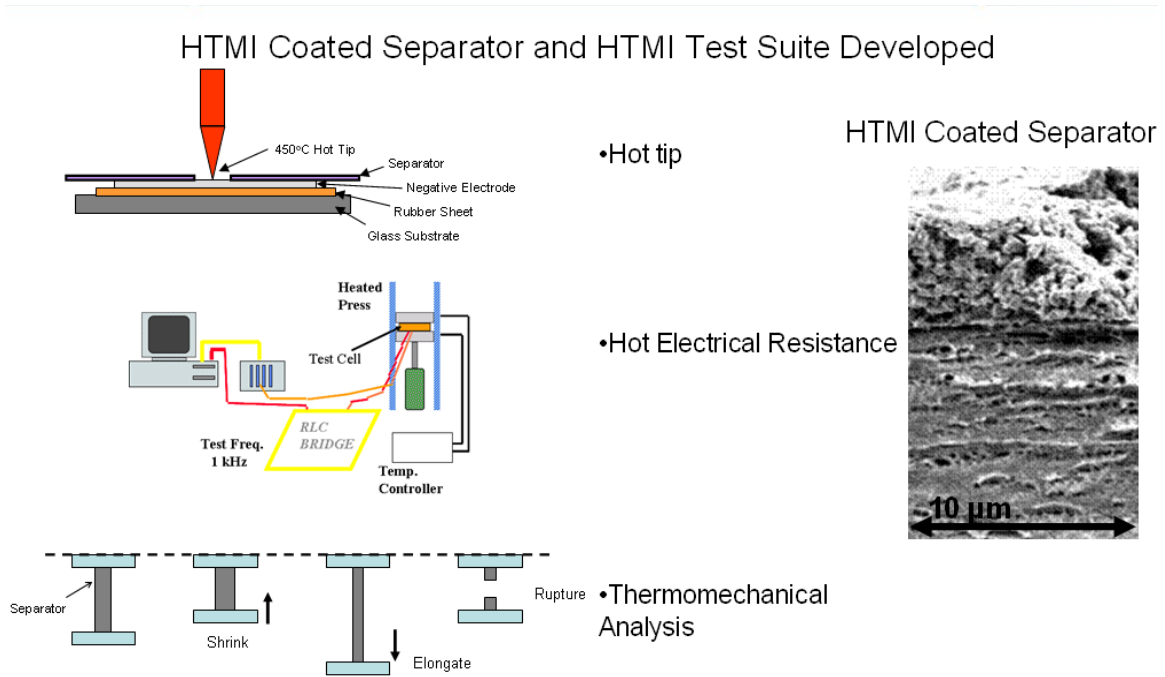


Figure 1. (left) HTMI Separator Test Suite, (right) new Celgard separator.

2010 FreedomCAR and Fuel Partnership Highlight

19 Amp-Hour Prismatic Cell Delivered

A123 Systems, United States Advanced Battery Consortium

A 19 Ah prismatic cell which is projected to meet U.S. Advanced Battery Consortium FreedomCAR and Fuel Partnership power and energy targets for 10 mile and 40 mile PHEV applications has been created by A123 Systems and USABC. The nanophosphate system strength is in power capability, therefore program focus has been on optimizing energy and life through improved materials and design. Consistent improvements in cell performance characteristics have enabled a 23 percent reduction in Battery Scaling Factor (BSF), and significantly reduced system cost, during this program. Safety and abuse testing conducted on the cell and module level have resulted in acceptable EUCAR ratings of ≤ 4 .

The most recent accomplishment has been the development of a Gen 1.5 prismatic cell with modified electrodes and cell design to improve power, energy, cycle life and calendar life. Ten-second peak power for discharge and regen both improved over 100 percent from Gen 1 to Gen 1.5 designs, and energy increased 36 percent. Preliminary testing of both calendar and cycle life are consistent with the anticipated improvement. During 2010, the prototype and process development were completed, design validation testing was completed, process validation initiated and a U.S. production facility opened in Livonia, Michigan.

A 10-mile PHEV module and pack design was developed and initial prototypes are under construction, with delivery to the national labs planned for Q1 2011, prior to the conclusion of this program. Remaining efforts are focused on characterizing Gen 1.5 cell cycle and calendar life performance, and on completing cell, module and pack deliveries to the national laboratories for testing.

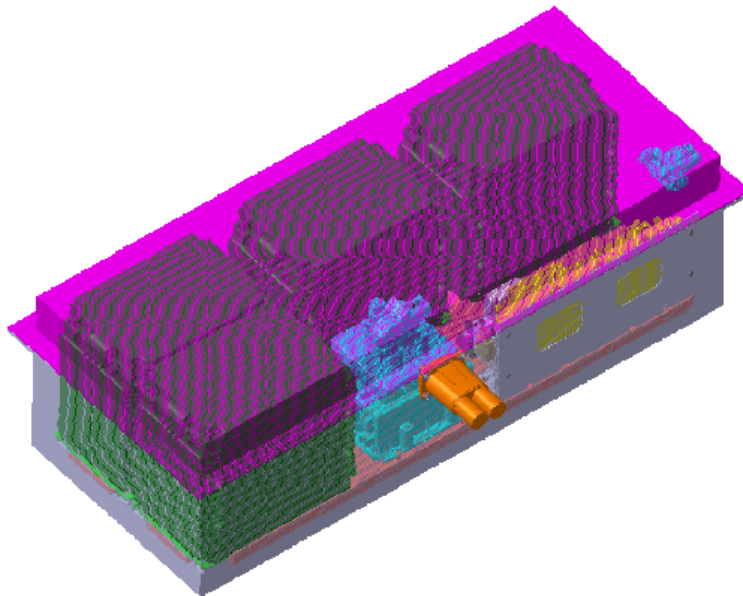


Figure 1. A123 Systems 10-mile PHEV Pack.

2010 FreedomCAR and Fuel Partnership Highlight

Advanced Separators for HEV/PHEVs

ENTEK Membranes LLC, United States Advanced Battery Consortium

Separators are an integral part of the performance, safety and cost of lithium-ion batteries. ENTEK is focused on manufacturing separators with an interconnected three dimensional inorganic network that prevents high temperature shrinkage and internal shorts. They produced a 20-30 microns thick, inorganic-filled separator that shrank less than 3.3 percent after heating the separator in an inert atmosphere for one hour at 200°C, compared with a shrinkage of nearly 100 percent for traditional lithium-ion battery separators under the same conditions.

These separators have been produced without compromising other desirable properties such as high porosity (> 65 percent), excellent wettability and very low resistance derating factor (MacMullin Number < 3). The excellent stability of the separator at high temperature is expected to improve abuse tolerance of lithium-ion cells (e.g. internal short circuit). Electrochemical testing in standard battery (18650 format) cells indicated improved performance with ceramic-filled separators compared to unfilled separators: better capacity retention on both cycling (>1,000 full depth cycles) and long-term stand at high temperature (60°C). Future work is focused on evaluating the abuse tolerance of lithium-ion cells built with such separators.

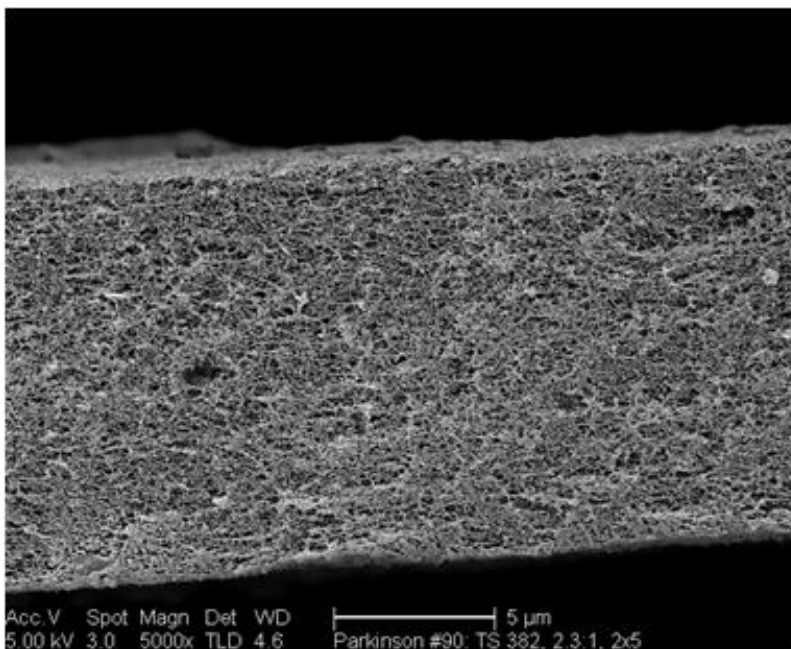


Figure 1. Scanning electron micrograph of an inorganic-filled separator.

2010 FreedomCAR and Fuel Partnership Highlight

Surface-Coated, High-Energy Battery Cathode Demonstrates Improved Cycling and Capacity

Argonne National Laboratory

Cells with $\text{Li}_{3-2x}\text{Ni}_x\text{PO}_4$ -coated electrodes showed improved rate, better thermal stability, and enhanced cyclability. Previously, uncoated 'layered-layered' $x\text{Li}_2\text{MnO}_3 \cdot (1-x)\text{LiMO}_2$ systems in which M is predominantly Mn, Ni and Co, yield high capacities (240-250 mAh/g), and operate at high voltages which would yield much higher energy density cells and thus smaller and less expensive batteries. However, these materials had rate and cycle life limitations.

Coin cells with untreated $0.5\text{Li}_2\text{MnO}_3 \cdot 0.5\text{LiNi}_{0.44}\text{Co}_{0.25}\text{Mn}_{0.31}\text{O}_2$ electrodes and electrodes surface treated with 5 wt% LiNiPO_4 were cycled five times between 2.0 and 4.6 V. Cells were then disassembled and the thermal stability of the charged cathodes was studied by differential scanning calorimetry (DSC). The data, in Figure 1, showed that the amount of heat generated from an uncoated electrode (1881 J/g) was suppressed by the 'Li-Ni- PO_4 ' coating (1205 J/g) which should translate into a more abuse tolerant lithium-ion cell.

The cycling behavior of the untreated and surface-treated electrodes in a full cell is shown in Figure 2. Cycling of untreated electrodes in full-cell configurations results in ~25% capacity fade over 100 cycles. In contrast, Li-Ni- PO_4 -treated electrodes exhibited superior cycling stability, fading of only ~10% over 100 cycles. Future work will focus on surface studies of phosphates and fluorides and will use complementary experimental and theoretical approaches to improve the surface stability, rate capability and cycle life of high capacity Mn-rich oxide electrodes at high voltages.

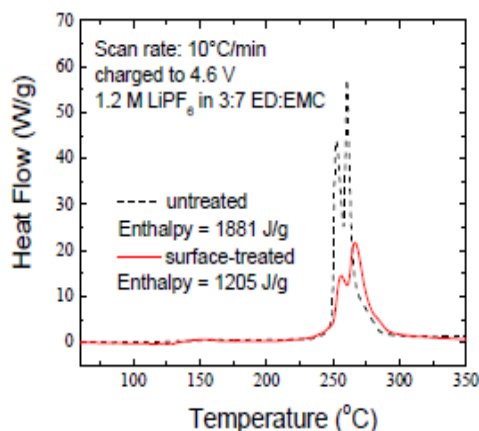


Figure 1. DSC data of untreated and LiNiPO_4 surface treated $0.5\text{Li}_2\text{MnO}_3 \cdot 0.5\text{LiNi}_{0.44}\text{Co}_{0.25}\text{Mn}_{0.31}\text{O}_2$ electrodes after being charged to 4.6 V.

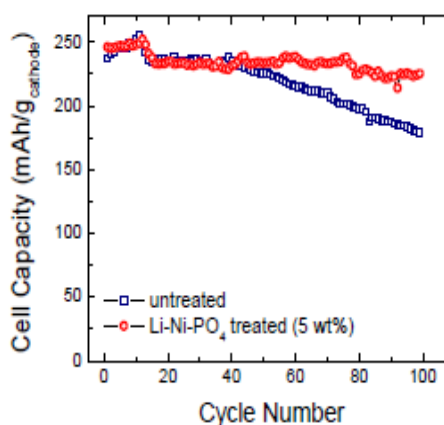


Figure 2. Cycling data of untreated and LiNiPO_4 -treated electrodes in a full cell.

2010 FreedomCAR and Fuel Partnership Highlight

Pre-Lithiating Graphite, Silicon, and Tin Anodes Reduces First Cycle Irreversible-Capacity-Loss

Lawrence Berkeley National Laboratory

First cycle loss is a significant issue for many high-energy anode materials, including Silicon (Si), Tin (Sn) and intermetallic materials. It reduces the energy density of the cell because one must compensate for it by adding "sacrificial" material to the cell.

Lawrence Berkeley National Laboratory has discovered that lithium-nitride metathesis (e.g., $4\text{Li}_3\text{N} + 7\text{Si} = \text{Li}_{12}\text{Si}_7 + 2\text{N}_2$) is useful in preparing partially-lithiated anode-materials, which help to reduce the first cycle loss. The open circuit voltage of the pre-lithiated anode is much lower than that of the untreated material, substantially reducing the lithium lost during the first charge cycle, as measured by 1st Coulombic efficiency and shown in Figure 1 below. The reactions can be carried out in the presence of carbon black so that subsequent mixing is unnecessary.

In the future, this team will identify binders and solvents that are compatible with partially prelithiated anode materials and establish optimum prelithiation levels for tin, silicon and graphite.

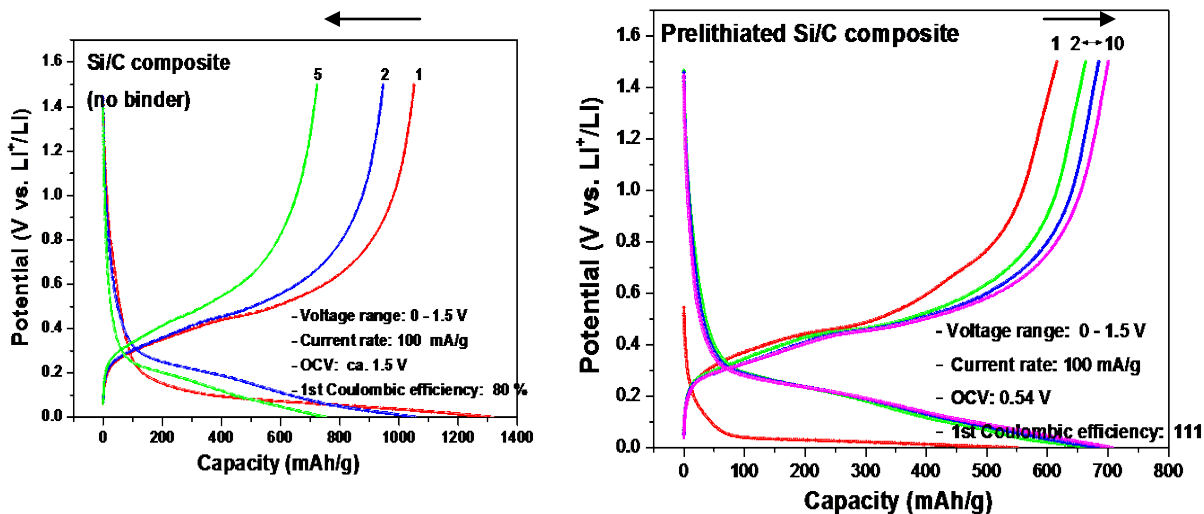


Figure 1. Comparison of untreated and treated Si anodes and resulting 1st cycle coulombic efficiency improvements.

2010 FreedomCAR and Fuel Partnership Highlight

Synthesis of a High-Voltage Cathode Material with Improved Stability

Lawrence Berkeley National Laboratory

Researchers have investigated the performance of the high-voltage cathode material $\text{LiNi}_{1/2}\text{Mn}_{3/4}\text{O}_4$. This new material has been proposed as a good partner for a higher voltage anode (like lithium titanate), resulting in a safe, high-energy battery. The aim of this effort was to compare performance of particles with identical chemistry but different morphologies and eventually to enable the use of this high-voltage cathode. Two types of particles were obtained using hydrothermally synthesized precursors, 1- μm highly nanostructured cuboids (labeled ex- MnCO_3) and 1- μm long by 150-nm wide sticks (labeled ex- MnO_2). The cycling data of these two samples is shown in Figure 1 with the best material in the hydroxide series (BM900C, labeled BM, a 1 μm aggregated octahedra). Despite the nanostructured character of ex- MnO_2 and ex- MnCO_3 , BM900C shows much better performance. These results suggest that nanostructuring $\text{LiNi}_{1/2}\text{Mn}_{3/4}\text{O}_4$ does not provide improved performance, especially since smaller sizes will lead to increased surface area and, therefore, more potential for electrolyte decomposition.

In view of the improved performance of BM900C based $\text{LiNi}_{1/2}\text{Mn}_{3/4}\text{O}_4$, the sample was submitted for advanced electrode testing in FY2011, including the use of novel electrolytes with improved stability at voltages above 4.5 V.

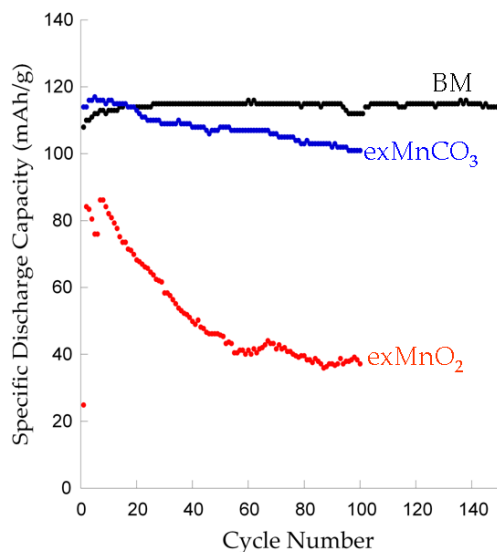


Figure 1. Performance of $\text{LiNi}_{1/2}\text{Mn}_{3/4}\text{O}_4$ samples as electrodes at 1C rate.

2010 FreedomCAR and Fuel Partnership Highlight

Improved Performance of High-Energy Battery Anodes

National Renewable Energy Laboratory

This team of researchers applied “atomic layer deposition” (ALD) coatings to increase the rate capability and cycle life of molybdenum oxide (MoO_3) nanoparticles as lithium anode material, promising significantly enhanced energy density and possibly safety benefits compared to graphitic anodes. In another method, adding 5 percent single wall carbon nanotubes to iron oxide made with an inexpensive hydrothermal process enabled a binder-free negative electrode with durable high-rate cycling as shown in Figure 1. The two techniques have the potential to address the issue of high-volume expansion of some high capacity materials in pursuit of high-energy batteries for electric vehicles. Sample results are shown in the Figure 2 below. Note that the performance of the ALD coated electrodes is significantly better than that of the ALD coated particles and the uncoated electrode.

Future work will involve the continued optimization of full battery cells with the Argonne National Laboratory's high-energy layered/layered cathode for performance testing.

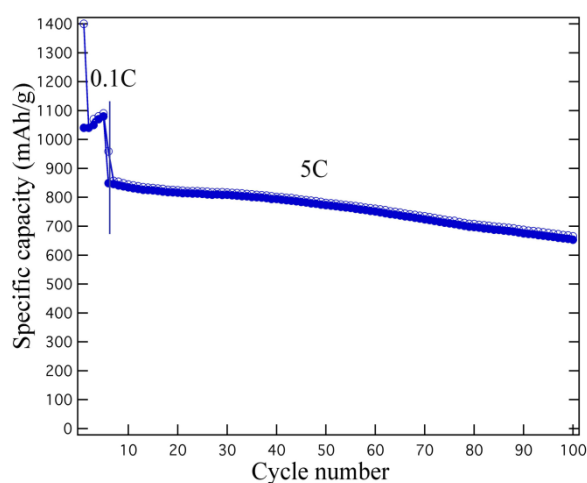


Figure 1. High-rate cycling of Fe_3O_4 anodes with single-walled carbon nanotubes.

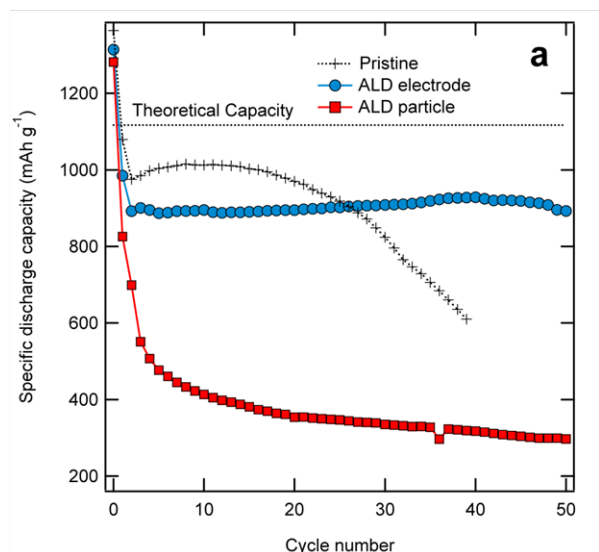


Figure 2. Cycling stability of MoO_3 anodes with and without ALD coating.

2010 FreedomCAR and Fuel Partnership Highlight

New Electrolyte Additive for Lithium-Ion and Lithium-Air Batteries

Brookhaven National Laboratory

Researchers have designed, developed, synthesized, characterized and tested new electrolytes for high voltage lithium-ion and lithium-air batteries. Stable, high voltage electrolytes are critical components needed to expedite the deployment of lithium-ion batteries in traction applications, and lithium-air batteries possess one of the highest energy densities possible. This research, conducted in collaboration with the Chinese Academy of Science in China, has resulted in a new boron-based additive that demonstrates functionalities of both boron-based anion receptors and stable Solid Electrolyte Interphase (SEI) film formation (a stable SEI is critical for long life operation). Anion receptors are sought to enhance the Li transference number, which should enhance rate capability dramatically. One such additive is shown in Figure 1 below. The ability to dissolve LiF, Li₂O₂ and Li₂O is necessary for Li/air cells and demonstrated in Figure 2. A provisional patent application was recently filed at the U.S. Patent and Trademark Office.

In the future, this additive will be further evaluated in collaboration with other laboratory and university research groups.

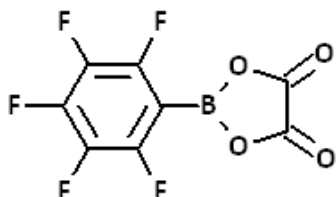


Figure 1. PFPBO, which combines the structure of both TFPFB and LiBOB, is a good anion receptor and a good SEI formation additive.

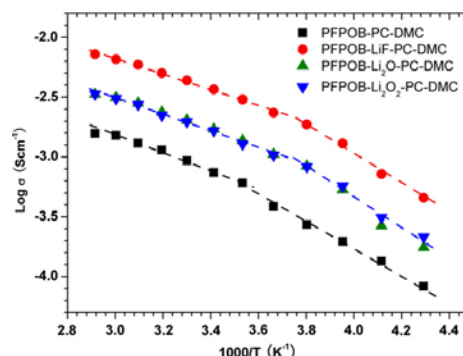


Figure 2. Temperature-dependent conductivities of different electrolytes containing PFPBO additive show good capability to dissolve LiF, Li₂O₂ and Li₂O.

2010 FreedomCAR and Fuel Partnership Highlight

Improved Thermal Performance Using a Coated Cathode Material

Sandia National Laboratories, Argonne National Laboratory

This team evaluated the thermal response of several positive and negative electrode materials in standard battery (18650) cells to correlate the materials-level results to improve safety of real energy storage devices. As part of the DOE Advanced Battery Research (ABR) program, lithium-ion battery materials with improved thermal stability are developed and evaluated in full-scale cells - a process that is important for the adoption of these new technologies. Accelerating rate calorimetry (ARC) is used to characterize the onset of exothermic reactions and determine a heat generation profile up to and even during a high-order thermal runaway reaction.

Coating cathode materials with an inert film (AlF_3 , Al_2O_3 , etc.) were studied in order to improve their overall thermal stability (which includes interfacial reactivity with the electrolyte, mitigation of oxygen reactivity, etc.). Materials-level characterization by differential scanning calorimetry (DSC) shows improved stability in AlF_3 -coated Nickel Manganese Cobalt (NMC) (a standard Li-ion cathode material) powders over uncoated NMC with an increase in the decomposition onset temperature of $\sim 20^\circ\text{C}$. The figure below shows an ARC profile of normalized heating rate (C/min-Ah) as a function of temperature for 18650 battery cells built with uncoated NMC (red trace) and AlF_3 -coated NMC (blue trace) cathodes. These results show a 10 percent reduction in the total heat generation of the AlF_3 -coated NMC cell (related to the ΔT in the ARC profile) and a significant reduction in the kinetic parameter peak-heating rate during runaway compared to the uncoated NMC cell; consistent with DSC observations of the powder materials.

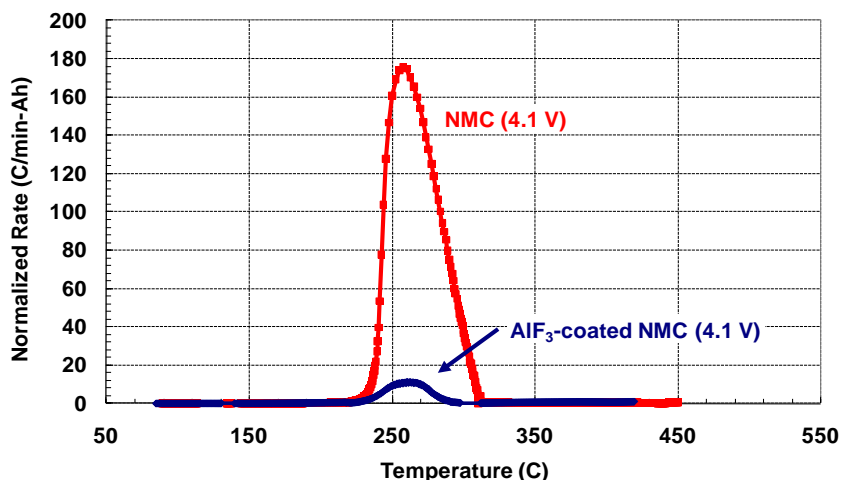


Figure 1. Normalized heating rate (C/min-Ah) as a function of temperature for standard 18650 battery cells with NMC (red trace) and AlF_3 -coated NMC (blue trace) cathodes.

2010 FreedomCAR and Fuel Partnership Highlight

In Situ NMR Observation of the Formation of Metallic Lithium Microstructures

SUNY Stony Brook through Lawrence Berkeley National Laboratory

Lithium (Li) metal anodes would significantly improve volumetric and gravimetric energy density of lithium-ion cells. However, the formation of dendrites following cycling leads to short circuits, particularly at high rates, rendering this class of batteries unacceptable for transportation application. SUNY Stony Brook through Lawrence Berkeley National Laboratory has developed an *in situ* Nuclear Magnetic Resonance (NMR) approach to provide time-resolved, quantitative information about the nature of metallic Li deposited on Li-metal electrodes. The new method relies on the ability of radio frequency (rf) waves – used to excite the Li nuclei – to penetrate bulk Li metal. The so-called “skin-depth” corresponding to about 15 μm can be exploited to differentiate between bulk and dendritic Li, to monitor the growth of micron-sized dendritic/mossy Li, and to determine what Li participates in the electrochemistry.¹ In Figure 1 below, the change in the intensity of the NMR signal can be explained only if the majority of the Li was deposited as μm -sized deposits on charging of a LiCoO_2 -Li cell. Furthermore, this μm -sized Li was consumed during the subsequent discharge. In collaboration with A.S. Best and A.F. Hollenkamp (CSIRO, Australia), this methodology was used to explore dendrite growth in symmetric cells, containing Li electrodes only. In that system, since the mass of Li metal was constant on cycling, it was very simple to measure the fraction of mossy Li, since this followed directly from the increase in the Li-metal signal. The approach was used to explore the effect of different electrolytes and additives on the extent of dendrite growth. In the future, this technique will be used to improve understanding of this class of batteries and further explore correlations between rate, electrolytes and additives and Li dendrite formation.

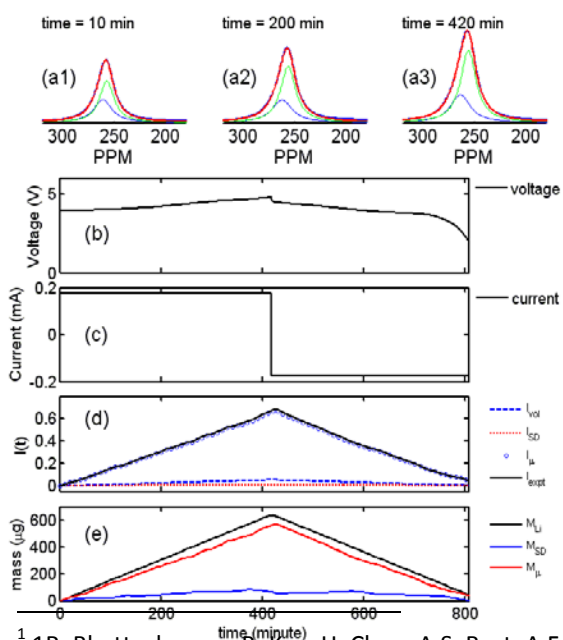


Figure 1 - ^7Li NMR spectra of metallic Li (a 1-3), vs. time in a LiCoO_2 cell, for one charge-discharge cycle. Voltage and the applied current (C/10 rate) are plotted in (b) and (c). The measured Li-metal intensity ($I_{\text{exp}}(t)$) is shown as a solid black line in (d), where the signal ($S(t)$) has been normalized to the signal at $t=0$, to give $I_{\text{exp}}(t) = [S(t)-S(t=0)]/S(t=0)$. Theoretical values of $I(t)$, calculated under various assumptions are shown for comparison: (i) no skin depth issues $I_{\text{vol}}(t)$ (blue dashed line), (ii) all of Li is smoothly deposited $I_{\text{SD}}(t)$ (red dotted line), (iii) all of Li deposited/stripped forms microstructure $I_{\mu}(t)$ (blue circles; eqn 16). Only $I_{\mu}(t)$ provides a good fit to the experimental data, the small deviation being due to a small amount of smoothly deposited Li. $I_{\text{exp}}(t)$, with total mass of Li deposited or stripped $M_{\text{Li}}(t)$, can be used to calculate the mass of deposited Li, $M_{\text{SD}}(t)$ and Li microstructures $M_{\mu}(t)$, taking into account of the skin-depth problem (e).

¹ R. Bhattacharyya, B. Key, H. Chen, A.S. Best, A.F. Hollenkamp, and C.P. Grey, *Nat. Mater.*, 9, 504-510 (2010).

2010 FreedomCAR and Fuel Partnership Highlight

Development of High-Rate Anode Using Graphene Building Blocks

Pacific Northwest National Laboratory

Silicon (Si) anodes are capable of up to 10 times the energy density of graphitic anodes, but quickly lose capacity due to particle isolation caused by its large volume expansion and contraction during cycling. PNNL has developed a novel multiphase, self-assembly approach using graphene as a building block to construct graphene nanocomposites with active metal oxide or Si materials. This approach may be able to hold the active Si directly against the electrically conducting graphene, offering enhanced cycle life.

The surfactants used in this approach link the metal ions or Si to graphene sheets, resulting in self-assembly of metal oxides/Si and graphene into composite nanostructures. The paper-like electrodes were made without using binders or other additives, which further increase their energy density.

TiO₂/graphene anodes prepared by this approach have demonstrated excellent rate capability (~100 mAh/g at 30C rate), Figure 1, and cycling stability, Figure 2. Si/graphene composite anode has demonstrated a capacity of 960 mAh/g in 35 cycles based on the anode weight. This result is reasonable compared to other approaches, but does show the feasibility of this approach.

In the future, this team plans to optimize the composition of Si/graphene to balance high capacity and cycling ability and the size and morphology of Si and graphene in the Si/graphene composite to increase the utilization of Si. Further improvements in cycling stability of Si by optimizing a new binder developed by PNNL and by using new additives are expected.

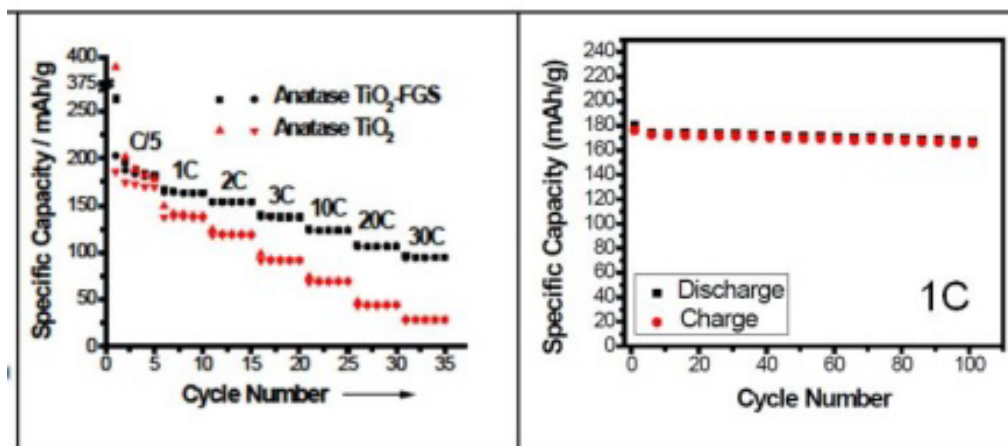


Figure 1. Rate performance of anatase TiO₂ and anatase TiO₂/graphene composite.

Figure 2. Cycling stability of anatase TiO₂ and anatase TiO₂/graphene composite at 1C rate.

2010 FreedomCAR and Fuel Partnership Highlight

Automotive Fuel Cell System Cost Modeling Shows Progress Toward Cost Targets

Directed Technologies Inc., TIAX LLC

Fuel cell (FC) cost analysis is critical for demonstrating the significant progress that has been made through research and development activities and in identifying areas of future research focus to further reduce costs. Recent studies by teams at Directed Technologies Inc. and TIAX have independently estimated the cost of an automotive fuel cell system at high volume production (500,000 units/yr) to be \$51/kW and \$53/kW, respectively, a decrease in cost of ~\$10/kW over the past year and over \$50/kW since 2006. The yearly progress of the FC system cost projections as a function of annual production volume is shown in Figure 1. Furthermore, projections for an estimated 2015 FC system show the potential for significant further cost reductions, although more work is required to meet the 2015 system cost target of \$30/kW.

One team's cost study is based on the automotive fuel cell power plant system model developed at Argonne National Laboratory (ANL), while the other team has proposed their own system with input and feedback from industry and ANL. The two models have recently converged on a realistic fuel cell system design. Both teams derived their own manufacturing process assumptions, obtained price quotations for raw materials and validated their assumptions with extensive industry interaction, peer review and FreedomCAR and Fuel Partnership Fuel Cell Tech Team reviews. The analyses have been refined by replacing less rigorous quotation-based material and component analyses with detailed, bottom-up cost analyses. Analyses have also been used to help evaluate potential for further cost reduction. Balance of plant components, in particular compressor/expanders, and bipolar plate surface treatment technologies have been identified as focus areas for possible future cost reductions.

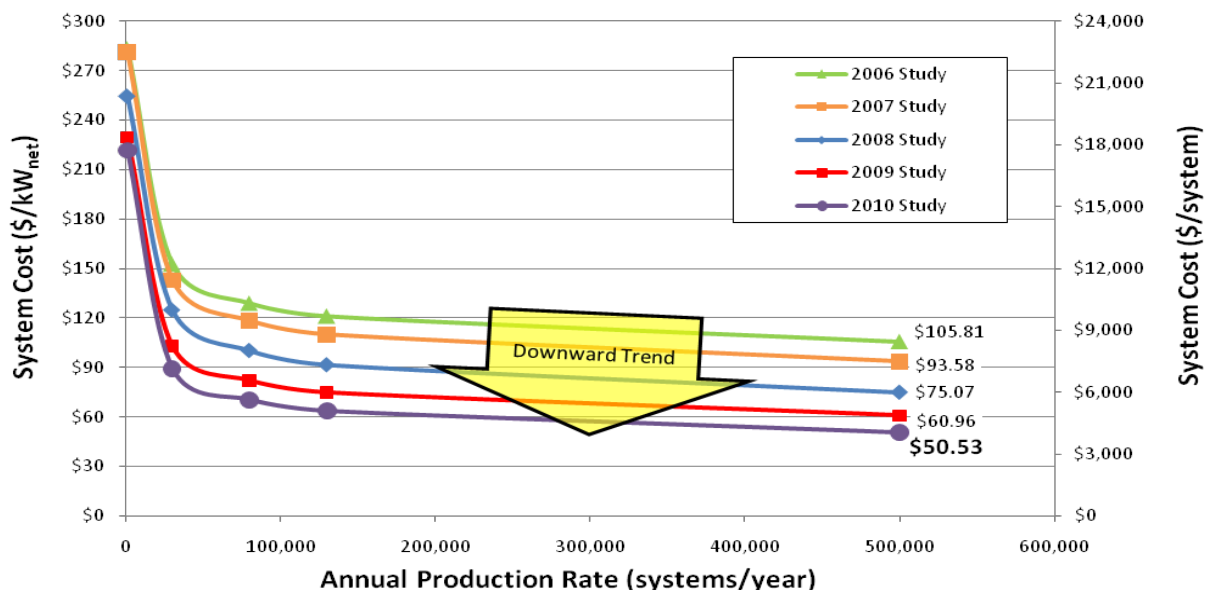


Figure 1. Projections for automotive fuel cell system cost since 2006 for various production volumes (DTI).

2010 FreedomCAR and Fuel Partnership Highlight

New Ultra-Low Platinum Loading Fuel Cell Catalyst has 7X Improved Activity and High Stability

Argonne National Laboratory

Lowering the loading of platinum group metal (PGM) catalyst is one of the primary pathways toward lowering the cost of fuel cell vehicles. One way to lower PGM loading is to create a PGM catalyst with higher activity, so less catalyst is needed and cost is reduced. Researchers found a way to improve catalyst activity by not only fabricating an alloy of platinum and nickel, but also by using a combination of an acid treatment and an annealing step to create a surface on which a "skin" of platinum exists. This skin positioned atop a nickel-rich layer represents "nanosegregation," where the compositions of neighboring atomic layers can be very different, resulting in activity advantages due to compaction of platinum-platinum interatomic distances.

Starting with the alloy nanoparticle, the acid treatment removes nickel from the surface, which leaves a "skeleton" of low coordination platinum in which the platinum atoms are not adjacent to many other platinum atoms. This usually has a negative impact on activity. The annealing that follows serves to smooth the nanoparticle surface, providing for higher platinum coordination and the resulting platinum skin. The activity measurements shown in Figure 1 demonstrate that these steps yield higher activity. The combination of acid leaching and annealing can generate PtNi nanoparticles with seven times higher activity per unit surface area than baseline commercial Pt nanoparticles. Furthermore, the nanosegregated PtNi nanoparticles do not suffer from decay in activity or surface area after 30,000 cycles between 0.5 and 1.1 V. The next steps in the project are further optimization of composition and scale-up to quantities needed for fuel cell testing.

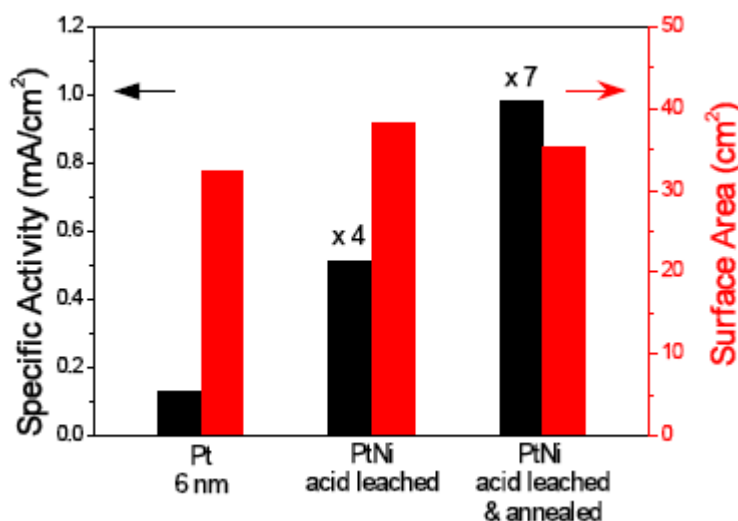


Figure 1. Alloy catalysts that are acid leached and annealed show higher activity per unit surface area than baseline platinum catalyst.

2010 FreedomCAR and Fuel Partnership Highlight

Systems Analysis Shows Significant Cost Savings Possible by Easing Peak-Power Efficiency Target

Argonne National Laboratory

An important task of the U.S. Department of Energy Fuel Cell Technologies Program is to assess the present status and future potential of the technology. This assessment allows for cost estimation and enables benchmarking the technology's potential impact on greenhouse gas reduction, petroleum consumption reduction and market impact, etc. Automotive fuel cell system analysis supports this critical activity by developing the baseline fuel cell system architecture and models used in the program. This system architecture is based on the combined data and feedback from various stakeholders and experts including automotive manufacturers, DOE project contractors, research laboratories and the literature. The end product serves as a publicly available, peer-reviewed consensus of the technology status and is utilized for cost assessments and program analyses. The model is also used to provide input and guidance for many DOE hydrogen fuel cell projects. Examples include: operating conditions for balance of plant projects (humidifiers, compressors, water & thermal management projects), impact of impurities on fuel cell stacks (to assist in evaluation and development of fuel specification requirements), optimization and trade-off studies highlighting areas of potential significant benefit.

For example, a trade-off study indicated that significant stack cost reduction can be realized, approaching the \$20/kW 2015 stack cost target, if the peak-power target system efficiency is relaxed from the DOE target of 50% to 45%. This easing of the efficiency target has little adverse impact on real-world fuel economy (approximately 1-2 miles/kg-H₂).

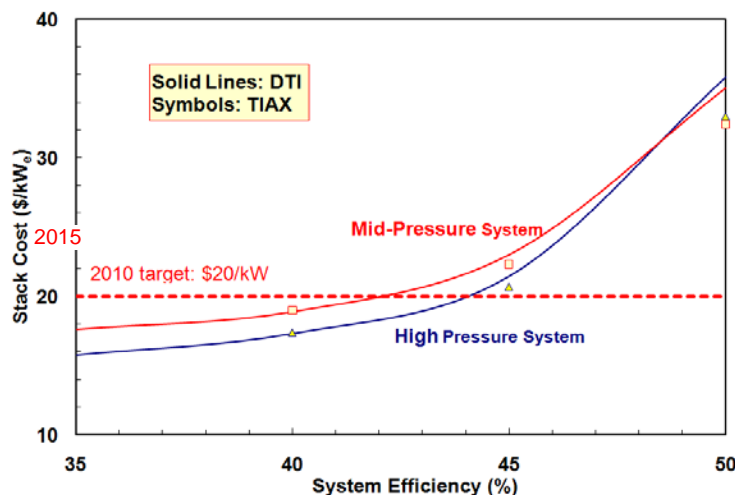


Figure 1. Trade-off analysis of stack cost vs. maximum power fuel cell system efficiency based on the 2010, DOE funded, cost analysis data.

2010 FreedomCAR and Fuel Partnership Highlight

New Composite Membranes Show Improved Durability without Compromising Performance

Vanderbilt University

Using a “forced assembly” approach a Vanderbilt University team fabricated a phase separated fuel cell membrane composed of conductive nanofibers interwoven with a more stable polymer. Consequently, this enabled the decoupling of the mechanical and proton-conducting functions of the fuel cell membrane, as the conductive polymers themselves are known to swell excessively under extended fuel cell operation.

Vanderbilt University researchers start with a low equivalent weight (EW) proton conducting polymer and a stable non-conductive polymer such as polyphenyl sulfone. The two polymers are simultaneously electrospun to form an interconnected mat with each polymer forming a continuous phase. The mat is then heated to melt the conductive polymer while maintaining the non-conductive fiber network, forming a thin, nonporous film. This novel method of simultaneous electrospinning of two distinct polymer phases allowed Vanderbilt to remove a process step where the conductive polymer mat was impregnated with an expensive urethane-based resin. Thus, the new process is both simpler and less expensive. Preliminary work has focused on using Nafion[®] Perfluorosulfonic Acid (PFSA) as the conductive polymer.

Figure 1 shows that the composite membrane matches the fuel cell performance of non-composite Nafion[®] counterparts made with the same polymer. Figure 2 shows that the durability of the composite membrane is more than double that of the non-composite Nafion[®] 212. Next steps include using lower EW PFSA conductive polymers from 3M (see 3M accomplishment) and highly conductive hydrocarbon conductive polymers from Case Western Reserve University (2009 accomplishment) to further improve fuel cell performance.

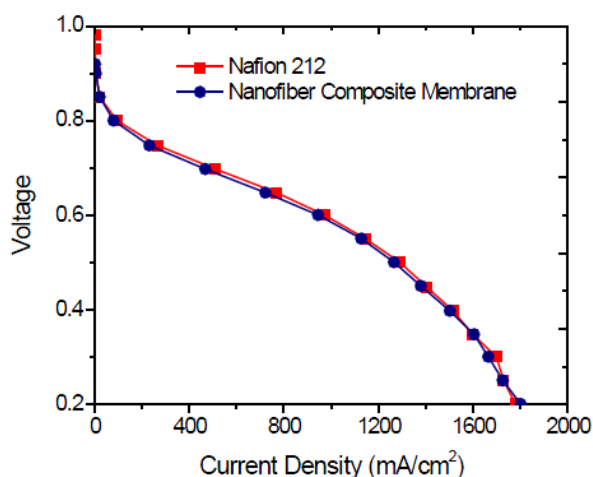


Figure 1. Fuel cell performance of Vanderbilt nanofiber composite membrane compared to Nafion[®] 212. 33

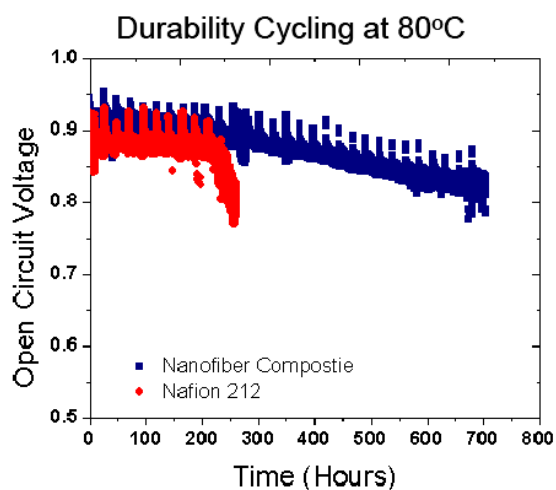


Figure 2. Accelerated durability testing of Vanderbilt nanofiber composite membrane compared to Nafion[®] 212.

2010 FreedomCAR and Fuel Partnership Highlight

Improved Resolution for Imaging Water in Operating Fuel Cells Aids Developers

National Institute for Standards and Technology

Managing flow inside the gas channels of a fuel cell is critical for removing the water that is created during the electrochemical reaction. If the water is not effectively removed, it may accumulate to the point that it blocks the flow of gas to catalyst reaction sites. Conversely, removing too much water inhibits the retention of sufficient moisture in polymer electrolyte membranes to efficiently conduct protons. Fuel cells must also endure temperatures below which water freezes both while in operation and when shut down. Development of effective operating strategies relies on the developers knowing where the water is within a fuel cell stack during operation.

Measuring the through-plane water content in a fuel cell is critical to understanding this complicated heat and mass transport environment. National Institute of Standards and Technology researchers have developed and refined a non-intrusive neutron imaging technique for visualizing and quantifying water inside an operating fuel cell. A limit of neutron imaging is the achievable spatial resolution, which is primarily dominated by the detector. This effect is clearly demonstrated in Figure 1, where the water content in a fuel cell was measured using three different detectors at similar operating conditions. Installation of a new “13 micron” microchannel plate detector allows researchers to directly measure the water content and distribution in the porous media with unprecedented detail and resolution. This state-of-the-art instrument has provided a 20-fold improvement in the spatial resolution over the last 4 years. This improved resolution has enabled discrimination of water in the different material layers within an operating fuel cell. This tool has been valuable for fuel cell research and development into both materials and the stack.

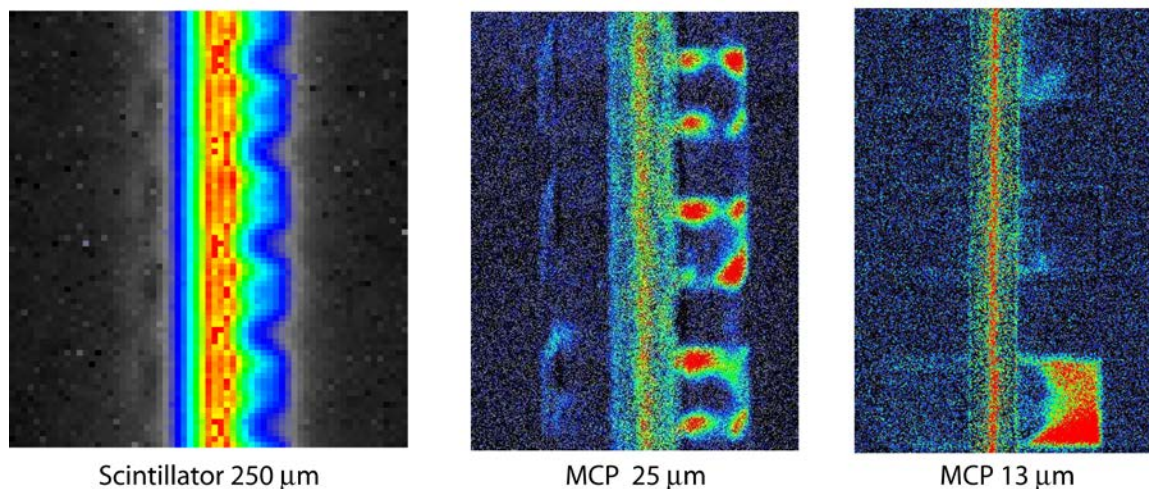


Figure 1. Effect of spatial resolution on measuring the through-plane water content in an operating, PEM, fuel cell.

2010 FreedomCAR and Fuel Partnership Highlight

Improved Performance and Stability of Non-Precious Metal Cathode Catalysts

Los Alamos National Laboratory

A Los Alamos National Laboratory team has synthesized new non-precious metal catalysts with greater than 60-fold improvement in activity for oxygen reduction over the last two years. Additionally, significant strides have been made in demonstrating the stability of these non-precious metal catalysts. This accomplishment represents a significant advancement toward removing precious metals from proton exchange membrane fuel cells and, therefore, lowering cost.

The most active materials are Cyanamide-Fe-C catalysts. A 9-fold activity improvement was gained over the past year by selecting a better carbon support and incorporating a sulfur-containing precursor. While these materials have not yet been tested for durability, significant progress has been gained on stabilizing another family of materials, polyaniline (PANI)-Fe-C catalysts. The results of voltage cycling between 0.6 and 1.0V in a fuel cell on these materials are shown in Figure 1. The high power performance actually increases with voltage cycling, while there are slight performance losses in the lower power region (inset).

There are still significant remaining challenges to be addressed to enable use of these non-precious metal catalysts in automotive fuel cell systems. An additional 5-fold improvement in performance is required to meet Partnership targets. Also, the stability of the most active materials is still unproven. Finally, electrode optimization for H₂/Air performance to minimize mass transport losses is required.

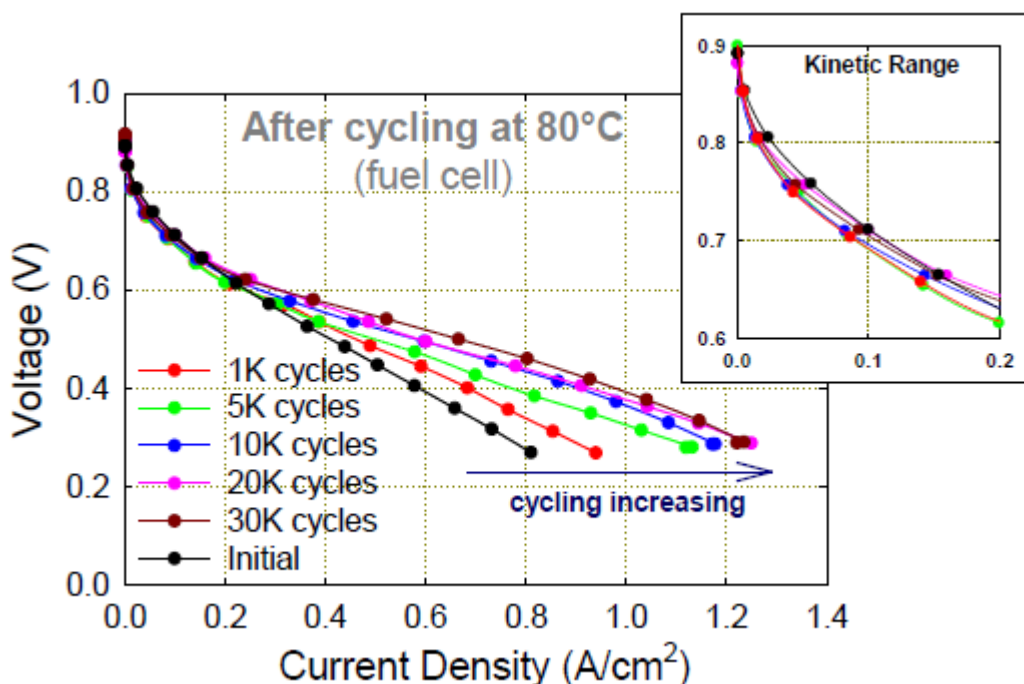


Figure 1. Performance of LANL non-precious metal (PANI-Fe-C) catalysts after voltage cycling between 0.6 and 1.0V in a H₂/O₂ cell.

2010 FreedomCAR and Fuel Partnership Highlight

Hollow Platinum Nanoparticles Developed for Stable, High-Activity Fuel Cell Catalysts

Brookhaven National Laboratory

One of the primary routes toward decreasing the cost of fuel cell vehicle technology is reducing the amount of platinum group metal (PGM) catalyst used. By increasing the amount of activity per unit mass of PGM (also known as "mass activity"), the mass of PGM on the vehicle can be reduced. Conventionally, platinum catalyst exists in the catalyst layers of a fuel cell in the form of nanoparticles. Researchers have created nanoparticles that use less platinum by removing platinum from the center of the nanoparticles. Transmission Electron Microscope images of these hollow spheres are shown in Figure 1. The particle diameters range from 4-8 nm, but the platinum itself occupies only a 1-2 nm thick shell.

The mass activity of the hollow spheres, as fabricated, has been shown to be 1.1 A/mg_{Pt}, which exceeds both literature baselines (0.1-0.16 A/mg_{Pt}) and the FreedomCAR and Fuel Partnership target (0.44 A/mg_{Pt}).

This measurement was performed *ex-situ* in a standard electrochemical cell (not an operating fuel cell). Since degradation of nanoparticles has usually been shown with voltage cycling between 0.65 and 1.05 V, the platinum hollow spheres were subjected to 6000 cycles between these potentials *ex-situ*. After 6000 cycles, the mass activity was 0.58 A/mg_{Pt} or 67 percent of the starting value, and the same as the activity shown after 3000 cycles (see Figure 2). The mass activity at which the hollow spheres stabilized under cycling is still higher than FreedomCAR and Fuel Partnership targets. The next steps for this project are to scale up platinum hollow sphere production to larger batches and to integrate the catalyst into an operating fuel cell.

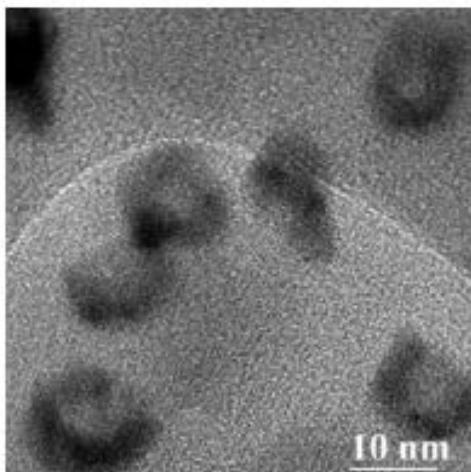


Figure 1. Hollow Pt nanoparticles approximately 4-8 nm in diameter containing 1-2 nm thick Pt shells.

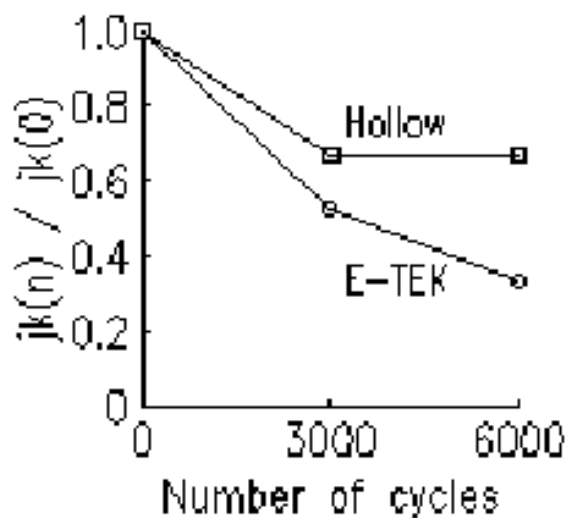


Figure 2. Normalized mass activity of BNL hollow nanoparticles and commercial (E-TEK) catalysts as function of voltage cycles between 0.65 and 1.05 V.

2010 FreedomCAR and Fuel Partnership Highlight

Fuel Cells Can Recover from Ammonia Contamination in Both Fuel and Air Streams

Los Alamos National Laboratory

This Los Alamos National Laboratory research team studied the effects of impurities in both the hydrogen fuel stream and the air stream on the performance and durability of fuel cells. This work is critical to help set the fuel quality specifications, determine what on-board air purification systems are required, and to develop *in-situ* recovery methods for contaminant removal. LANL has focused on the effects of hydrogen sulfide (H₂S), ammonia (NH₃) and hydrocarbons in the fuel stream and atmospheric SO_x and NO_x in the air stream.

NH₃ is particularly relevant because it can exist as a contaminant in both the hydrogen fuel and air streams that enter the fuel cell. This year, significant progress was made in understanding the primary poisoning mechanisms of ammonia contamination, as well as in developing strategies to recover from ammonia poisoning. The team has shown that no matter whether NH₃ is introduced from the fuel or air stream, the effects are the same. In a fuel cell environment, NH₃ is ionized to become NH₄⁺. The water soluble NH₄⁺ cation can easily move across the fuel cell to the regions where it is damaging: namely, the membrane, where it binds to the membrane's functional sites needed for proton conduction, and the cathode, where it slows the oxygen reduction reaction. Fuel cell performance decreases steadily upon introduction of 48 parts per million of NH₃ to the air stream, as shown in Figure 1. Figure 1 also shows that the performance recovers slowly after the NH₃ introduction is stopped. Both experiments and models indicate that the NH₃ is slowly removed from the cell as it is dissolved in water produced by the fuel cell reactions. Next steps include validation of a cation degradation model and developing strategies for faster recovery from ammonia poisoning.

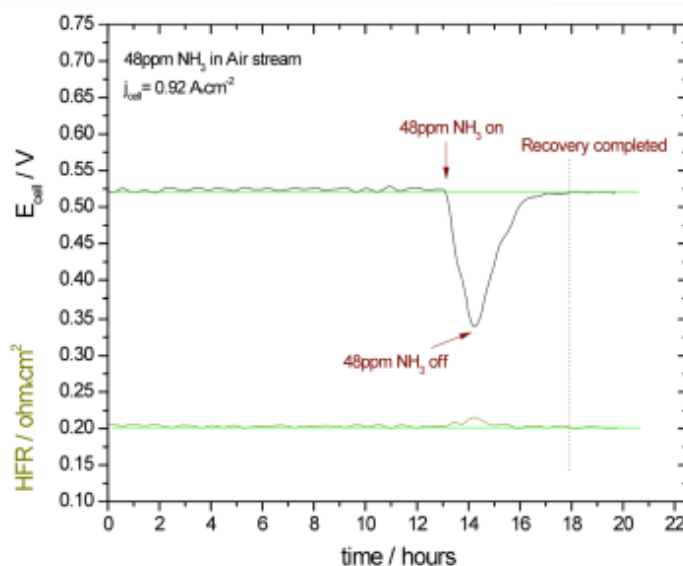


Figure 1. Fuel cell performance and recovery during ammonia poisoning from air stream.

2010 FreedomCAR and Fuel Partnership Highlight

Better Water Management Improves Transient Performance of Low Platinum-Loading Catalysts

3M

New electrocatalysts developed by 3M meet or exceed most of the DOE 2015 catalyst performance and durability targets in 50 cm² cell tests. Furthermore, the nano-structured, thin-film (NSTF) catalyst-based membrane electrode assemblies (MEA's) in original equipment manufacturer (OEM) short stacks (<20 cells) have demonstrated specific power densities greater than 0.2 gPt/kW, successful 10°C cold and -20°C freeze-start and lifetimes of 2,000 hours under various automotive system-relevant operating cycles. Significant improvements in oxygen reduction reaction activity with new alloys and processing methods were demonstrated, and further improvements are anticipated. They also demonstrated 6,500 hours of load cycling with MEA's made with 0.05/0.10 mg/cm² platinum group metal (PGM) loading.

The biggest remaining challenge for NSTF MEA's is performance at wet conditions such as cold start and transients. The research team has made significant advances in understanding and improving water management issues associated with these ultra-thin NSTF electrodes. They demonstrated a new paradigm for water management of these thin electrode layers by using sub-atmospheric anode pressure and high liquid water permeability anode gas diffusion layers (GDL's) that enables: a) steady-state current density up to 2.0 A/cm² at 30 to 35°C with NSTF MEAs, and b) 5 second 0 -1 A/cm² load transients at 50°C and 140 percent relative humidity (RH). A schematic of this new paradigm is depicted in Figure 1. 3M also demonstrated a hybrid MEA with a gradient cathode catalyst construction that enables steady-state 1 A/cm² operation at 30°C, successful load transient 0 -1 A/cm² step at 40°C, 140 percent RH, and comparable 80°C performance to standard NSTF MEA's.

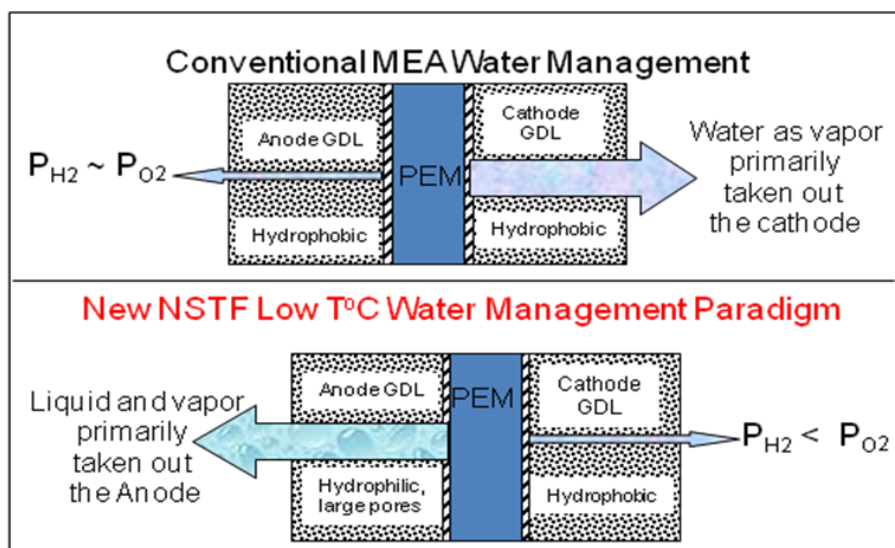


Figure 1. New Water Management Paradigm

2010 FreedomCAR and Fuel Partnership Highlight

Simultaneous Water Visualization and Resistance Measurements Can Be Used to Develop Fuel Cell Shut-Down Strategy

Rochester Institute of Technology

For fuel cell vehicle technology to be commercialized, vehicles will require the same capability to start in cold temperatures as can be expected from conventional internal combustion engine vehicles. Because fuel cell vehicles produce water, water must be purged on shutdown of the vehicle in order to prepare the fuel cell stack for startup during freezing conditions. Without purging, ice blockages in the flow channels and Gas Diffusion Layers (GDL) will prevent the entrance of gases to the stack. However, since the ion-conducting materials (i.e. ionomers) in the fuel cell membranes and electrode layers need to remain humidified to perform adequately, the purge cannot completely dry out the cell. The Rochester Institute of Technology team, in collaboration with General Motors, has used both *in-situ* neutron imaging (at NIST - see page 34 for related accomplishment) and high-frequency resistance (HFR) measurements simultaneously to show how much purging can be done before ionomers begin to dry. As shown in Figure 1, the purge does remove water, although the removal of water does not immediately increase HFR. Only after some duration – after the GDL is essentially dry - does the ionomer water begin to be removed and the HFR increase. Therefore, using data from this experiment, an on-board vehicle purge strategy can be designed. The team also demonstrated the capability to show which vehicle operating conditions create the wettest conditions following operation, so the purge strategy can be designed to be robust for all conditions.

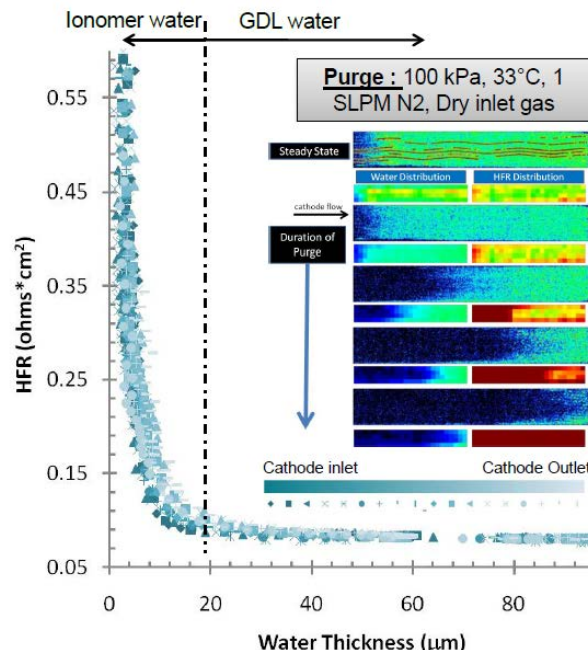


Figure 1. Neutron imaging shows that longer purge duration results in drying of a cell (green in inset). Moving from right to left in the main figure, water content ("thickness") decreases, but high-frequency resistance (HFR) remains level until water begins to be removed from proton-conducting phases (i.e. ionomers) that should remain wet.

2010 FreedomCAR and Fuel Partnership Highlight

New Fuel Cell Membranes Show Promise to Meet High-Temperature Operation Targets

3M

This 3M group is developing new polymers as well as new stabilizing and conductivity enhancing components to provide a fuel cell membrane that meets all FreedomCAR and Fuel Partnership membrane technical targets, including high temperature performance and durability. They focused on gaining a better fundamental understanding of structure property relationships relevant to conductivity and durability to aid in this development. One of the new materials meets most of the membrane targets. The new perfluoroimide acid (PFIA) polymer electrolyte membrane meets the Partnership's 30°C and 80°C (low temperature) area specific resistance targets and nearly meets the high temperature (120°C) target. This membrane also meets Partnership's membrane chemical stability targets.

Researchers synthesized new polymers with two and three acid-sites per sidechain that show enhanced conductivity and lower swelling in boiling water compared to conventional one-site perfluorosulfonic acid (PFSA) polymers with the same equivalent weight (EW). The multi-acid sidechains allow membranes to retain higher crystallinity by utilizing the same polymer backbone as a higher EW PFSA. One of these, the 625 EW PFIA, allows 3M to make membranes with conductivity exceeding 100 mS/cm, at 120°C and 40 percent RH with lower swelling than that for a 700 EW PFSA membrane. 3M has also developed a 575 EW PFIA polymer that shows even higher conductivity. Figure 1 shows the conductivity of these PFIA membranes compared to PFSA membranes at 120°C. The 575 EW membrane has >150 mS/cm conductivity at 40 percent RH and >80 mS/cm at 25% RH. Figure 2 shows conductivity of these membranes at 80°C. The 575 EW membrane meets the 100 mS/cm conductivity target at 40 percent RH.

The group also developed new additives and an optimized fabrication process to improve durability. Use of mechanical stabilization concepts enabled the PFIA membranes to meet DOE membrane mechanical durability targets. Resistance measurements on these mechanically stabilized membranes will be completed in 2011.

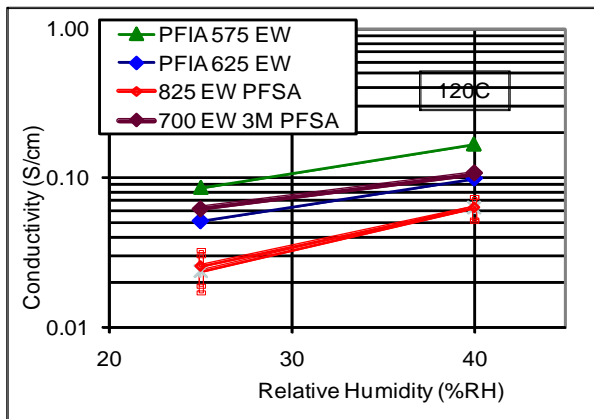


Figure 1. Conductivity vs. RH at 120°C

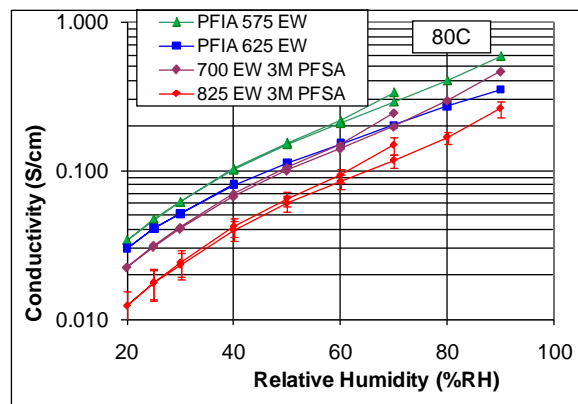


Figure 2. Conductivity vs. RH at 80°C

2010 FreedomCAR and Fuel Partnership Highlight

Advanced High-Strength Steel Matches Aluminum Performance and Light Weight with Reduced Cost

United States Automotive Materials Partnership-A/SP 340

The American Iron and Steel Institute (AISI) and the Auto-Steel Partnership (A/SP) have demonstrated the ability to reduce body-in-white system weight by 25 percent using Advanced High-Strength Steel (AHSS) when compared to traditional steel designs. The project objective was to determine if similar success could be achieved using AHSS for suspension and chassis systems, where the reduction in unsprung mass benefits both fuel efficiency and vehicle handling characteristics. The approach of this project was to develop steel-intensive front lower control arm (FLCA) designs that meet the mass and performance of the baseline forged aluminum design at 30 percent less cost, and significant weight reduction when compared to traditional steel and cast iron designs.

The baseline FLCA design was a Chevrolet Malibu/Buick Lacrosse aluminum forged component design (Figure 1). The control arm is a challenging baseline component as it is one of the lightest weight designs as determined from a benchmarking study. An iterative optimization strategy was used to minimize the mass of each design while meeting the specified structural requirements. The optimization process was successful and resulted in two stamped steel control arm designs, referred to as the clamshell design and I-beam design, and the forged control arm design.

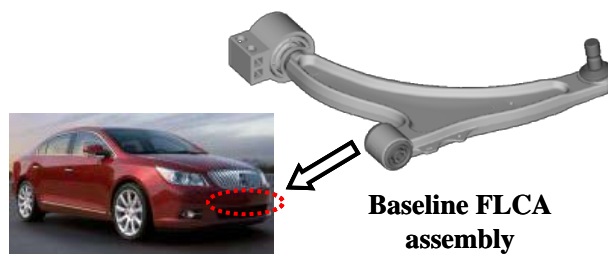


Figure 1. Baseline OEM FLCA Assembly

- The **Clamshell Design** is predicted to have equivalent mass to the baseline assembly with up to a 34 percent cost reduction potential at a production volume of 250,000 vehicles per year. The design is deemed production feasible based on forming simulations and industry welding examples. The design is 46 percent lighter than the average steel FLCA assembly for vehicles with similar foot prints per A2MAC1 benchmarking data.
- The **I-beam Design** is predicted to have the highest buckling resistance and high stiffness with a 2 percent (0.05 kg) higher mass than the baseline assembly, with up to a 21 percent cost reduction potential at a production volume of 250,000 vehicles per year. The design is deemed production feasible based on typical welding process development and industry tube bending examples.

The **Forged Design** is predicted to have the highest stiffness and durability performance (no welds) of all designs with a 4 percent (0.13 kg) higher mass than the baseline assembly, assuming an aggressive 3 mm minimum gage manufacturing target.

2010 FreedomCAR and Fuel Partnership Highlight

Minimum Weight SMC Assemblies Free from Bond-Line Read-Through

United States Automotive Materials Partnership – ACC 932

Sheet molding compound (SMC) is an option for building lighter weight closure panel assemblies than comparative steel assemblies. Unfortunately, the presence of adhesive-induced distortions (i.e. Bond-Line Read-Through (BLRT)) on assemblies causes manufacturers to increase the thickness of the outer panel which eliminates the weight savings. The Automotive Composites Consortium (ACC) completed this project to enable elimination of these distortions without adding weight. Implementation of the lessons learned and modeling tools developed in this project will allow manufacturers to reduce the thickness of the outer panels in composite closure panel assemblies and achieve a 25 percent weight reduction.

The ACC Bond-Line Read-Through (BLRT) project developed a measurement system for quantifying the visual severity of BLRT-induced distortions. The team completed a series of experiments to discover what factors determine the severity of the distortions and developed and validated a finite element modeling methodology for predicting the severity of the distortions.

This project has shown that BLRT is fundamentally caused by differential shrinkage between the adhesive and the substrate as the assembly cools from bonding temperature to room temperature. The distortions caused by thermal shrinkage alone will not, however, necessarily be severe enough to be visible. Other factors that contribute to the visibility of the distortions are: a) abrupt variations in the thickness of the adhesive bead, b) the adhesive material properties and c) the sectional stiffness of the substrate. The effect of variation in the adhesive bead geometry on the severity of the distortion is illustrated in Figure 1. The finite element modeling methodology developed in this project will enable manufacturers to eliminate objectionable distortions by evaluating and modifying part designs prior to cutting molding tools. The manufacturing guidelines developed will help parts manufacturers better control their processes and enable the use of thinner panels.

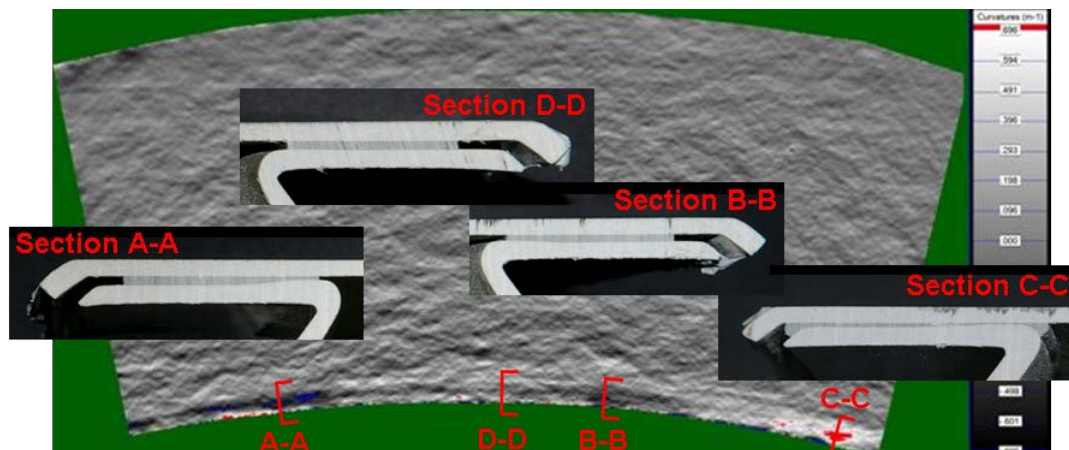


Figure 1. Curvature map with associated sections showing that the severity of the distortion was dependent on the cross-sectional geometry of the adhesive.

2010 FreedomCAR and Fuel Partnership Highlight

Reliability Tools for Resonance Inspection

United States Automotive Materials Partnership – NDE 901

Resonant (acoustic) inspection (RI) offers unique capabilities for nondestructive safety- and performance-critical inspections of lightweight metal castings. Sound in the range of 100 to 100,000 Hz can readily penetrate small to very large castings and is sensitive to heat treatment, porosity, cracks and at least some oxide inclusions. Resonance inspection also has significantly lower capital and piece costs than either radiographic testing (RT) or fluorescent penetrant inspection (FPI). In fact, resonance inspection is already used for 100% inspection of many traditional castings such as knuckles, rocker arms, master cylinders and brake calipers. Despite these advantages, resonant inspection has not achieved full automotive industry acceptance because sensitivity and repeatability cannot be assured with current implementations. Working with RI system vendors and casting vendors, this project is developing new tools to improve the robustness of RI in production. There are 3 tasks underway:

1. Standardized processes

A detailed Resonance Inspection Process Development Flow Chart has been completed. The Process Development Flow Chart provides a check-off process for establishing an RI plan. This Flow Chart has been evaluated during the selection and inspection of production knuckle castings and non-production solid cylindrical castings.

2. Integrated tools to improve probability of detection (POD) of critical defects

The material and resonance frequency variations of knuckles have been extensively measured. Figure 1 describes the very small variations associated with knuckles made with a single cavity mold during a single shift. The repeatability variation of RI is typically very low (<100 ppm).

3. Finite element sort modules

To have a useful predictive tool, it is necessary to integrate all the physics into a software tool bench. The overall design of the tool bench was completed including the data structures; inputs, outputs and processing algorithms for each module; and a graphical user interface.

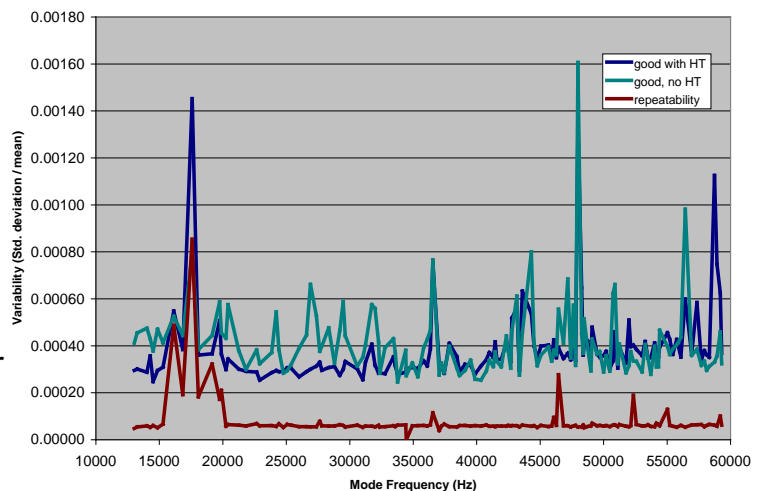


Figure 1. Frequency variation of 118 resonances with repeatability, heat treatment, and no heat treatment.

2010 FreedomCAR and Fuel Partnership Highlight

Development of High-Volume Warm Forming of Low-Cost Magnesium Sheet

United States Automotive Materials Partnership - AMD602

There are two major barriers to the application of magnesium sheet components in vehicle structures: 1) limited formability of magnesium sheet and 2) the cost of producing the sheet itself. A warm forming process similar to the one demonstrated for aluminum with the USAMP Warm Forming Project (AMD307) can be used to significantly improve the formability of magnesium sheet. The current project leveraged the accomplishments of AMD307 to develop equipment, lubricant, simulation and forming equipment for the cost effective forming of magnesium sheet. A warm forming cell capable of 5 jobs per minute was designed and built to demonstrate the efficient forming of magnesium sheet. The target application for this process was deep drawn panels that could be used for automotive door inners.



Figure 1. Warm forming cell capable of five jobs per minute and pans stamped at 350°C from five different magnesium alloys.

The cost of magnesium sheet is driven by the high conversion costs of rolling an ingot into sheet form. This is a direct result of the hexagonal close-packed structure of magnesium that requires the sheet to be rolled in small increments often with annealing steps between rolling passes. Continuous casting is a technology with the potential to reduce this cost dramatically. By casting directly into sheet form, continuous casting offers a higher production rate, a smaller capital investment and significantly less energy and labor when compared with the conventional direct-chill (DC) ingot-casting process.

In this project, continuous-cast sheet produced by five of the major global magnesium suppliers was included to determine suitability for the warm forming process. The new warm forming system was used as a standard test bed for the evaluation of these materials and will be for new magnesium sheet materials produced in the future. This project has proven that warm forming can be used to significantly improve formability of magnesium sheet and the cost of the sheet can be reduced through the application of continuous casting technology.

2010 FreedomCAR and Fuel Partnership Highlight

Friction Stir and Ultrasonic Solid State Welding Enable Joining of Magnesium to Steel

Pacific Northwest National Laboratory, Oak Ridge National Laboratory

The use of magnesium as a structural material has the potential to provide significant vehicle weight savings. However, the joining of magnesium to other materials is a significant challenge. A joining project performed by both PNNL and ORNL focused on joining magnesium to steel by two different techniques: ultrasonic spot welding and friction stir welding.

Ultrasonic spot welding (USW): Significant advances demonstrated that this

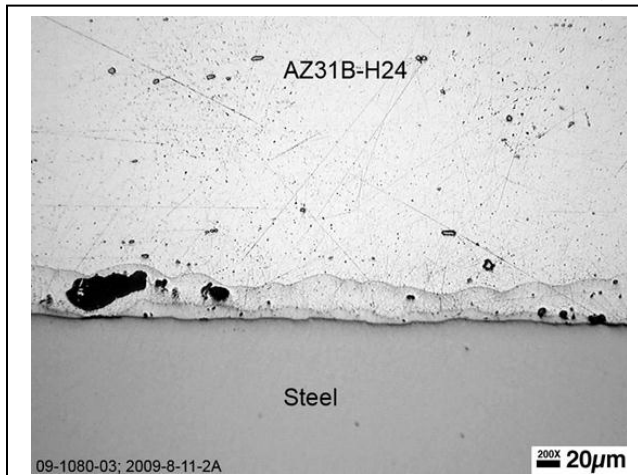


Figure 1. Optical micrograph of magnesium of type AZ31B-H24 mild steel USW interface (unetched) highlighting interfacial reaction between the AZ31B and the zinc coating on the mild steel.

technique is capable of making magnesium-steel joints of potentially useful strength levels. Reproducible spot welds with high strength could be made between magnesium and hot-dip galvanized (HDG) mild steel (Figure 1), but not between magnesium and bare, uncoated steel. The lap-shear strengths for magnesium (AZ31B-H24) spot welded to HDG steel were comparable to those of resistance-spot-welded joints of magnesium to magnesium (AZ31-AZ31).

Friction stir welding: Previous results have demonstrated that solid-state friction stir welding technologies could be used to join magnesium of type AZ31B to various automotive sheet steel alloys.

This year's focus was to develop tooling and processing parameters that resulted in increasing weld strengths from 60 percent to more than 90 percent of the strength of drawing quality base metal sheet steel. Understanding the flow of material in the joint between steel and magnesium resulted in a patent application for friction stir tooling that enhances bonding between dissimilar materials. New tools resulting from this work are shown in Figure 2. Utilizing tooling developed during this project, joints between 2.3-mm thick AZ31B magnesium alloy and a 0.8-mm thick Drawing Steel Type B were shown to consistently exceed 90 percent of the tensile strength of the steel sheet.

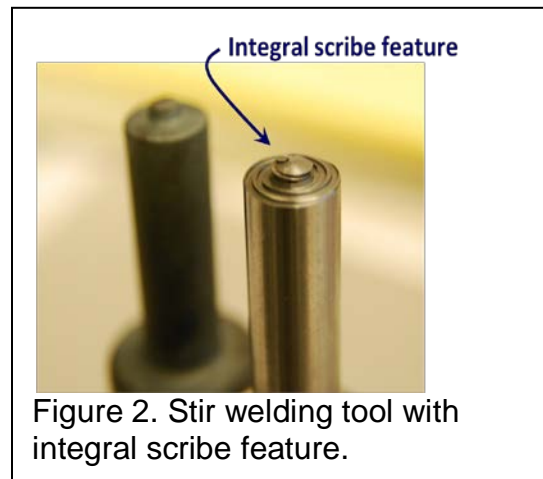


Figure 2. Stir welding tool with integral scribe feature.

2010 FreedomCAR and Fuel Partnership Highlight

Friction Stir Spot Welding of Advanced High Strength Steel

Pacific Northwest National Laboratory, Oak Ridge National Laboratory

The use of Advanced High-Strength Steels (AHSS) reduces vehicle weight. However, joining AHSS is challenging because one must maintain the microstructures that govern their significantly improved properties. For this reason, melting AHSS using traditional welding technology is undesirable. The technique of friction stir spot welding (FSSW), a solid-state welding process, is being evaluated for joining AHSS. Because friction stir spot welding does not require melting, concerns about defects associated with metal solidification are eliminated, and the potential for interactions with zinc coatings that degrade joint properties and tooling are minimized. Studies have shown that friction stir spot welding is also highly energy efficient.

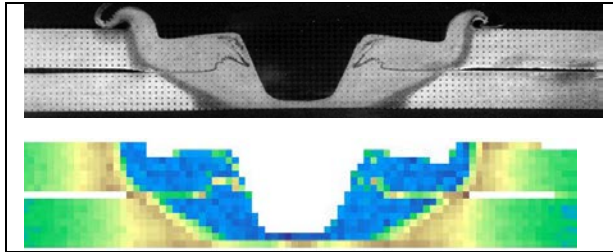


Figure 1. Cross-sectional views of FSSW in hot-stamp boron steel; optical image (top), image representation of hardness measurements (bottom).

This shared study between ORNL and PNNL significantly advances the use of friction stir spot welding of AHSS. Specific major accomplishments include demonstrating that high-strength joints can be achieved on both bare and zinc-coated AHSS, see Figure 1. Strategies for optimizing the process were identified. Additionally, a variety of materials were evaluated for stir tooling and the impact of tooling costs on the overall cost of implementing friction stir spot welding was estimated through cost modeling. The importance of reducing the cost of stir tools was confirmed, as shown in Figure 2. More recent efforts indicate that transformation-induced plasticity (TRIP) steel can also be friction stir spot welded to produce high-strength joints.

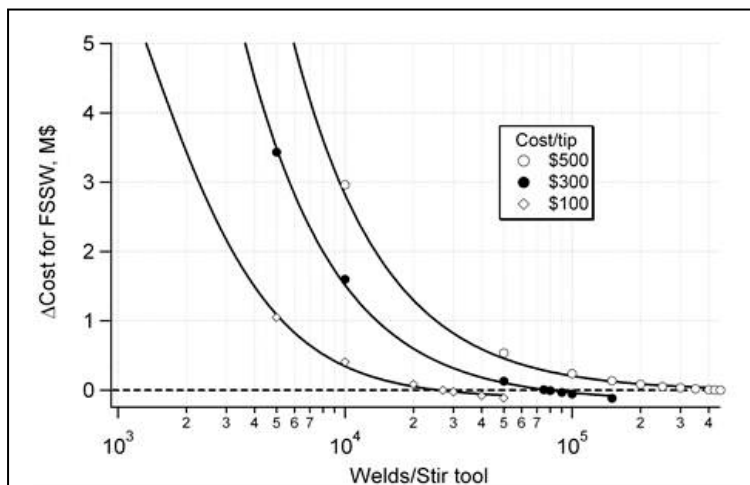


Figure 2. Variations in cost of FSSW relative to resistance spot welding depending on stir tool cost and life.

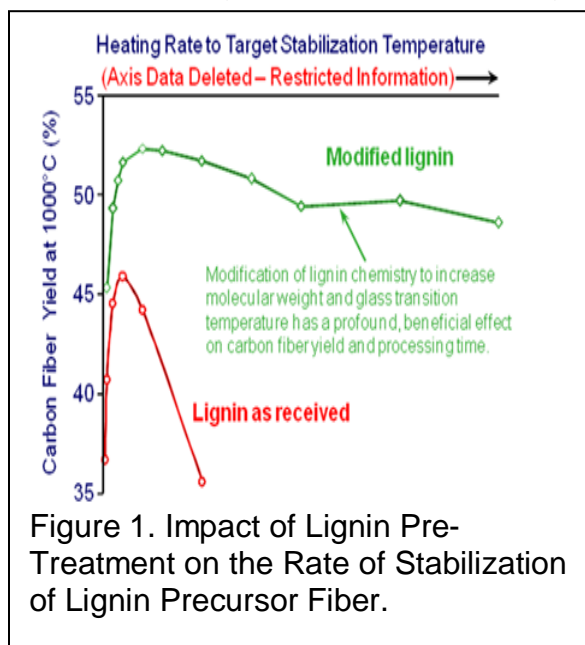
2010 FreedomCAR and Fuel Partnership Highlight

Stabilization Time of Lignin Precursor Fiber Reduced from Days to Minutes

Oak Ridge National Laboratory

Advances were made in two distinct, but related areas of lignin-based carbon fiber production: 1) the development of a technique for continuous processing of discontinuous lignin precursor fiber tows (bundles of thousands of fibers roughly 18 inches in length), including the identification of the thermal conditions under which the precursor fiber could be satisfactorily converted into carbon fiber; and 2) the substantial acceleration of lignin precursor fiber stabilization rates for subsequent conversion into carbon fiber.

Simply attaching each end of the bundle of lignin precursor fibers to the polyacrylonitrile-based carbon fiber tow used to make the lignin fiber tense and pulling it through the furnace equipment proved to be a considerable challenge due to the fragile nature of the lignin precursor fiber. Modifications were made to the precursor evaluation line to better accommodate bundles of lignin fiber, and different methods for attaching the bundle to the pull tow were evaluated. It became clear that the relatively low glass transition temperature (T_g) and melting point (T_m) of the lignin fiber were not conducive to stabilization of the fiber in a practical timeframe. Based on extensive thermal analysis studies, a proprietary method was developed for raising the T_g and T_m of the precursor fiber through pre-treatment of the lignin before melt spinning. The beneficial impact of this lignin pre-treatment is highlighted in the Figure 1.



To comply with Export Control regulations, the specific heating rates are not shown. However, the data demonstrated that the time required for satisfactory stabilization of lignin precursor fiber could be reduced from more than two days to less than 15 minutes through the initial pre-treatment of the lignin precursor material. There were indications that the stabilization time could be reduced further, opening up the possibility of stabilizing the lignin fiber “on-the-fly” by passing the spun fiber through a heated chamber on the melt-spinning equipment immediately after spinning. Furthermore, upon conversion of the rapidly stabilized precursor fiber, the yield of carbon fiber (at 1000°C) increased from 46 to 53 percent, a

significant gain with respect to the economics of carbon fiber production. These findings emphasize the importance of lignin chemistry with respect to both the processing of lignin into carbon fiber and the properties of the carbon fiber obtained.

2010 FreedomCAR and Fuel Partnership Highlight

Accelerating Advanced Technology Introduction through Plug-and-Play Architecture Modeling

Argonne National Laboratory

Autonomie, a new plug-and-play powertrain and vehicle simulation program, facilitates rapid, flexible evaluation of new powertrain/propulsion technologies on engineers' personal computers. Building hardware is an expensive way to confirm advanced technology vehicle performance. To reduce development costs and improve time to market, it is imperative that greater emphasis be placed on modeling and simulation.

Autonomie builds on the Powertrain Systems Analysis Toolkit (PSAT), a simulation program that has been successfully used to assess the fuel consumption and performance of advanced vehicles for more than a decade. The increased complexity and diversity of the vehicle and powertrain technologies led to a partnership, initiated by General Motors in 2007, to develop this next generation of automotive simulation tools. Autonomie adds a plug and play powertrain and vehicle architecture modeling and development environment as shown in Figure 1 below. It supports the rapid evaluation of new powertrain/propulsion technologies and fuels for improving fuel economy through virtual design and powertrain controls-based analysis in a math-based simulation environment.

Autonomie:

- Unifies the entire engineering organization for efficient operation
- Connects entire models in less than a minute compared to hours or days
- Promotes reuse and exchange of models industry-wide by incorporating legacy models from Simulink and other automotive expert tools
- Simulates systems, subsystems and entire vehicles
- Sorts technology quickly to reduce need for hardware build iterations
- Supports all the model-based design processes from Model-in-the-Loop to Software-in-the-Loop, Hardware-in-the-Loop, etc.
- Manages models, data, processes, results and control code from research to production using configuration and database management
- Promotes complete customer customization via the open architecture

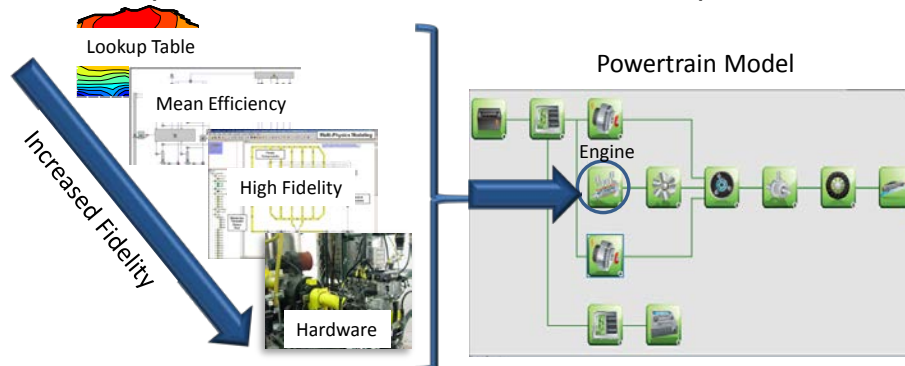


Figure 1. Autonomie provides increased fidelity in vehicle and powertrain simulation to support ever-increasing advanced vehicle powertrain complexity.

2010 FreedomCAR and Fuel Partnership Highlight

Accelerating Control Development Using Hardware in a Virtual System Environment

Argonne National Laboratory

Using Autonomie a generic process has been successfully defined to provide a seamless link between software and hardware. To reduce development time and introduce technologies faster to the market, companies are turning to Model Based Design (MBD). In MBD, the development process centers around a system model, from requirements capture and design to implementation and test. Engineers can skip over a generation of system design processes on the basis of hand coding and use graphical models to design, analyze and implement the software that determines machine performance and behavior. Since MBD includes many steps (e.g., Model-in-the-Loop, Software-in-the-Loop and Hardware-in-the-Loop) and engineers have to iterate numerous times between software and hardware for each step, a generic process is necessary to accelerate the development.

To evaluate the impact of non-modeled phenomena such as thermal behavior and emissions on fuel efficiency, Argonne has developed two tests set up with a battery and an engine. For the battery-in-the-loop, a battery cycler is used to charge and discharge the battery in order to mimic transient, in-vehicle scenarios for the battery. Similarly, engine-in-the-loop has been implemented on a 2.2 L Opel SIDI Engine and an AC engine dynamometer capable of fast transient response. Noise in feedback signal, system time response and command and feedback delay issues, which are critical to real-time behavior of the system, have been addressed to replicate real world behavior.

The same steps can be used to evaluate the benefits of engine, batteries or electric machines. Powertrain configurations, plant models and controls can now be quickly modified in simulation and evaluated in hardware. Such evaluation saves significant control and hardware development time since development and tuning can be performed without the need for the rest of the powertrain to be physically present.

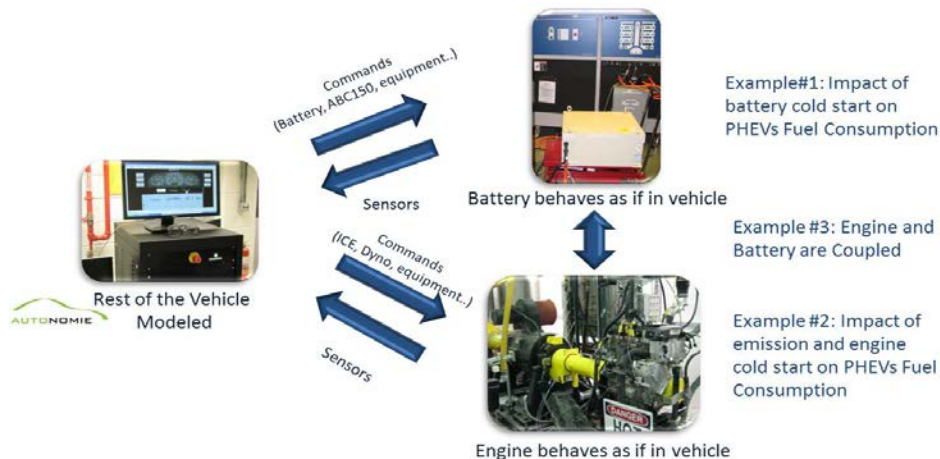


Figure 1. Engine and Battery in the loop using Autonomie.

2010 FreedomCAR and Fuel Partnership Highlight

Grid-Connected Electric Drive Vehicle and Charging Studies Demonstrate Petroleum Reductions

Idaho National Laboratory, ECOTality

Idaho National Laboratory (INL) testing and data collection supports the U.S. Department of Energy (DOE), Vehicle Systems Analysis Technical Team and DOE's Advanced Vehicle Testing Activities. This includes testing of grid-connected electric drive vehicles (EDVs) in on-road fleets, on the test track and in laboratory settings to demonstrate real-world petroleum reduction potentials of the various EDV technologies. More than 100 testing partners collected vehicle performance and charging behavior from more than 300 EDVs (including 260 plug-in hybrid electric vehicles - PHEVs) in 26 states and Canada. As FY10 ended, INL initiated data collection from an additional 28,000 PHEVs, pure electric vehicles (EVs), extended range electric vehicles (EREVs), Level 2 electric vehicle supply equipment (EVSE) and fast chargers.

EDV performance and infrastructure testing accomplishments include:

- 3 million PHEV test miles documented, showing driving/charging profiles during 265,000 trips, 53,000 charging events, 135 million watt-hours of electricity use
 - PHEV petroleum use impacts captured from <-20°C to >40°C temperatures, driver aggressiveness, and varying battery state of charge
- 5.2 HEV million test miles on 22 models documented, showing an average 21.8 percent mpg decrease (range 8 to 28.7 percent) from air conditioning use, and 17.9 to 45.6 HEV fleet real world mpg
- Real world usage data collection started for 9,000 OEM EVs, PHEVs and EREVs
 - 19,000 Level 2 EVSE and 340 fast chargers deployed privately and publicly
- Initiated the development of a charging codes and standards DOE workshop, vehicle-to-grid codes and standards review/report and demonstrated real-world EDV grid impacts
- 64 EDV presentations, papers and reports were produced to support DOE

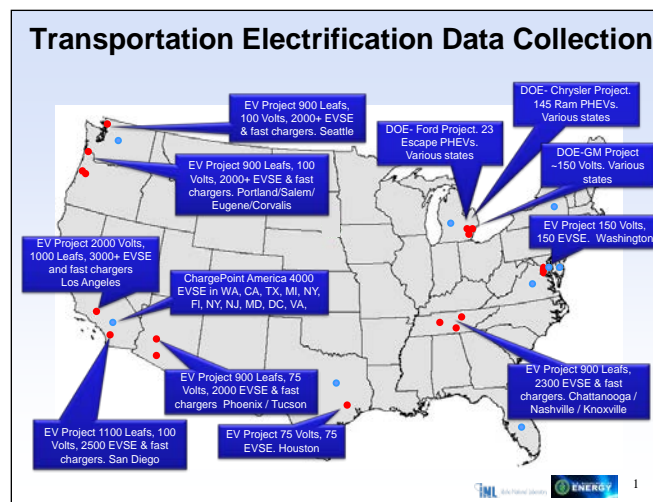


Figure 1. Locations of 28,000 EVs, PHEVs, EREVs, EVSE and fast chargers from which INL will collect data.

2010 FreedomCAR and Fuel Partnership Highlight

A Standard Practice for Testing PHEVs Developed and Balloted

Argonne National Laboratory

It was recognized in 2006 that existing techniques for testing PHEVs were inadequate for accurately characterizing the highly evolving and diverse types of PHEVs. In response, the Society of Automotive Engineers (SAE) task force SAE J1711 created a fair and effective testing procedure for PHEV fuel and energy consumption. The task force was assembled with experts from Ford, Chrysler, GM, Honda, Toyota, Nissan, Mitsubishi, U.S. EPA, National Renewable Energy Laboratory, California Air Resources Board, Environment Canada, Southern California Edison and the Japan Automotive Research Institute.

Argonne National Laboratory (ANL) guided and managed the very challenging development of the complex procedures for testing the fuel and electrical energy consumption of PHEVs. Subtle differences in definitions, calculation or test methods have a radical impact in the overall outcome, or rating of the PHEV in question. Thus, proper and consistent test procedures are critical to the continued assessment and advancement of PHEV technologies. If done incorrectly, improper testing and vehicle assessment procedures could delay introduction of these vehicles into the marketplace for years or decades.

Given the extensive experience and position as a world-leading center of expertise in testing advanced vehicles, it was ANL's task to ensure the final product (SAE J1711) properly assessed technologies that offered benefits such as displacing petroleum. For example, an earlier simple version of the procedure resulted in false optimum design characteristics that automakers may have designed the vehicles to exploit. ANL recognized this problem and invented a new and more precise calculation procedure that properly weights the electrified mode of operation no matter how large the battery pack chosen by the OEM.

In May of 2010, SAE J1711 was balloted and published as a recommended standard practice for testing HEVs and PHEVs. Later, a companion document was balloted through SAE that includes the weighting factors used when analyzing PHEV results based upon national driver surveys and local driving data collection (SAE J2841).

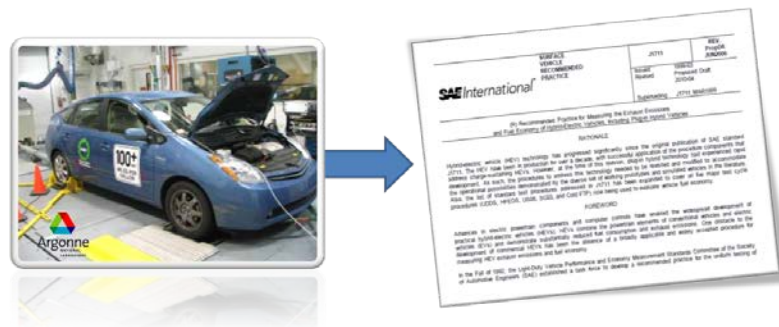


Figure 1. Many Test Programs Were Used to Optimize PHEV Procedures for SAE J1711.

2010 FreedomCAR and Fuel Partnership Highlight

European Hybrid Vehicle Demonstrates Fuel Consumption Benefits and Emissions Trade-Offs

Oak Ridge National Laboratory

A European MY2008 BMW 1 series 120i featuring a Lean Gasoline Direct Injected (LGDI) engine was benchmarked on U.S. drive cycles and steady state operation conditions in order to evaluate technologies not currently available in the U.S. The vehicle also featured two micro-hybrid functionalities: engine Stop-Start (MSA in figures below) and Intelligent Alternator Control (IGR in figures below) which provides some coast-down energy regeneration and efficient battery charging algorithms. The vehicle was operated in various modes (lean vs. stoichiometric, with and without micro-hybrid features) to quantify the fuel economy associated with each mode.

Lean operation consistently demonstrated better fuel economy than stoichiometric-only operation although improvements varied between 4 and 15 percent with drive cycles. Fuel economy results are shown in Figure 1. The more aggressive the drive cycle, the more occurrences of high speed and high load points where the engine will run stoichiometric (even in lean mode) and therefore the smaller the improvement. Stop-Start generates a 3.3 percent fuel economy improvement on the FTP cycle and 2.2 percent on a US06 drive cycle. Intelligent Alternator Control improved fuel economy by 2.5 percent on an FTP cycle.

The vehicle meets the U.S. Tier II bin 5 regulation levels for carbon monoxide, total hydrocarbons and particulate matter regardless of the engine operating mode. Lean operation NO_x emissions exceed U.S. Tier II Bin5 NO_x level of 0.05g/mile (at 50000 miles) by a factor of two whereas stoichiometric-only operation emissions are within the limits. Micro-hybrid features did not have a significant effect on NO_x emissions. See Figure 2. It is important to note that this vehicle is calibrated for European certification drive cycles; as such, emissions might not be optimized and could potentially be improved with a U.S.-specific calibration.

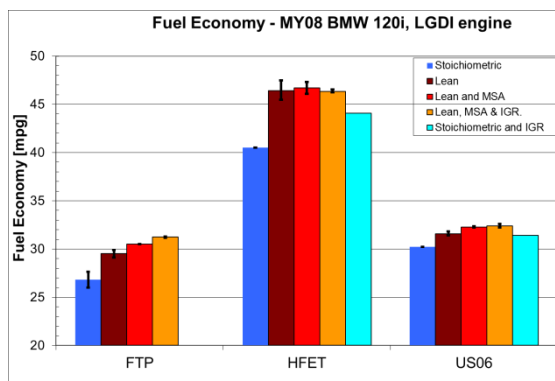


Figure 1. Fuel Economy as a Function of Vehicle Mode and Drive Cycle.

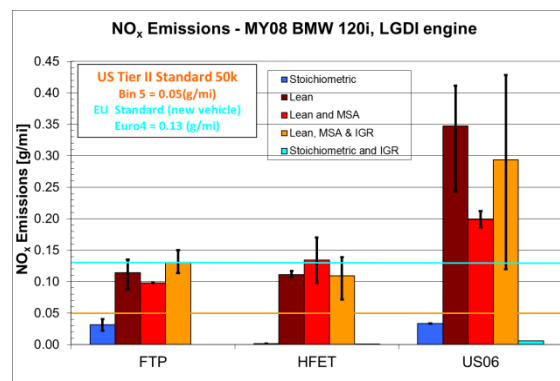


Figure 2. NO_x Emissions as a Function of Vehicle Mode and Drive Cycle.

2010 FreedomCAR and Fuel Partnership Highlight

PHEV Bus Reduces Fuel Consumption Up to 50%

National Renewable Energy Laboratory

Plug-in Hybrid Electric Vehicle (PHEV) technology may reduce fuel consumption and tailpipe emissions in many medium and heavy duty vehicle vocations, including school buses. The true magnitude of these reductions is best assessed by comparative testing over relevant drive cycles.

Real-world school bus drive-cycle data (614 operating shifts and 73 unique vehicles), and selected similar standard drive cycles for testing on a chassis dynamometer were collected and analyzed. A first-generation PHEV school bus from International Corporation (2007 model year) equipped with a 6.4 L engine and an Enova PHEV drive system, comprised of a 25 kW/80 kW (continuous/peak) motor and a 370 volt Li-ion battery pack. For a baseline comparison, a Bluebird 7.2 liter 2008 model year conventional school bus also was tested. Both vehicles were tested over the Urban Dynamometer Driving Schedule for Heavy-Duty Vehicles (UDDSHDV), the Rowan University Composite School Bus Cycle (RUCSBC) and the Orange County Bus Cycle (OCC) in order to capture a range of typical driving activity.

Relative to the baseline school bus, the PHEV fuel savings in charge-depleting (CD) mode ranged from slightly more than 30 percent on the UDDSHDV and RUCSBC cycles to a little more than 50 percent on the OCC cycle. However, the larger fuel savings lasted over a shorter driving distance, as the fully charged PHEV school bus would initially operate in CD mode for some distance, then in a transitional mode and finally in a charge-sustaining (CS) mode for continued driving. Figure 1 illustrates fuel and electricity consumption as a function of distance driven since recharge for the OCC.

In CS mode, the tested bus showed up to 5 percent reduction in fuel consumption and somewhat higher NO_x emissions than the baseline comparison bus. Further refinements to realize hybridization fuel savings in CS mode and calibrations focused on reducing NO_x could lead to both higher fuel economy and lower NO_x emissions in the next generation PHEV bus design.

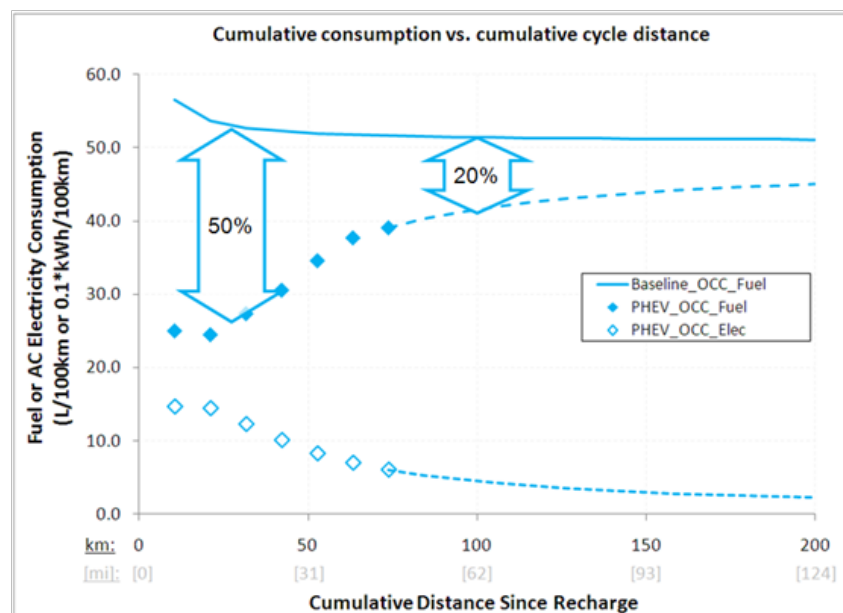


Figure 1. Cumulative Consumption Rate vs. Distance (OCC).

2010 FreedomCAR and Fuel Partnership Highlight

Thermal Preconditioning Restores Range Up to 19%

National Renewable Energy Laboratory

Plug-in electric vehicles (PEV) represent a unique opportunity to thermally precondition a vehicle when they are plugged into an off-board power source. The charge depleting (CD) range of a PEV is limited by on-board battery capacity, which is used not only for driving but also for other loads. Notably, climate-control loads (heating and cooling) can reduce the PEV's CD range and/or cause the internal combustion engine to operate more frequently in a Plug-in Hybrid Electric Vehicle (PHEV). During hot or cold weather, the climate-control load on the on-board power source is high at startup to cool down or to warm up the vehicle from a thermal-soaked condition to a comfortable condition. If the cool down or warm up can be accomplished during battery charging, the higher transient climate-control load on the vehicle's power source could be reduced, or eliminated. The reduction of the climate-control load due to preconditioning has the potential to reduce fuel consumption, partially restore CD range, and improve battery life.

The Powertrain Systems Analysis Toolkit (PSAT) vehicle simulation program was further developed to calibrate models of three relevant PEV platforms: a blended plug-in hybrid electric vehicle (PHEV) with a 15-mile (24-km) electric range (PHEV15), a series PHEV with a 40-mile (64-km) electric range (PHEV40) and an electric vehicle with a 100-mile (161-km) electric range (EV). Second, NREL surveyed literature and test data to develop representative air conditioning and heater load profiles. Next, NREL simulated PEV performance with and without thermal preconditioning over the EPA city and highway drive cycles, and for three different ambient temperature scenarios. Finally, battery wear was characterized using a physically justified semi-empirical lithium ion battery life model. Figure 1 presents the impacts of climate control and benefits of thermal preconditioning on the PHEV15 performance.

This analysis shows that climate control system loads can significantly increase fuel consumption (up to 60.7 percent) and decrease CD range (up to 35.1 percent) in PEVs. When compared to no thermal preconditioning, thermal preconditioning can provide a moderate reduction in fuel consumption (up to 2.7 percent, as well as partially restore CD range (up to 19.2 percent). Pre-cooling of electric-drive vehicle batteries is predicted to reduce capacity fade by 2 to 7 percent and resistance growth by 3 to 14 percent in hot (35°C) ambient conditions.

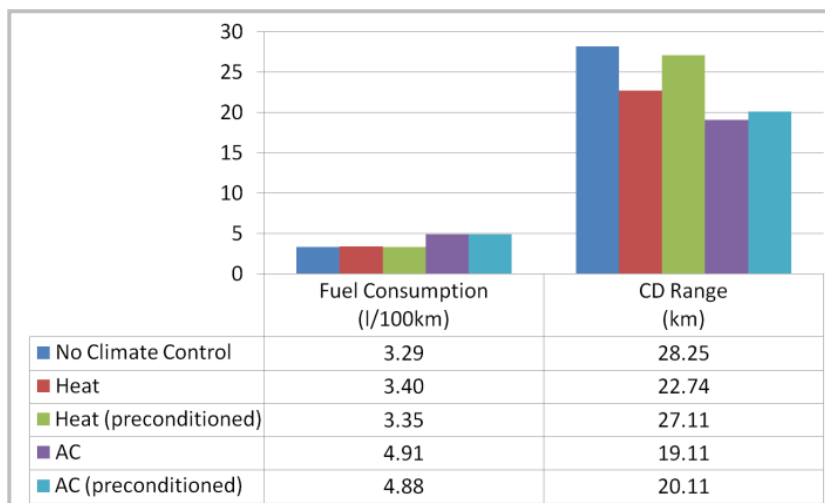


Figure 1. PHEV15 performance

2010 FreedomCAR and Fuel Partnership Highlight

Hydrogen Threshold Cost Updated

National Renewable Energy Laboratory Systems Integration Office

In 2010, the U.S. Department of Energy (DOE) developed a hydrogen threshold cost analysis to determine the cost at which hydrogen is projected to be competitive with gasoline. The threshold cost will guide DOE's hydrogen and fuel cell research and development activities and will be updated periodically. It is pathway independent with respect to hydrogen production and delivery technology options.

The Fuel Pathways Integration Technical Team (FPITT) reviewed the Department of Energy's analysis process, methodology, assumptions and data, providing industry perspective. The methodology sets a threshold cost such that consumers' costs (\$/mile) in a hydrogen fuel cell vehicle will be equal to or less than the competitive gasoline hybrid electric vehicle in 2020. It provides a range reflecting variability in future fuel efficiency improvement factors, competitive gasoline cost and incremental vehicle cost compared to competing vehicles as shown in Figure 1.

The base case of the hydrogen threshold cost analysis was based on the Energy Information Administration's 2009 Reference Case projection of gasoline cost in 2020, DOE projections of the fuel economy (estimated using the Powertrain System Analysis Toolkit), and DOE projections of the incremental cost of hydrogen fuel cell vehicles relative to other advanced vehicle technologies. Sensitivity and stochastic analyses were performed to substantiate the hydrogen threshold cost range of \$2-4/gge. The upper end (\$4/gge) of the range was selected because it corresponds with the base case results of the analysis, the lower end (\$2/gge) of the range corresponds with the analytical results using either the low gasoline cost projection or a conservative incremental vehicle cost of \$0.04/mile. The range incorporates most of the costs resulting from the stochastic analysis. Details are available in an October 15, 2010, presentation to the Hydrogen and Fuel Cell Technical Advisory Committee (www.hydrogen.energy.gov/htac_meeting_oct10.html).

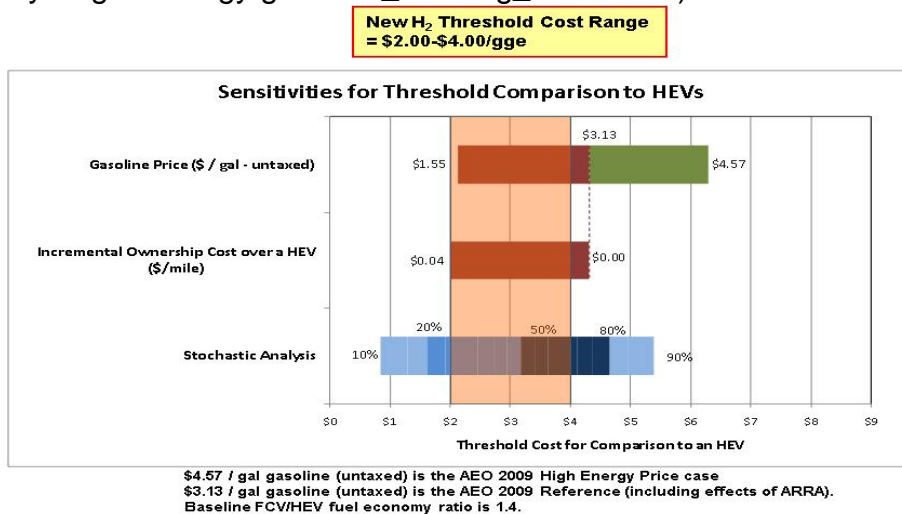


Figure 1. Sensitivities of Hydrogen Threshold Cost Range to Gasoline Price and Incremental Cost

Source: DOE/NREL October 15, 2010, presentation to the Hydrogen and Fuel Cell Technical Advisory Committee

2010 FreedomCAR and Fuel Partnership Highlight

Hydrogen Costs from Fuel Cell Combined Heat and Power

National Renewable Energy Laboratory

NREL's Fuel Cell Power Model predicts that hydrogen costs from molten carbonate fuel cell (MCFC)-based combined heat, hydrogen, and power (CHHP) systems are lower than those from stand-alone steam methane reforming (SMR) fueling stations at hydrogen production rates below 130-180 kg/day.

The SMR station was scaled to ~600 kg/day hydrogen capacity using a standard engineering scaling factor. Smaller stations were modeled by assuming lower capacity factors for the 600 kg/day station. The CHHP system used a MCFC, which was scaled linearly from 1,400 kW to 200 kW maximum electrical output. The compression, storage and dispensing portions of both types of facilities were identical. Fuel cell utilization was assumed to be 95 percent, the CHHP electricity price was set equal to the grid price (\$0.08/kWh), the CHHP heat price was assumed to be equal to the natural gas price at 80 percent efficiency, and the fuel cell uninstalled cost was assumed to be \$2,500/kW. Both the MCFC and the SMR modeled systems have PSA hydrogen purification to achieve hydrogen purity for fuel cell vehicles with a PSA discharge pressure of 300 psi. The dispensed hydrogen pressure in the modeled systems is sufficient for 5,000 psi on-board storage. Additional details of the analysis can be found in the Fuel Cell Power Model and the H2A Production and Delivery Models.

Since hydrogen is a side product of the stationary fuel cell system in CHHP service and electricity is the main product, hydrogen can be economically produced in small quantities from the fuel cell system. During the early stages of fuel cell vehicle adoption, the demand for hydrogen is expected to be low, dispersed and uncertain. Fuel cell based CHHP systems may be ideally suited for these applications because hydrogen can be economically produced in small quantity.

Figure 1 illustrates hydrogen costs and sensitivities to natural gas prices for CHHP (without tax incentives) and SMR pathways. For both natural gas cost cases, the CHHP cost is lower than the SMR cost at low hydrogen-production levels. At a natural gas cost of \$9/MBtu, the fuel cell CHHP system produces hydrogen more economically than the dedicated SMR station for production rates less than about 130 kg/day. At a natural gas cost of \$5/MBtu, the fuel cell CHHP system produces hydrogen more economically for production rates less than about 180 kg/day.

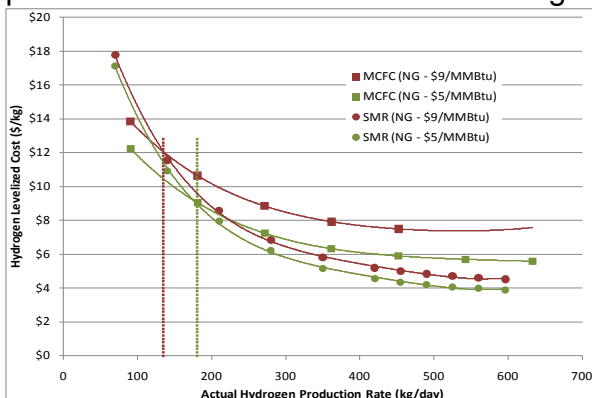


Figure 1: Delivered Hydrogen Cost from MCFC CHHP and SMR at 2 Natural Gas Costs

Source: NREL November 2010

2010 FreedomCAR and Fuel Partnership Highlight

Infrastructure Costs for Coal-Based Hydrogen Production

National Renewable Energy Laboratory

Analysis of infrastructure requirements and costs for central coal-based hydrogen production revealed that costs for installation of hydrogen pipelines, CO₂ pipelines, and rail spurs are of a similar order of magnitude on a per-mile basis. The sites most favorable for coal-based hydrogen production are those located near demand centers and carbon sequestration sites as shown in Figure 1a.

Costs were calculated for rail transport of coal to the plant, pipeline transport of hydrogen to demand centers and pipeline transport of CO₂ to sequestration sites. These costs were then adjusted for terrain and right-of-way (ROW) costs associated with land use. The results were used to calculate a minimum total infrastructure cost for potential plant locations nationwide. Four analyses were performed:

Infrastructure Analysis

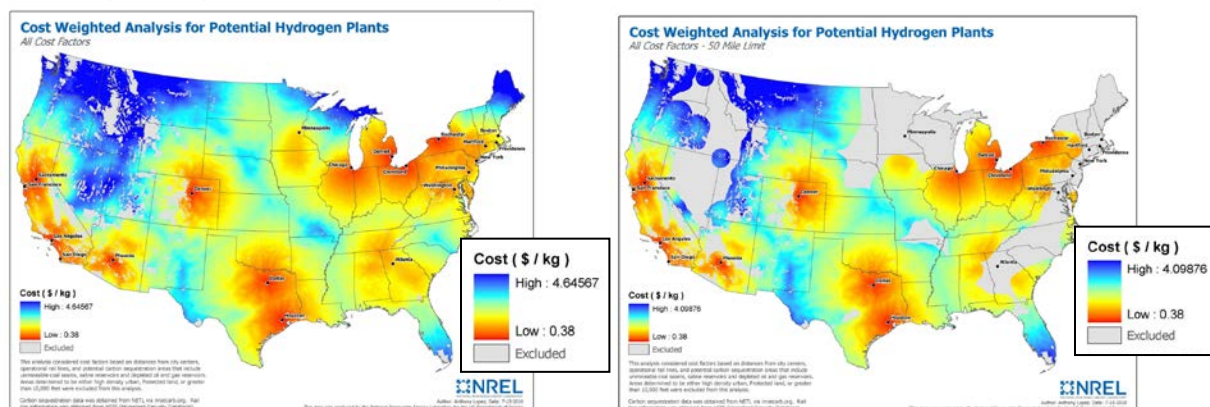
- Baseline (considering distances only)
- Considering terrain
- Considering ROW/land use
- Combined terrain and ROW considerations

Range of Infrastructure Costs (\$/kg H₂)

\$0.38–\$3.83
\$0.38–\$3.87
\$0.38–\$4.20
\$0.38–\$4.65

Infrastructure costs vary widely depending on the distance between the hydrogen production plant and carbon sequestration sites and demand centers. Terrain near demand centers tends to be navigable; therefore, it does not affect infrastructure costs dramatically. In contrast, ROW costs are higher near demand centers because these areas tend to be more urban.

Figure 1b shows results of a similar analysis after limiting the distance from a hydrogen plant to a carbon sequestration site to 50 miles. The costs for demand centers are differentiated primarily by their distance to carbon sequestration sites. As illustrated in Figure 1b, a number of hydrogen demand centers are not located near carbon sequestration sites resulting in higher infrastructure costs or excluding them from adopting coal gasification for hydrogen production.



a – Unadjusted

b – Adjusted for 50-mile Sequestration Limit

Figure 1. Coal Hydrogen Plant Infrastructure Costs Adjusted for Terrain and ROW.

Source: NREL July 2010

2010 FreedomCAR and Fuel Partnership Highlight

Development of a Centrifugal Hydrogen Pipeline Gas Compressor

Concepts NREC

Concepts NREC has completed a Phase 1 feasibility design of a full-scale, six-stage centrifugal compressor for use in hydrogen pipelines that is expected meet all DOE targets. A two-stage prototype will be fabricated in FY11 and tested in FY12. Hydrogen pipelines are a key component for a future low-cost hydrogen distribution infrastructure, and the pipelines will require high-reliability centrifugal compressors. No such compressors currently exist, so their development is a crucial enabler for widespread deployment of hydrogen as a transportation fuel.

	DOE Target	Projected Performance
Efficiency	98%	98%
Capacity (kg/day)	100,000-1,000,000	240,000
Leakage	<0.5%	0.0%
H ₂ Purity	99.99%	99.99%
Discharge Pressure	>1,000 psig	1,285 psig
Cost	\$6.2M	\$4.5M
Size	300-350 ft. ²	175-200 ft. ²

Using state-of-the-art aerodynamic design and structural modeling analyses, the team at Concepts NREC developed a high-performance centrifugal compressor with only 6 stages, each operating at 2,000 ft/sec tip speed. The compressor uses commercially available, proven state-of-the-art bearings, gas shaft seal and high speed gearing technology to reduce developmental risks and increase system reliability at a competitive cost.

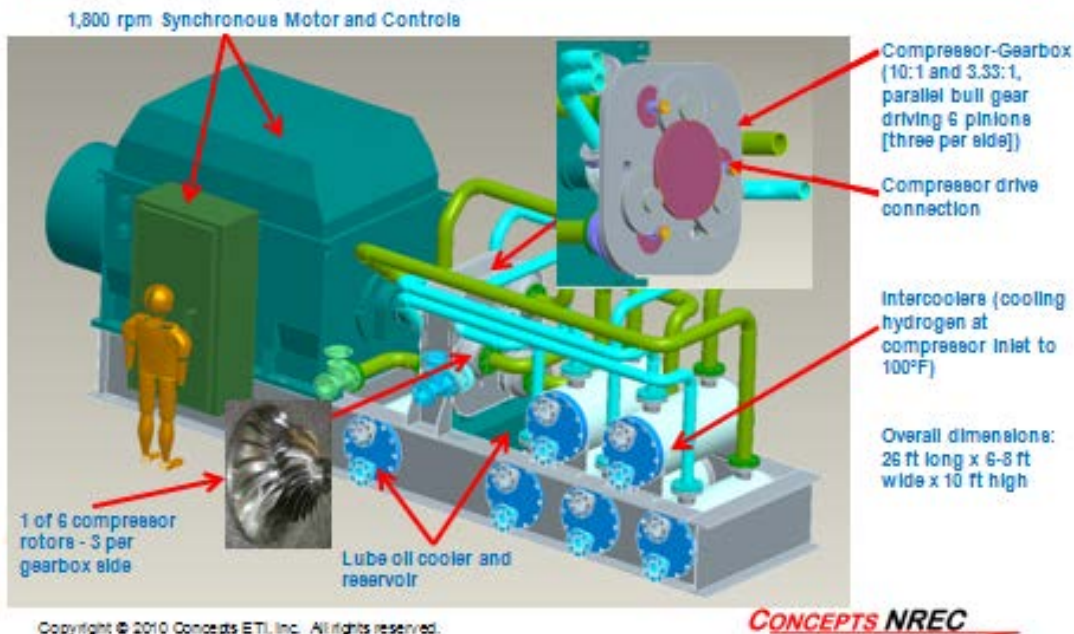


Figure 1. Hydrogen Compressor Phase I Feasibility Design Results: 240,000 kg/day; 350 to 1,285 psig; motor power is 6,300 kW

2010 FreedomCAR and Fuel Partnership Highlight

Hydrogen Selective Membranes as Reactors/Separators for Distributed H₂ Production

Media and Process Technology Inc.

Media and Process Technology Inc. (MPtech), a U.S.-based ceramic membrane developer and manufacturer, has successfully developed hydrogen selective membranes suitable as separators and/or reactors for the purification of syngas generated as part of a reforming process. The work is part of a project to develop a highly efficient and low-temperature membrane-based water gas shift (WGS) reactor for distributed hydrogen production. Membranes are fabricated by depositing a palladium (Pd) thin film over a ceramic membrane substrate at intermediate temperatures of 200 to 350°C. This temperature range is also optimal for the membranes for hydrogen separation and/or WGS reactor applications. Utilizing MPtech's commercial ceramic membrane as a substrate makes the hydrogen selective membrane much less expensive and more readily available for field applications. The Pd membrane developed is capable of delivering a high-purity hydrogen product with high hydrogen recovery ratios. Progress towards performance targets for the Pd membrane is summarized below.

- ❑ Field tested the full-scale Pd membrane with a syngas feed stream generated from diesel reforming.
- ❑ Exceeded the DOE 2010 cost target of \$1000/ft² by an order of magnitude (~\$100/ft²) due to cost savings resulting from deposition of a thin layer of Pd (~1 μm) on low-cost, off-the-shelf ceramic tubular supports.
- ❑ Improved the Pd membrane pure H₂ flux 200% from 50 SCFH/ft² to 150 SCFH/ft², within 40% of the DOE 2010 target of 250 SCFH/ft². The project has achieved a membrane cost per unit H₂ flux that is five-fold lower than the DOE target.
- ❑ Demonstrated ΔP operating capability of 1,000 PSI, 250% higher than the DOE 2010 target of 400 PSI.

Two months of testing of a full-scale integrated membrane WGS reactor showed:

- ❑ Improved hydrogen recovery from 75% to 87%, exceeding the DOE 2010 target.
- ❑ Achieved 99.99% hydrogen permeate quality, meeting the DOE 2010 target.

FY2011 plans include completion of a full-scale tubular membrane field test demonstrating >99.999% H₂ purity, >85% H₂ recovery and H₂ flux of 120 scfh/ft² @ 20 psig over 700 hours of operation.



Figure 1. Advanced hydrogen separation membranes and assembled separation unit.

2010 FreedomCAR and Fuel Partnership Highlight

New Benchmark Efficiency for Photoelectrochemical Water-Splitting Devices

NREL/DOE PEC Working Group

This NREL/DOE PEC team has achieved a new laboratory-scale performance benchmark of 18 percent solar-to-hydrogen (STH) conversion efficiency (i.e., the direct conversion efficiency of solar energy to chemical energy under standard 1-sun illumination) in its GaAs/GaInP₂ photoelectrode system (Figure 1). Renewable solar hydrogen production via photoelectrochemical (PEC) water splitting is a high-priority pathway in the U.S. Department of Energy's (DOE) hydrogen research and development portfolio. Significant improvements over the previous benchmark of 12.4 percent [1] (Figure 2) were achieved through component and device optimizations, including adding a catalyst to the GaInP₂ surface, and the use of a thin-film RuO₂ counter-electrode. Although this 18 percent STH benchmark far exceeds the DOE's 2018 efficiency target of 12 percent, technical barriers do remain in yield, durability and cost of producing this water-splitting system. The DOE is actively engaged in validating the reproducibility of this new world-record performance, and in developing pathways for addressing the remaining durability and cost issues for attaining technology readiness (i.e., 16 percent STH efficiency with 15,000 hour lifetime, and meeting the long-term DOE cost targets for hydrogen production [2].)

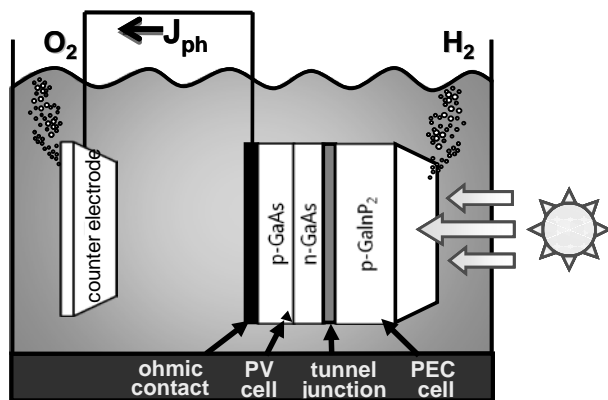


Figure 1. NREL GaAs/GaInP₂ tandem PEC device for solar hydrogen production

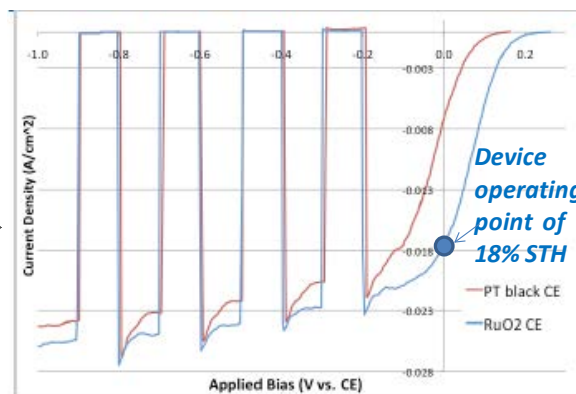


Figure 2. Recent component optimizations have resulted in GaAs/GaInP₂ device efficiencies up to 18 percent STH

¹ Oscar Khaselev, John A. Turner, A Monolithic Photovoltaic-Photoelectrochemical Device for Hydrogen Production via Water Splitting. *Science* **1998**, 280, 425-427.

² U.S. Department of Energy Fuel Cell Technologies Program "Multi-Year Research, Development and Demonstration Plan" **2007**, <http://www1.eere.energy.gov/hydrogenandfuelcells/mypp/pdfs/production.pdf>, 3.1-1.

2010 FreedomCAR and Fuel Partnership Highlight

SAE J2579 TIR and GTR Coordination

Los Alamos National Laboratory, National Renewable Energy Laboratory,
and Sandia National Laboratories

Development of performance-based and harmonized international codes, standards and regulations is critical to fair and open competition in worldwide markets for hydrogen and fuel cell vehicles. Teaming with the U.S. Department of Transportation, the U.S. Department of Energy (DOE) is an active participant in the United Nations/Economic Commission for Europe World Harmonization of Vehicle Regulations (referred to as WP.29) and its efforts on hydrogen and fuel cell vehicle regulations. Consistent, high-level, technical representation, including technical proposals and scientific data from the automobile industry, is needed in these regulatory development activities in order to ensure that North American interests and concerns are properly considered in the development of global codes, standards and regulations.

The drafting on the Global Technical Regulation (GTR) for hydrogen and fuel cell vehicles has progressed based on the technical proposals and data from the supported codes and standards organizations. A significant number of performance-based requirements, testing protocols, and research and analysis that originated from the Society of Automotive Engineers (SAE) J2579 Technical Information Report (TIR) for Fuel Systems in Fuel Cell and other Hydrogen Vehicles have been incorporated into the GTR. Both OEMs and DOE, with the national laboratories, supported the development and validation of test requirements for SAE J2579 TIR. They also provided or supported the participation of experts who provided extensive technical input to the GTR, coordinated testing required for the GTR, and worked with GTR members outside of meeting venues to resolve critical issues.

The SAE J2579 TIR working group also has made significant progress in developing a localized fire test and assessing Compressed Natural Gas cylinder failures. DOE and Sandia National Laboratories conducted several tank and early market workshops to collect data and information from hydrogen and natural gas vehicle demonstration activities along with real-world applications in Canada, Brazil, China, India and the U.S. During the past decade, the highest frequencies of natural gas cylinder failures were due to vehicle fires and the localized fire sub-set of these failures, which are not currently addressed in the standards. In the past year, the SAE J2579 TIR working group has created an industry-first localized fire-test method based on vehicle and system fire-test-data to address this failure mode.

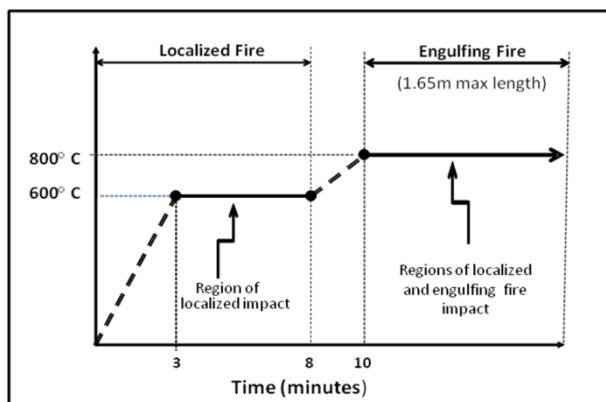


Figure 1. Preliminary Temperature Profile

2010 FreedomCAR and Fuel Partnership Highlight

SAE J2601 Hydrogen Fueling Protocol

SAE Interface Working Group, Powertech Labs

A major accomplishment in 2010 was the publication of SAE Technical Information Report (TIR) J2601 – Fueling Protocols for Light Duty Gaseous Hydrogen Surface Vehicles. This technical report provides guidance for common fueling across all gaseous hydrogen fuel cell vehicles within a reasonable time (3-5 minutes with adequate pre-cooling) while ensuring that safety limits for pressure, bulk gas temperature and density are not exceeded. This common protocol is a key enabler for future development of commercial hydrogen fueling infrastructure.

The U.S. Department of Energy (DOE) has supported the development of J2601 (Figure 1) in several ways. DOE helped fund the Multi-Client Study at Powertech Labs, in which an array of OEM hydrogen storage tanks were experimentally fueled to understand the fuel conditioning (pre-cooling) requirements as a function of initial tank conditions and fueling speed. This work guided the subsequent modeling activity of the SAE Interface Working Group members in the construction of fueling protocol lookup tables. These lookup tables form the basis of the J2601 protocol by defining how fuel is delivered to the station-vehicle interface, including pre-cooling level, pressure ramp rate and target pressure for end of fill.

DOE also funded follow-on testing at Powertech Labs for confirmation of the J2601 lookup tables (Figure 2). In this testing, a boundary set of hydrogen storage tanks were fueled over a range of conditions, including extreme hot soak and extreme cold, due to cold soak plus the cooling effect of high-load driving. This testing provided a check against the model-based lookup tables and was a pre-condition for putting the document out to the Working Group for concurrence.

SURFACE VEHICLE TECHNICAL INFORMATION REPORT <small>SAE International</small>		SAE TIR J2601 MAR2010 Issued 2010-03
Fueling Protocols for Light Duty Gaseous Hydrogen Surface Vehicles*		
RATIONALE The implementation of hydrogen vehicles into the market necessitates having a universal fueling protocol for every vehicle. The goal is to achieve a "customer acceptable" fueling, which means a full tank of hydrogen within a reasonable amount of time without exceeding the temperature, pressure and density (SDC) limits. However, fueling performance may be limited by the pre-cooling capacity of the station dispenser. SAE TIR J2601 establishes industry-wide fueling protocol guidelines for the fueling of gaseous hydrogen into on-road passenger vehicles operating with nominal working pressures (NWP) of 35 MPa and 70 MPa. Fueling stations should employ fueling algorithms and equipment to conduct the fueling process within these guidelines. Vehicles filled at stations using these protocols should be designed appropriately for fueling according to these guidelines. SAE TIR J2579 provides guidance for qualifying the vehicle hydrogen storage system (HSS) for operation at specific nominal working pressures.		
TABLE OF CONTENTS		
1.	SCOPE.....	2
2.	REFERENCES.....	4
3.	DEFINITIONS.....	6
4.	ABBREVIATIONS AND SYMBOLS.....	9
5.	GENERAL REQUIREMENTS FOR FUEL SYSTEM AND INTERFACE.....	10
6.	DEFINITION OF FUELING STATION DISPENSER TYPES.....	11
7.	COMMON PROCEDURES FOR COMPRESSED HYDROGEN FUELING.....	12
8.	NON-COMMUNICATION FUELING PROCEDURE.....	15
9.	COMMUNICATION FUELING PROCEDURE.....	20
10.	PERFORMANCE TESTS TO VERIFY COMPLIANCE WITH FUELING PROTOCOLS.....	22
11.	NOTES.....	24
11.1	Marginal Indices.....	24
<small>SAE Technical Standards Board Rules provide that "This report is published by SAE to advance the state of technical and engineering sciences. The use of this report is advisory; it is not applicable and liability for any technical use, including any patent infringement arising therefrom, is the sole responsibility of the user." SAE reserves each technical report or standard every five years at which time it may be reaffirmed, revised, or cancelled. SAE invites your written comments and suggestions. Copyright © 2010 SAE International. All rights reserved. No part of this publication may be reproduced, stored in a retrieval system or transmitted, in any form or by any means, electronic, mechanical, photocopying, recording, or otherwise, without the prior written permission of SAE. TO PLACE A DOCUMENT ORDER: Tel: 877-606-7323 (toll free USA and Canada) Tel: +1 724-776-4800 (outside USA) Fax: 724-776-4789 Email: CustomerService@sae.org SAE values your input. To provide feedback on this Technical Report, please visit http://www.sae.org/technical/standards/J2601_201003</small>		

Figure 1. SAE TIR J2601 – March 2010

Type A (-40°C)																																																																																																																																																																																																																																																																																																																					
A-70 1-7kg	Actual Fueling Duration (min) Add intermediate leak check times up to 18 sec after every 25MPa increase in fueling pressure Initial Tank Pressure, P _i (BPSI)																																																																																																																																																																																																																																																																																																																				
Ambient Temperature, T _{amb} (°C)	<table border="1"> <tr> <th></th> <th>2</th> <th>5</th> <th>10</th> <th>15</th> <th>20</th> <th>25</th> <th>30</th> <th>35</th> <th>40</th> <th>50</th> <th>60</th> <th>70</th> <th>> 70</th> </tr> <tr> <th>> 50</th> <td>notched</td><td>notched</td><td>notched</td><td>notched</td><td>notched</td><td>notched</td><td>notched</td><td>notched</td><td>notched</td><td>notched</td><td>notched</td><td>notched</td><td>notched</td> </tr> <tr> <th>45</th> <td>5</td><td>4</td><td>4</td><td>4</td><td>3</td><td>3</td><td>2</td><td>2</td><td>1</td><td>1</td><td>0</td><td>0</td><td>notched</td> </tr> <tr> <th>40</th> <td>4</td><td>3</td><td>3</td><td>3</td><td>3</td><td>2</td><td>2</td><td>1</td><td>1</td><td>0</td><td>0</td><td>0</td><td>notched</td> </tr> <tr> <th>35</th> <td>3</td><td>3</td><td>3</td><td>2</td><td>2</td><td>2</td><td>1</td><td>1</td><td>0</td><td>0</td><td>0</td><td>0</td><td>notched</td> </tr> <tr> <th>30</th> <td>3</td><td>2</td><td>2</td><td>2</td><td>2</td><td>1</td><td>1</td><td>0</td><td>0</td><td>0</td><td>0</td><td>0</td><td>notched</td> </tr> <tr> <th>25</th> <td>3</td><td>2</td><td>2</td><td>2</td><td>2</td><td>1</td><td>1</td><td>0</td><td>0</td><td>0</td><td>0</td><td>0</td><td>notched</td> </tr> <tr> <th>20</th> <td>3</td><td>2</td><td>2</td><td>2</td><td>2</td><td>1</td><td>1</td><td>0</td><td>0</td><td>0</td><td>0</td><td>0</td><td>notched</td> </tr> <tr> <th>15</th> <td>2</td><td>2</td><td>2</td><td>2</td><td>2</td><td>1</td><td>1</td><td>0</td><td>0</td><td>0</td><td>0</td><td>0</td><td>notched</td> </tr> <tr> <th>10</th> <td>2</td><td>2</td><td>2</td><td>2</td><td>2</td><td>1</td><td>1</td><td>0</td><td>0</td><td>0</td><td>0</td><td>0</td><td>notched</td> </tr> <tr> <th>5</th> <td>2</td><td>2</td><td>2</td><td>2</td><td>2</td><td>1</td><td>1</td><td>0</td><td>0</td><td>0</td><td>0</td><td>0</td><td>notched</td> </tr> <tr> <th>0</th> <td>2</td><td>2</td><td>2</td><td>2</td><td>2</td><td>1</td><td>1</td><td>0</td><td>0</td><td>0</td><td>0</td><td>0</td><td>notched</td> </tr> <tr> <th>-5</th> <td>2</td><td>2</td><td>2</td><td>2</td><td>2</td><td>1</td><td>1</td><td>0</td><td>0</td><td>0</td><td>0</td><td>0</td><td>notched</td> </tr> <tr> <th>-10</th> <td>2</td><td>2</td><td>2</td><td>2</td><td>2</td><td>1</td><td>1</td><td>0</td><td>0</td><td>0</td><td>0</td><td>0</td><td>notched</td> </tr> <tr> <th>-15</th> <td>2</td><td>2</td><td>2</td><td>2</td><td>2</td><td>1</td><td>1</td><td>0</td><td>0</td><td>0</td><td>0</td><td>0</td><td>notched</td> </tr> <tr> <th>-20</th> <td>2</td><td>2</td><td>2</td><td>2</td><td>2</td><td>1</td><td>1</td><td>0</td><td>0</td><td>0</td><td>0</td><td>0</td><td>notched</td> </tr> <tr> <th>-25</th> <td>2</td><td>2</td><td>2</td><td>2</td><td>2</td><td>1</td><td>1</td><td>0</td><td>0</td><td>0</td><td>0</td><td>0</td><td>notched</td> </tr> <tr> <th>-30</th> <td>2</td><td>2</td><td>2</td><td>2</td><td>2</td><td>1</td><td>1</td><td>0</td><td>0</td><td>0</td><td>0</td><td>0</td><td>notched</td> </tr> <tr> <th>-35</th> <td>2</td><td>2</td><td>2</td><td>2</td><td>2</td><td>1</td><td>1</td><td>0</td><td>0</td><td>0</td><td>0</td><td>0</td><td>notched</td> </tr> <tr> <th>-40</th> <td>2</td><td>2</td><td>2</td><td>2</td><td>2</td><td>1</td><td>1</td><td>0</td><td>0</td><td>0</td><td>0</td><td>0</td><td>notched</td> </tr> <tr> <th>< -40</th> <td>notched</td><td>notched</td><td>notched</td><td>notched</td><td>notched</td><td>notched</td><td>notched</td><td>notched</td><td>notched</td><td>notched</td><td>notched</td><td>notched</td><td>notched</td> </tr> </table>		2	5	10	15	20	25	30	35	40	50	60	70	> 70	> 50	notched	45	5	4	4	4	3	3	2	2	1	1	0	0	notched	40	4	3	3	3	3	2	2	1	1	0	0	0	notched	35	3	3	3	2	2	2	1	1	0	0	0	0	notched	30	3	2	2	2	2	1	1	0	0	0	0	0	notched	25	3	2	2	2	2	1	1	0	0	0	0	0	notched	20	3	2	2	2	2	1	1	0	0	0	0	0	notched	15	2	2	2	2	2	1	1	0	0	0	0	0	notched	10	2	2	2	2	2	1	1	0	0	0	0	0	notched	5	2	2	2	2	2	1	1	0	0	0	0	0	notched	0	2	2	2	2	2	1	1	0	0	0	0	0	notched	-5	2	2	2	2	2	1	1	0	0	0	0	0	notched	-10	2	2	2	2	2	1	1	0	0	0	0	0	notched	-15	2	2	2	2	2	1	1	0	0	0	0	0	notched	-20	2	2	2	2	2	1	1	0	0	0	0	0	notched	-25	2	2	2	2	2	1	1	0	0	0	0	0	notched	-30	2	2	2	2	2	1	1	0	0	0	0	0	notched	-35	2	2	2	2	2	1	1	0	0	0	0	0	notched	-40	2	2	2	2	2	1	1	0	0	0	0	0	notched	< -40	notched																																						
	2	5	10	15	20	25	30	35	40	50	60	70	> 70																																																																																																																																																																																																																																																																																																								
> 50	notched	notched	notched	notched	notched	notched	notched	notched	notched	notched	notched	notched	notched																																																																																																																																																																																																																																																																																																								
45	5	4	4	4	3	3	2	2	1	1	0	0	notched																																																																																																																																																																																																																																																																																																								
40	4	3	3	3	3	2	2	1	1	0	0	0	notched																																																																																																																																																																																																																																																																																																								
35	3	3	3	2	2	2	1	1	0	0	0	0	notched																																																																																																																																																																																																																																																																																																								
30	3	2	2	2	2	1	1	0	0	0	0	0	notched																																																																																																																																																																																																																																																																																																								
25	3	2	2	2	2	1	1	0	0	0	0	0	notched																																																																																																																																																																																																																																																																																																								
20	3	2	2	2	2	1	1	0	0	0	0	0	notched																																																																																																																																																																																																																																																																																																								
15	2	2	2	2	2	1	1	0	0	0	0	0	notched																																																																																																																																																																																																																																																																																																								
10	2	2	2	2	2	1	1	0	0	0	0	0	notched																																																																																																																																																																																																																																																																																																								
5	2	2	2	2	2	1	1	0	0	0	0	0	notched																																																																																																																																																																																																																																																																																																								
0	2	2	2	2	2	1	1	0	0	0	0	0	notched																																																																																																																																																																																																																																																																																																								
-5	2	2	2	2	2	1	1	0	0	0	0	0	notched																																																																																																																																																																																																																																																																																																								
-10	2	2	2	2	2	1	1	0	0	0	0	0	notched																																																																																																																																																																																																																																																																																																								
-15	2	2	2	2	2	1	1	0	0	0	0	0	notched																																																																																																																																																																																																																																																																																																								
-20	2	2	2	2	2	1	1	0	0	0	0	0	notched																																																																																																																																																																																																																																																																																																								
-25	2	2	2	2	2	1	1	0	0	0	0	0	notched																																																																																																																																																																																																																																																																																																								
-30	2	2	2	2	2	1	1	0	0	0	0	0	notched																																																																																																																																																																																																																																																																																																								
-35	2	2	2	2	2	1	1	0	0	0	0	0	notched																																																																																																																																																																																																																																																																																																								
-40	2	2	2	2	2	1	1	0	0	0	0	0	notched																																																																																																																																																																																																																																																																																																								
< -40	notched	notched	notched	notched	notched	notched	notched	notched	notched	notched	notched	notched	notched																																																																																																																																																																																																																																																																																																								
Type B (-20°C)																																																																																																																																																																																																																																																																																																																					
B-70 1-7kg	Actual Fueling Duration (min) Add intermediate leak check times up to 18 sec after every 25MPa increase in fueling pressure Initial Tank Pressure, P _i (BPSI)																																																																																																																																																																																																																																																																																																																				
Ambient Temperature, T _{amb} (°C)	<table border="1"> <tr> <th></th> <th>3</th> <th>5</th> <th>10</th> <th>15</th> <th>20</th> <th>25</th> <th>30</th> <th>35</th> <th>40</th> <th>50</th> <th>60</th> <th>70</th> <th>> 70</th> </tr> <tr> <th>> 50</th> <td>notched</td><td>notched</td><td>notched</td><td>notched</td><td>notched</td><td>notched</td><td>notched</td><td>notched</td><td>notched</td><td>notched</td><td>notched</td><td>notched</td><td>notched</td> </tr> <tr> <th>50</th> <td>41</td><td>39</td><td>36</td><td>33</td><td>30</td><td>24</td><td>18</td><td>13</td><td>7</td><td>1</td><td>0</td><td>0</td><td>notched</td> </tr> <tr> <th>45</th> <td>29</td><td>28</td><td>25</td><td>23</td><td>21</td><td>17</td><td>13</td><td>9</td><td>5</td><td>1</td><td>0</td><td>0</td><td>notched</td> </tr> <tr> <th>40</th> <td>21</td><td>20</td><td>19</td><td>17</td><td>16</td><td>13</td><td>10</td><td>7</td><td>4</td><td>1</td><td>0</td><td>0</td><td>notched</td> </tr> <tr> <th>35</th> <td>15</td><td>14</td><td>14</td><td>13</td><td>12</td><td>10</td><td>7</td><td>5</td><td>3</td><td>1</td><td>0</td><td>0</td><td>notched</td> </tr> <tr> <th>30</th> <td>11</td><td>11</td><td>11</td><td>10</td><td>10</td><td>8</td><td>6</td><td>4</td><td>2</td><td>0</td><td>0</td><td>0</td><td>notched</td> </tr> <tr> <th>25</th> <td>11</td><td>10</td><td>10</td><td>9</td><td>8</td><td>6</td><td>5</td><td>3</td><td>1</td><td>0</td><td>0</td><td>0</td><td>notched</td> </tr> <tr> <th>20</th> <td>8</td><td>8</td><td>8</td><td>7</td><td>6</td><td>5</td><td>4</td><td>2</td><td>1</td><td>0</td><td>0</td><td>0</td><td>notched</td> </tr> <tr> <th>15</th> <td>7</td><td>6</td><td>6</td><td>5</td><td>5</td><td>4</td><td>3</td><td>2</td><td>1</td><td>0</td><td>0</td><td>0</td><td>notched</td> </tr> <tr> <th>10</th> <td>6</td><td>5</td><td>5</td><td>4</td><td>4</td><td>3</td><td>2</td><td>1</td><td>0</td><td>0</td><td>0</td><td>0</td><td>notched</td> </tr> <tr> <th>5</th> <td>5</td><td>5</td><td>4</td><td>4</td><td>3</td><td>3</td><td>2</td><td>1</td><td>0</td><td>0</td><td>0</td><td>0</td><td>notched</td> </tr> <tr> <th>0</th> <td>5</td><td>5</td><td>4</td><td>4</td><td>3</td><td>3</td><td>2</td><td>1</td><td>0</td><td>0</td><td>0</td><td>0</td><td>notched</td> </tr> <tr> <th>-5</th> <td>5</td><td>5</td><td>4</td><td>4</td><td>3</td><td>3</td><td>2</td><td>1</td><td>0</td><td>0</td><td>0</td><td>0</td><td>notched</td> </tr> <tr> <th>-10</th> <td>5</td><td>5</td><td>4</td><td>4</td><td>3</td><td>3</td><td>2</td><td>1</td><td>0</td><td>0</td><td>0</td><td>0</td><td>notched</td> </tr> <tr> <th>-15</th> <td>5</td><td>5</td><td>4</td><td>4</td><td>3</td><td>3</td><td>2</td><td>1</td><td>0</td><td>0</td><td>0</td><td>0</td><td>notched</td> </tr> <tr> <th>-20</th> <td>5</td><td>5</td><td>4</td><td>4</td><td>3</td><td>3</td><td>2</td><td>1</td><td>0</td><td>0</td><td>0</td><td>0</td><td>notched</td> </tr> <tr> <th>-25</th> <td>5</td><td>5</td><td>4</td><td>4</td><td>3</td><td>3</td><td>2</td><td>1</td><td>0</td><td>0</td><td>0</td><td>0</td><td>notched</td> </tr> <tr> <th>-30</th> <td>5</td><td>5</td><td>4</td><td>4</td><td>3</td><td>3</td><td>2</td><td>1</td><td>0</td><td>0</td><td>0</td><td>0</td><td>notched</td> </tr> <tr> <th>-35</th> <td>5</td><td>5</td><td>4</td><td>4</td><td>3</td><td>3</td><td>2</td><td>1</td><td>0</td><td>0</td><td>0</td><td>0</td><td>notched</td> </tr> <tr> <th>-40</th> <td>5</td><td>5</td><td>4</td><td>4</td><td>3</td><td>3</td><td>2</td><td>1</td><td>0</td><td>0</td><td>0</td><td>0</td><td>notched</td> </tr> <tr> <th>< -40</th> <td>notched</td><td>notched</td><td>notched</td><td>notched</td><td>notched</td><td>notched</td><td>notched</td><td>notched</td><td>notched</td><td>notched</td><td>notched</td><td>notched</td><td>notched</td> </tr> </table>		3	5	10	15	20	25	30	35	40	50	60	70	> 70	> 50	notched	50	41	39	36	33	30	24	18	13	7	1	0	0	notched	45	29	28	25	23	21	17	13	9	5	1	0	0	notched	40	21	20	19	17	16	13	10	7	4	1	0	0	notched	35	15	14	14	13	12	10	7	5	3	1	0	0	notched	30	11	11	11	10	10	8	6	4	2	0	0	0	notched	25	11	10	10	9	8	6	5	3	1	0	0	0	notched	20	8	8	8	7	6	5	4	2	1	0	0	0	notched	15	7	6	6	5	5	4	3	2	1	0	0	0	notched	10	6	5	5	4	4	3	2	1	0	0	0	0	notched	5	5	5	4	4	3	3	2	1	0	0	0	0	notched	0	5	5	4	4	3	3	2	1	0	0	0	0	notched	-5	5	5	4	4	3	3	2	1	0	0	0	0	notched	-10	5	5	4	4	3	3	2	1	0	0	0	0	notched	-15	5	5	4	4	3	3	2	1	0	0	0	0	notched	-20	5	5	4	4	3	3	2	1	0	0	0	0	notched	-25	5	5	4	4	3	3	2	1	0	0	0	0	notched	-30	5	5	4	4	3	3	2	1	0	0	0	0	notched	-35	5	5	4	4	3	3	2	1	0	0	0	0	notched	-40	5	5	4	4	3	3	2	1	0	0	0	0	notched	< -40	notched																								
	3	5	10	15	20	25	30	35	40	50	60	70	> 70																																																																																																																																																																																																																																																																																																								
> 50	notched	notched	notched	notched	notched	notched	notched	notched	notched	notched	notched	notched	notched																																																																																																																																																																																																																																																																																																								
50	41	39	36	33	30	24	18	13	7	1	0	0	notched																																																																																																																																																																																																																																																																																																								
45	29	28	25	23	21	17	13	9	5	1	0	0	notched																																																																																																																																																																																																																																																																																																								
40	21	20	19	17	16	13	10	7	4	1	0	0	notched																																																																																																																																																																																																																																																																																																								
35	15	14	14	13	12	10	7	5	3	1	0	0	notched																																																																																																																																																																																																																																																																																																								
30	11	11	11	10	10	8	6	4	2	0	0	0	notched																																																																																																																																																																																																																																																																																																								
25	11	10	10	9	8	6	5	3	1	0	0	0	notched																																																																																																																																																																																																																																																																																																								
20	8	8	8	7	6	5	4	2	1	0	0	0	notched																																																																																																																																																																																																																																																																																																								
15	7	6	6	5	5	4	3	2	1	0	0	0	notched																																																																																																																																																																																																																																																																																																								
10	6	5	5	4	4	3	2	1	0	0	0	0	notched																																																																																																																																																																																																																																																																																																								
5	5	5	4	4	3	3	2	1	0	0	0	0	notched																																																																																																																																																																																																																																																																																																								
0	5	5	4	4	3	3	2	1	0	0	0	0	notched																																																																																																																																																																																																																																																																																																								
-5	5	5	4	4	3	3	2	1	0	0	0	0	notched																																																																																																																																																																																																																																																																																																								
-10	5	5	4	4	3	3	2	1	0	0	0	0	notched																																																																																																																																																																																																																																																																																																								
-15	5	5	4	4	3	3	2	1	0	0	0	0	notched																																																																																																																																																																																																																																																																																																								
-20	5	5	4	4	3	3	2	1	0	0	0	0	notched																																																																																																																																																																																																																																																																																																								
-25	5	5	4	4	3	3	2	1	0	0	0	0	notched																																																																																																																																																																																																																																																																																																								
-30	5	5	4	4	3	3	2	1	0	0	0	0	notched																																																																																																																																																																																																																																																																																																								
-35	5	5	4	4	3	3	2	1	0	0	0	0	notched																																																																																																																																																																																																																																																																																																								
-40	5	5	4	4	3	3	2	1	0	0	0	0	notched																																																																																																																																																																																																																																																																																																								
< -40	notched	notched	notched	notched	notched	notched	notched	notched	notched	notched	notched	notched	notched																																																																																																																																																																																																																																																																																																								

Figure 2. 70MPa Fueling Times

2010 FreedomCAR and Fuel Partnership Highlight

Cryo-Compressed Tank Exceeds 2015 Weight and Volume Targets

Lawrence Livermore National Laboratory

Cryo-compressed hydrogen storage is projected to exceed DOE 2015 hydrogen storage weight and volume targets, however, reducing costs is still a challenge. Based on results from the existing third generation, 10.4 kg useable capacity, cryo-compressed tank, a scaled down tank with 5.6 kg of useable hydrogen is projected to achieve 5.7 wt. percent and 43 g/liter. This surpasses the 2015 targets of 5.5 wt. percent and 40 g/liter. Estimated costs are \$12/kWh (DOE 2010 target is \$4/kWh) when fabricated in high volume (500,000 per year), which compares favorably to other hydrogen storage technologies.

To achieve maximum capacity, the tank must be filled with liquid hydrogen. If liquid hydrogen is not available, the tank can be filled with high pressure (275 bar) compressed hydrogen, but its capacity is lowered to approximately one-fourth of its maximum capacity.

Dormancy (the length of time a tank can sit idle before venting occurs) is a concern for cryo-compressed tanks and is a function the efficiency of the tank insulation to prevent heat leakage from the environment into the tank. The constructed 10.4 kg useable capacity tank can sit for 8 days with no venting. Studies of para-ortho hydrogen conversion indicate this endothermic process can result in a doubling of the dormancy. The results also indicate that driving only 3-4 miles a day lowers the internal tank pressure and should eliminate venting altogether.



Figure 1. Generation 2 cryo-compressed hydrogen storage tank prototype (left). Generation 3 cryo-compressed hydrogen storage tank prototype (right).

2010 FreedomCAR and Fuel Partnership Highlight

12 Weight Percent Hydrogen Reversibility Demonstrated for Magnesium Borohydride

University of Hawaii, Sandia National Laboratories

Demonstrated reversibility of magnesium borohydride ($\text{Mg}(\text{BH}_4)_2$) has reinvigorated interest in high-capacity hydrogen storage materials. $\text{Mg}(\text{BH}_4)_2$ is a high-capacity material (14.8 wt. percent) that has been extensively studied. However, only modest reversibility had been demonstrated. Researchers identified a stable intermediate desorption species $\text{Mg}(\text{B}_{12}\text{H}_{12})_2$, that prevented extensive reversibility of the material. Reversibility of a material is necessary to allow direct refueling on a vehicle.

The team demonstrated that the stable intermediate can be overcome using 950 atmospheres of hydrogen pressure at 400°C to recharge the material and achieve 12 wt. percent reversible capacity, see Figure 1. Results indicate higher capacities might be realized. The high pressures and temperature of this method are too severe for use onboard vehicles but demonstrate there are possible pathways to achieve reversibility.

The team also demonstrated 2.4 wt. percent reversible capacity for $\text{Mg}(\text{BH}_4)_2$ using milder conditions. By only partially desorbing hydrogen, they avoid formation of the stable intermediate, $\text{Mg}(\text{B}_{12}\text{H}_{12})_2$, and are thus able to recharge the products under milder conditions (<100 atmospheres and 200°C). The combined results indicate that there may be pathways to circumvent and/or overcome apparent barriers to high-capacity hydrogen storage materials.

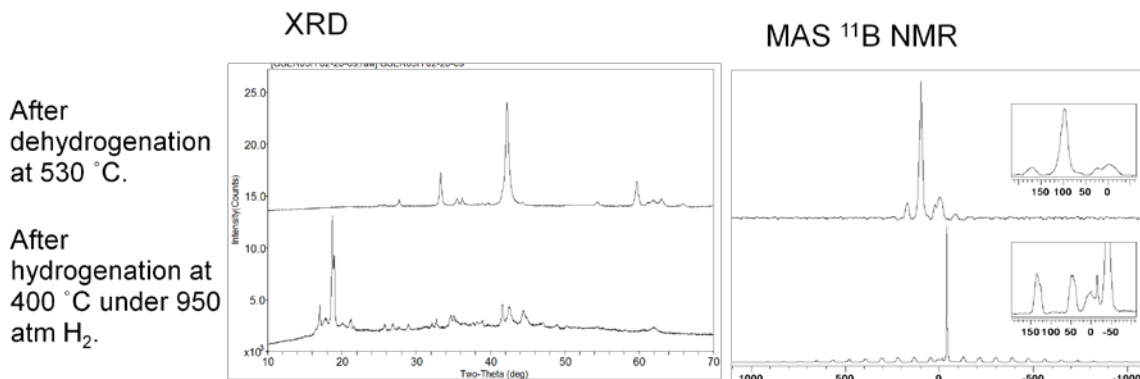


Figure 1. X-ray diffraction and NMR analyses of dehydrogenated (top) and subsequent rehydrogenated (bottom) materials show essentially complete recharging of magnesium borohydride.

2010 FreedomCAR and Fuel Partnership Highlight

“Optimized” Sorbents Designed and Synthesized for Hydrogen Storage

Texas A&M University

Metal organic frameworks (MOFs), large porous networks composed of metal ions and organic molecules, are promising materials for hydrogen storage. Interest stems from the following typical properties: a) favorable hydrogen uptake/release rates, b) reversibility for storage, and c) potential for low-cost synthetic scalability. One weakness is the current need for cryogenic temperature (e.g. 77K) for significant hydrogen storage. Until recently, approaches for the discovery of new MOF sorbents have been largely empirical (i.e., via trial-and-error). “Optimized” sorbents are designed by using linker type and composition “to tune” pore size distribution, surface area and MOF composition to impact hydrogen storage gravimetric and volumetric performance. Rational design of the sorbent structure was shown to yield high surface area, high-capacity sorbents.

During 2010, the Texas A&M team designed and synthesized a series of MOF structures (termed PCN-6X) using a variety of isostructural linkers to obtain high surface area (Figure 1a and 1b). Measurements on these MOFs confirms the expected ultra-high surface areas, up to 6000 m²/g for PCN-68, among the highest reported. Correspondingly, the team achieved exceptional excess gravimetric and volumetric H₂ uptakes, up to 6.8 percent by weight at 77K and 50 bar for PCN-68 (Figure 1c) and 35.0 g/L (based on crystal density) at 77K and 33 bar for PCN-61 (Figure 1d).

The team at Texas A&M is balancing design of materials with high surface area (that can result in low volumetric capacity) to optimize both gravimetric and volumetric performance. However, higher surface area materials also provide an opportunity for further addition of hydrogen-binding groups, increasing both the heat of hydrogen adsorption and density. Research along this theme is currently under way, and promises to improve the volumetric capacity at temperatures higher than 77K.

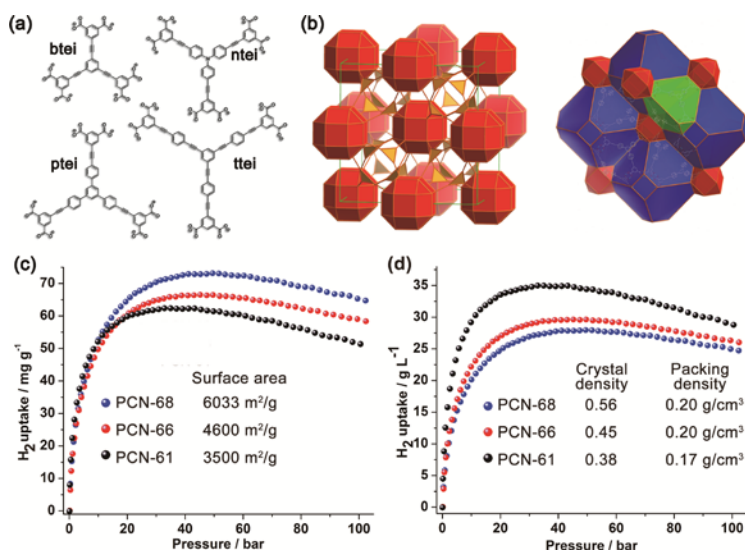


Figure 1: (a) Isostructural MOF linkers: btei (PCN-61), ntei (PCN-66), ptei (PCN-68) and ttei (PCN-610). (b) Reinforced joints around mesocavity in PCN-68. (c) Gravimetric and (d) volumetric H₂ uptake in PCN-6X series at 77K.

2010 FreedomCAR and Fuel Partnership Highlight

New Class of Lightweight Metal Hydrides Show Promise for Hydrogen Storage

The Ohio State University

A new class of hydrogen storage materials offers both high capacity and potential reversibility. New materials with larger hydrogen storage capacities are needed to reach the FreedomCAR and Fuel Partnership hydrogen storage targets for automotive applications. Researchers are investigating aluminoboranes, novel hydrides formed by boron (B) and aluminum (Al), with hydrogen capacities of 13-15 wt. percent. This work includes the synthesis of several AlB_yH_x compounds and their characterization by volumetric and calorimetric methods, mass spectrometry, infrared spectroscopy and nuclear magnetic resonance (NMR). The amorphous compound ($\text{AlB}_4\text{H}_{11}$) was prepared and its hydrogen release was studied. This hydride starts to release hydrogen above 100°C with over 11 wt. percent desorbed by 400°C . $\text{AlB}_4\text{H}_{11}$ exhibited partial reversibility of the 6 wt. percent hydrogen gas released below 250°C by absorbing hydrogen under moderate conditions (see Figure 1) to reform the original phases. The researchers confirmed they had regenerated the original composition using boron NMR (see Figure 2).

During the past year, the Ohio State University team has been investigating additional aluminoborane compounds including $\text{AlB}_5\text{H}_{12}$ and $\text{AlB}_6\text{H}_{13}$. The intent is to compare the properties and structures of these different aluminoboranes in order to identify their hydrogenation and dehydrogenation mechanisms. Catalytic screening and additional measurements are in progress to find pathways that reduce desorption temperatures and improve reversibility of aluminoborane compounds.

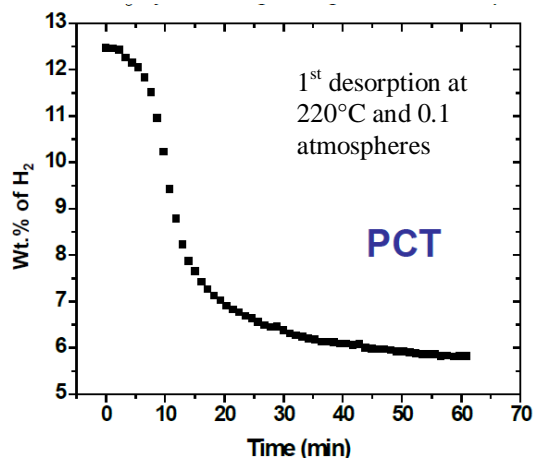


Figure 1. $\text{AlB}_4\text{H}_{11}$ releases 6.5 wt. percent hydrogen at 220°C with good kinetics.

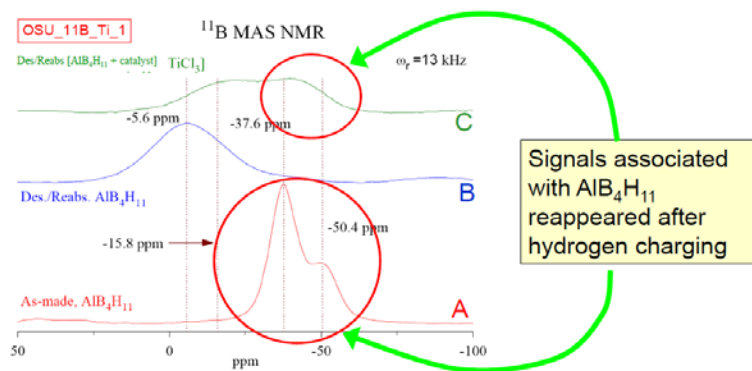


Figure 2. Solid state NMR shows partial reversibility under moderate conditions of 200°C , 90 atmospheres hydrogen for 5 hours.

2010 FreedomCAR and Fuel Partnership Highlight

New Techniques for Safe Hydride Containment

Sandia National Laboratories

Materials-based hydrogen storage tanks are less likely to fail when mechanical and chemical mitigation strategies are employed. Successful commercialization of metal-hydride-based hydrogen storage materials requires codes and standards. A technical understanding of material properties and identification of the system-level risks and possible hazard mitigation strategies are required to create appropriate codes and standards. To meet this goal, the Sandia National Laboratories (SNL) team developed theoretical and experimental methods and procedures to accomplish three tasks: 1.) quantifying the fundamental contamination processes, 2.) predicting processes during accident scenarios and 3.) identifying and demonstrating hazard mitigation strategies to enable the design, safe handling and operation of solid-state hydrogen storage systems.

During 2010, the team focused on the last two items. Initial Failure Mode and Effects Analysis (FMEA) indicated two significant failure modes of interest for further consequence analysis: breach-in-tank and fire impingement. The evolution of hydrogen from an alane bed reduces the extent of oxidation reaction during a breach-in-tank scenario; while in contrast, materials such as catalyzed sodium alanate proved to be much more reactive after exposure to dry air. Additionally, axisymmetric models revealed that in a pool fire scenario involving sodium alanate, system over-temperature and over-pressure can occur rapidly. As a result of these analyses, the team identified and tested two mitigation strategies including polymer additives to limit the extent and rate of oxidation reactions (Figure 1), and thermal shielding to limit the rate of temperature rise during a fire (Figure 2).

The team will continue to focus on optimizing mitigation strategies. Composite polymeric materials will be used to tune the structural properties of the mitigation materials. The mitigation strategies will be tested at full scale under “normal” life cycle conditions, and a design-for-safety toolkit for future advanced storage systems will be developed in collaboration with storage system engineers. The costs and effects on performance these mitigation strategies impose will also be investigated.

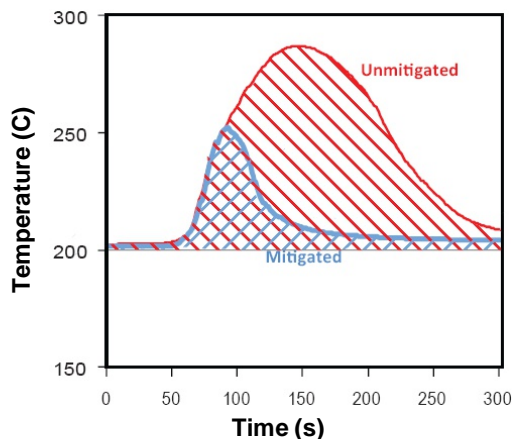


Figure 1. Polymer addition reduces energy released by 70 percent.

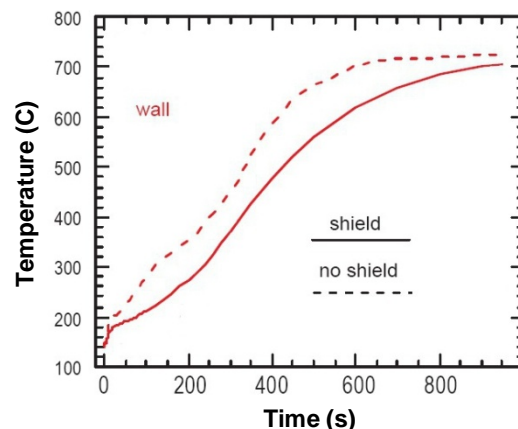


Figure 2. Modeling shows that shielding delays tank temperature rise.

2010 FreedomCAR and Fuel Partnership Highlight

Performance and Cost Analyses Accelerate Development of Hydrogen Storage Technologies

Argonne National Laboratory, TIAX, LLC

High-level performance and cost analyses have guided DOE research strategies and expedited improvement of storage technologies. The DOE applied hydrogen-storage program studies a wide range of technologies with the potential to store sufficient hydrogen to enable a driving range greater than 300 miles. These technologies include physical storage (e.g., compressed gas, cryogenic liquid/gas) and material-based storage (e.g., reversible hydrides, sorbents and regenerable chemical storage compounds). The FreedomCAR and Fuel Partnership hydrogen storage performance targets are based upon a complete storage system. System performance and cost analysis tools are essential for evaluating hydrogen storage technologies by projecting system performance and large volume (i.e. 500,000 units/yr) manufacturing cost based on the material's operating properties, and then identifying the most valuable areas for improvement.

The teams analyzed the impact of multiple compressed gas tank systems and tank constructions (type 3 versus type 4) on performance and costs at 350 bar and 700 bar (see Figure 1 for 700 bar vessel system performance). They have also made significant updates in their assessments of various storage systems (e.g., cryo-compressed, adsorbents and chemical systems). Figure 2 shows the projected costs for several systems at large-scale manufacturing volumes. The team also evaluated the efficiency, greenhouse gas emissions and total ownership cost. These results provide an important indication in the status of the hydrogen storage options and their remaining gaps.

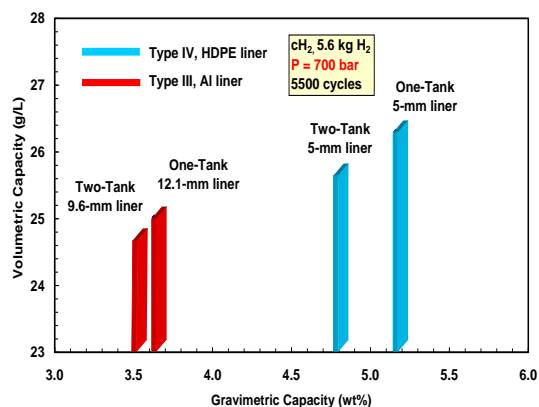


Figure 1. Predicted gravimetric and volumetric capacities for 700-bar compressed gas tanks.

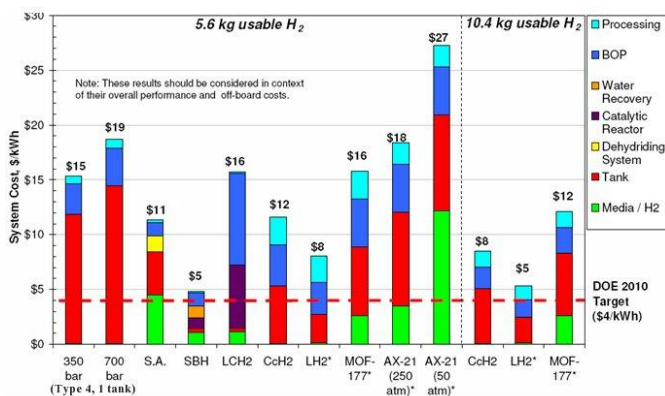


Figure 2. Projected cost comparison for high-volume production of on-board hydrogen storage systems. Storage basis, left to right: compressed gas at 350, 700 bar, sodium alanate, sodium borohydride H₂, liquid hydrogen carrier, cryo compressed, Liquid H₂, MOF cryo-absorbent, activated carbon.

2010 FreedomCAR and Fuel Partnership Highlight

Universal Vehicle Energy-Use Communications Technology Developed

Argonne National Laboratory, University of Michigan-Dearborn

A software-defined radio (SDR) is being developed for plug-in vehicle-grid interface and connectivity to the electric power supply. A breadboard version of this technology has been demonstrated for potential use in energy management processes. An important aspect of grid connectivity is the ability to communicate between the vehicle and the grid operator. This enables energy use management and billing for electricity use independent of location.

The technology, which was demonstrated in prototype form in FY 2010, acts like a flexible modem to support communication irrespective of where the vehicle is located around the world. The prototype was demonstrated on a non-optimized evaluation board, and the technical details are listed below.

The successful development has led to a plan to develop and test a one-chip communication solution in FY 2011.

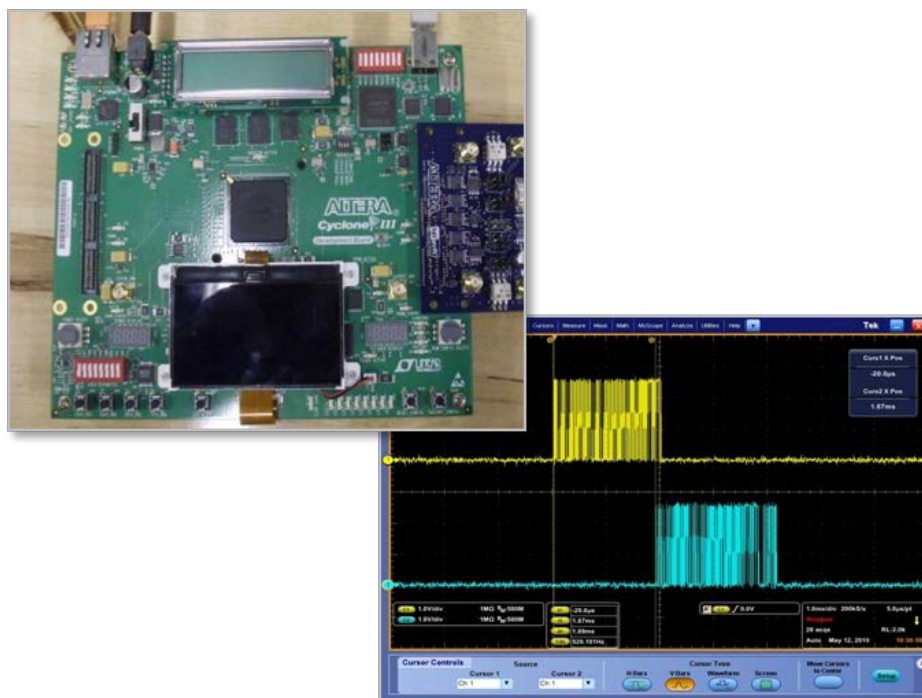


Figure 1. Software Defined Radio (SDR); evaluation board and OFDM modulation/demodulation example

- Enables Single Chip Communication Solution for Vehicle-Grid Communication
- Flexible Universal Metropolitan Area Network
- OFDM modulation achieved in 16,000 gate FPGA
- Programmed for Zigbee (IEEE 802.15.4-2006)
- UMAN (IEEE 802.15.4g); flexible baseband frequency

2010 FreedomCAR and Fuel Partnership Highlight

Compact Low-Cost Revenue-Grade Sub-Meter Demonstrated

Argonne National Laboratory, Viola Enterprises, 2G Engineering

This research team developed a compact current monitor with communication capability that enables differential electricity pricing. The FreedomCAR and Fuel Partnership Grid Interaction Technical Team (GITTT) is focused on the plug-in vehicle-grid interface and connectivity to the electric power supply. An important aspect of grid connectivity (and one that is required in some states) is the ability to separately meter electricity used by a plug-in vehicle – to enable differential pricing and encourage off-peak energy consumption.

To facilitate this capability, DOE sponsored the development of a very small, low-cost current sensor that would support an integrated measurement and communication device in a size comparable to the standard disconnect typically used for the air conditioner unit outside a residence. The FY 2010 project included the successful development of prototype current sensors and evaluation in the DTE Energy Metering Lab, confirming the potential to meet the requirements of a revenue-grade device. The prototype sensors and the specifics are listed below.

The successful development has led to a plan to fabricate a larger number of devices for field testing as part of ongoing vehicle/infrastructure demonstration efforts in FY 2011.

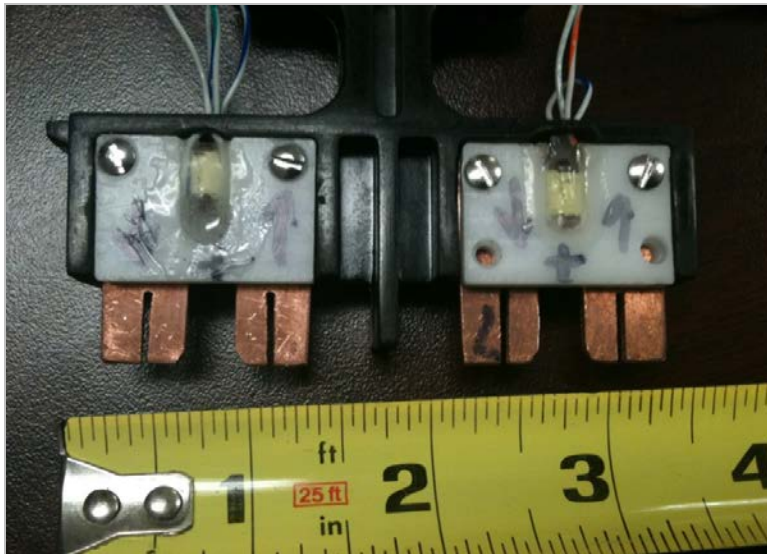


Figure 1: Low-cost current sensor

Enabler for small, low-cost revenue grade sub-meter

- Based on <\$5, 60A AC disconnect device
- Current sensor technology is > 0.1 percent accuracy
- 'Subtractive' meter is 0.3 percent class
- Communication based on Zigbee/UMAN via SDR
- Current sensors built into bus bars
- Single board metrology, 90x50x25 mm